



UNIVERSITÉ  
SORBONNE  
PARIS NORD



**THESE DE DOCTORAT DE L'UNIVERSITE SORBONNE PARIS NORD  
INSTITUT GALILEE**

Discipline Génie des Procédés

Option **Sciences des Matériaux**

Présentée et soutenue publiquement par

Ken Axxel CASTILLO ARVIZU

Pour obtenir le titre de

**Docteur de l'Université Sorbonne Paris Nord**

---

**Growth of thick and widened high quality boron doped single crystal diamond:  
Investigation and reduction of extended defects for the optimization of high power devices for a  
clean energy transition.**

---

Directeur de thèse: Jocelyn ACHARD

Co-Encadrant: Riadh ISSAOUI

Soutenue le 06/11/2023

**Devant le jury composé de:**

1	Didier CHAUSSENDE	Directeur de Recherche au CNRS	Rapporteur
2	Samuel SAADA	Directeur de Recherche au CEA, DRF	Rapporteur
3	Karine ISOIRD	Maitre de Conférences, LAAS	Examinatrice
4	Xavier DUTEN	Professeur des Universités, LSPM	Examineur
5	Jocelyn ACHARD	Professeur des Universités, LSPM	Directeur de thèse
6	Riadh ISSAOUI	Maitre de Conférences, LSPM	Co-encadrant de thèse

**“Accept the things to which fate binds you, and love the people with whom fate brings you together, but do so with all your heart.”  
— Marcus Aurelius, Meditations**

## Acknowledgments

Dedicated to my parents, who have always been my pillars of support in all my endeavors.

En primer lugar, quiero expresar mi profundo agradecimiento a los pilares que me han sostenido durante tantos años: mis padres. A Sandra Inés Arvizu Barrios, sin cuyas enseñanzas, consejos y amor, esto no habría sido posible. A mi padre, Horacio Castillo Requena, de quien he aprendido innumerables lecciones valiosas. Este trabajo está dedicado a ambos. También a mi pareja, Claudia Verónica Silva Juárez, quien me ha mostrado una faceta esencial de la vida. Su apoyo y amor, especialmente durante mis años en el extranjero, han sido invaluable. Gracias por cada sacrificio y por superar juntos cada obstáculo. A mis padrinos José Martín Díaz Medina y María Medina Araujo quienes también desde la distancia me apoyaron en todo momento.

This doctoral work was undertaken at the LSPM “Laboratoire des Sciences des Procédés et des Matériaux” of CNRS at the Université Sorbonne Paris Nord. I am deeply indebted to Jocelyn Achard for welcoming me, a stranger, into this project. This opportunity would not have materialized without the initial conversations with Riadh Issaoui, who introduced me to the project. My eternal gratitude goes to both of them. Additionally, I am thankful to CONACyT for their support for more than three years.

I owe immense gratitude to those who guided me in the laboratory. My co-advisor, Riadh Issaoui, worked closely with me, introducing me to the subject and patiently guiding my work. My thesis director, Jocelyn Achard, always provided invaluable insights and support. The entire diamond and carbon materials team contributed to my growth. Special mentions to Alexandre Tallaire and his kindness, Samir Farhat's honesty and transparency, Audrey Valentin's warmth, Ovidiu Brinza's unique teaching methods in complicated situations, Vianney Mille's patience, Fabien Bénédic's insightful comments, and Corinne Duluard quiet support, thanks to everyone for their guidance, knowledge, and kindness.

The lab was a mosaic of brilliant minds. From Nassim's ever-helpful demeanor, Sarah's genuine concern, Ludovic's early guidance, to Maria Konstantakopoulou's radiant warmth, each one has etched a memory in my heart. Their collective wisdom and camaraderie made the challenging days bearable and the good days memorable.

My fellow doctoral students were the comrades-in-arms in this intense journey. Miguel Sanchez, my guiding star from day one; Lino Martinez, my office partner and confidant; Ahmed Andalouci, with his wit and wisdom, whose inclusiveness made me feel at home; and Elyes Dhaouadi, whose profound conversations enriched my perspective and the unforgettable kindness of Wafa Alimi.

Without further ado to all my other fellow PhD students, such as Chaimaa, Midrel, Assane, Lounis, Damia, Lahcene, Rémi, Marie Charlotte, Ameni and without wanting to offend anyone by leaving them out, thank you all very much.

Muchas gracias a Dayana Bayarri, Fred Bayarri y sus hijos Arthur y Mila. Su hospitalidad y amabilidad al recibirme en Francia han sido invaluable. A Carlos Anaya, por su amabilidad y por recordarme el calor latino, siempre estarás en mis recuerdos. También, mis agradecimientos más sinceros al Dr. José Ricardo Silva Hernández, por darse el tiempo de aconsejarme en la parte final de redacción de esta tesis, lo aprecio mucho.

Siempre estaré eternamente agradecido con todas aquellas personas que, a pesar de la distancia, han dejado una huella imborrable en mi vida. Personas que, estando en México o en cualquier otro país, siempre tuvieron una palabra de aliento, como Adriana Muñiz, quien siempre estuvo presente en momentos de necesidad. A mis amigos de la maestría y la licenciatura, que, a pesar del tiempo y la distancia, supieron mantenerse en contacto; Oscar López, Emanuel García, Carlos Santamaría, entre otros, les agradezco profundamente.

## Table of content

General Introduction .....	4
Chapter I: State of art.....	8
1.1 Introduction.....	10
1.2 Diamond: An Outstanding material.....	11
1.3 Diamond classification.....	12
1.4 The diamond synthesis.....	13
1.4.1 High Pressure – High Temperature (HPHT) Diamond synthesis.....	16
1.4.2 The Chemical Vapor Deposition (CVD) diamond synthesis.....	17
1.5 Diamond growth type .....	21
1.5.1 CVD polycrystalline diamond.....	21
1.5.2 Nanocrystalline diamond .....	22
1.5.3 Heteroepitaxial diamond.....	22
1.5.4 CVD monocrystalline diamond.....	23
1.6 CVD single crystal diamond growth control at LSPM .....	24
1.6.1 Influence of temperature .....	24
1.6.2 Influence of the methane concentrations.....	25
1.6.3 Influence of the couple power and pressure .....	26
1.7 Defects and purity control in CVD diamond.....	27
1.7.1 Point defects: doping.....	27
1.7.2 Extended Defects: Dislocations .....	33
1.8 Electronic applications .....	41
1.9 Conclusion .....	42
1.10 References.....	44
Chapter II: Instrumentation for the sample manufacturing and characterization.....	51
2.1 Introduction.....	53
2.2 HPHT substrate treatment before growth .....	53
2.2.1 Diamond substrate cleaning.....	53
2.2.2 Choosing the correct side for the growth process .....	54
2.2.3 Surface treatment .....	55

2.3	CVD growth reactors .....	55
2.4	Characterization techniques.....	59
2.4.1	DiamondView™ .....	59
2.4.2	Confocal Laser Scanning Microscopy .....	60
2.4.3	Raman spectroscopy .....	62
2.4.4	Cathodoluminescence spectroscopy.....	67
2.4.5	Secondary Ion mass spectrometry (SIMS).....	75
2.5	Conclusions.....	79
2.6	References.....	80
3	Chapter III: Growth Parameters Optimization for Boron Doped CVD Diamond Growth and Stacking Layer Dislocation Study .....	82
3.1	Introduction.....	84
3.2	Growth parameters optimization for boron doped CVD diamond growth .....	85
3.2.1	Influence of sample position in the plasma .....	85
3.2.2	Influence of microwave power density .....	87
3.2.3	Influence of methane .....	92
3.2.4	Microwave power and (B/C) <sub>gas</sub> reduction.....	95
3.2.5	Measurements techniques for boron doping concentration.....	102
3.3	Exploring the Feasibility of Vertical Schottky Diodes with Diamond Layers: Investigations and Future Prospects .....	104
3.3.1	Stacking layer study.....	105
3.3.2	Interface analysis.....	113
3.4	Conclusions.....	119
3.5	References.....	120
	Chapter IV: Growth of large and thick boron doped single crystal diamond.....	122
4.1	Introduction.....	124
4.2	Lateral growth technique .....	125
4.2.1	Advantages and limitations of lateral growth .....	125
4.3	Conditions promoting lateral growth.....	125
4.3.1	First approach for lateral growth .....	127
4.3.2	Higher methane and oxygen levels during boron doped diamond deposition .....	130
4.3.3	Second approach using 1% oxygen in the gas phase .....	131

4.3.4	Third approach using 2% oxygen in the gas phase.....	134
4.4	Methods to obtain large and thick boron doped substrates .....	140
4.4.1	Widening of a 3x3mm <sup>2</sup> substrate .....	140
4.4.2	Widening of a 5x5mm <sup>2</sup> substrate .....	143
4.4.3	Overgrowth on macroscopic hole .....	145
4.4.4	Overgrowth on hole array on heteroepitaxial substrate .....	151
4.5	Conclusions.....	157
4.6	Perspectives.....	158
4.7	References.....	159
	General conclusions and outlook.....	161

# **General Introduction**



Diamonds, traditionally celebrated for their radiant beauty and hardness, have evolved beyond their aesthetic appeal to become a material with exceptional properties that have found a place in advanced technology. Despite their ancient origins, diamonds have been announced as the material of the future. The advent of laboratory diamond synthesis techniques, such as high-pressure, high-temperature synthesis (HPHT) and chemical vapor deposition (CVD), has expanded their use in various technological fields. These include anti-wear coatings, high-quality optical elements, radiation detectors and dosimeters. More recently, diamonds have found applications in quantum technologies, high-power high-frequency electronics, heat spreading, biochemical and electrochemical sensing and water treatment and purification systems.

The synthesis of diamond by CVD assisted by microwave plasma is a process that ensures optimal control of growth and doping rather than HPHT process and Hot Filament chemical vapor deposition (HFCVD). This process leads to the production of diamond crystals whose crystalline quality and purity often surpass that of the best natural crystals. This was the process I employed during my thesis work, testing a new cylinder chamber reactor at LSPM (Laboratoire des Sciences des Procédés et des Matériaux).

In the last decade, the CVD technique has matured sufficiently to allow the synthesis of monocrystals from several micrometers to several millimeters. This advancement has been limited to a few laboratories. Major companies like Element Six (a De Beers Group company) and Sumitomo have achieved industrial production of synthetic diamonds, along with startups like Diamfab, Diatope and the recently launched HiQuTe diamond, a spin-off of LSPM, that also could provide different diamond alternatives. These companies provide a variety of diamonds, ranging from single and polycrystalline, doped and undoped, large and small, from mechanical grade to optical and electronic grade. Synthetic diamonds are also gaining importance in the jewellery industry, where the color and transparency of the grown gemstones can be precisely controlled.

Despite these advancements, diamond technology is still in its early stages, and much progress is needed before it can claim a share of the dominance that silicon enjoys and becomes a common element in everyday life. The best so-called "electronic grade" crystals remain extremely difficult to obtain. These advances in diamond synthesis have also coincided with significant

developments in the field of diamond electronics. It is now clearly established that an increase in the doping rate induces a decrease in the activation energy, which even becomes negligible for concentrations greater than a few  $10^{20} \text{ cm}^{-3}$ . This mastery of the growth of thin layers of boron-doped diamond has made possible the manufacture of pseudo-vertical unipolar components based on diamond, showing the strong potential of this material. However, the components produced still have a significant series resistance limiting the value of the admissible currents. Thus, in order to reduce this parameter, the development of all-diamond vertical components seems essential. Such structures require the synthesis of very heavily doped thick diamond substrates, the first characteristic ensuring the necessary mechanical strength for handling the component and the second limiting as much as possible the electrical access resistance to the active component.

My thesis work was conducted in the context of exploring the exceptional properties of diamonds, particularly those heavily doped with boron. The primary focus was to develop the appropriate conditions for controlling the growth of thick films of diamond heavily doped with boron. This endeavor required optimizing a new reactor to aim for higher quality, longer deposition time, and stability. The work was built upon previous research conducted at the laboratory, but it also required the application of innovative strategies to overcome the scientific and technological challenges that arose. One of the main challenges was to incorporate boron homogeneously over long periods of time to obtain very thick crystals, ranging from a few hundreds of micrometers to 1 mm.

This research was part of the MOVEToDiam project, funded by the ANR (French National Research Agency). The project's main objective was the development of vertical power components, such as a MOSFET. However, to achieve such a complex device, the initial aim was a simpler one: a Schottky diode. Consequently, part of the samples produced during this thesis were used to create such components to evaluate their potential in this field.

This thesis work is structured as follows:

Chapter 1 provides a comprehensive review of the current state of the art in the growth of monocrystalline diamond films, with a particular emphasis on boron-doped diamond. This chapter also includes a brief overview of the interest and applications of boron-doped diamond in power electronics, based on existing components presented in the literature.

Chapter 2 discusses the experimental techniques used during my thesis. After describing the growth reactor used, the chapter delves into the theoretical principles of various characterization techniques. These techniques, used to observe and evaluate the properties of the crystals obtained during this thesis, were applied either at LSPM or in collaboration with other laboratories.

Chapter 3 presents the appropriate parameters for depositing thick layers of heavily boron-doped monocrystalline diamond. This chapter also explores the testing of different growth parameters such as microwave power density, different gas ratios, and substrate temperature. The latter part of the chapter delves into an interface study to assess the performance of a Schottky diode.

Finally, Chapter 4 focuses on strategies to the development of larger boron-doped diamonds, with an emphasis on lateral growth techniques and other potential dislocation control techniques. The goal is to achieve the largest possible substrates for various applications. This chapter presents several substrates with different modifications to reduce dislocations in the final layer. It also explores the use of more types of substrates than HPHT, such as CVD and heteroepitaxial substrates.

# **Chapter I: State of art**

## Summary

Chapter I: State of art.....	8
1.1 Introduction.....	10
1.2 Diamond: An Outstanding material.....	11
1.3 Diamond classification.....	12
1.4 The diamond synthesis.....	13
1.4.1 High Pressure – High Temperature (HPHT) Diamond synthesis.....	16
1.4.2 The Chemical Vapor Deposition (CVD) diamond synthesis.....	17
1.5 Diamond growth type.....	21
1.5.1 CVD polycrystalline diamond.....	21
1.5.2 Nanocrystalline diamond.....	22
1.5.3 Heteroepitaxial diamond.....	22
1.5.4 CVD monocrystalline diamond.....	23
1.6 CVD single crystal diamond growth control at LSPM.....	24
1.6.1 Influence of temperature.....	24
1.6.2 Influence of the methane concentrations.....	25
1.6.3 Influence of the couple power and pressure.....	26
1.7 Defects and purity control in CVD diamond.....	27
1.7.1 Point defects: doping.....	27
1.7.2 Extended Defects: Dislocations.....	33
1.8 Electronic applications.....	41
1.9 Conclusion.....	42
1.10 References.....	44

## 1.1 Introduction

In this chapter, I will present the state of the art related to the synthesis of diamond films, the importance related to the doping obstacles coupled with the development of applications based on this exceptional material, more particularly in the context of their use in high power electronics.

In recent years, remarkable progresses have been achieved in the field of diamond research in academic laboratories, leading to the creation of new companies in this field as Element Six, Diamond Foundry, DiamFab and HiQuTe Diamond, among others. Even if the accomplished works affect a large area related to synthetic diamonds, in this introduction, only some aspects will be discussed in depth while others will only be briefly discussed and the reader will have at his disposal the references in terms of journal articles, book chapters or website to go further.

A brief description of the crystallographic structure of diamond will be presented along with the electrical, mechanical, thermal and optical properties that make it an exceptional material for a very large panel of high-end applications. Then, the different diamond synthesis techniques will be discussed and more particularly the technique of Microwave Assisted Plasma Chemical Vapor Deposition (MPACVD) which has been used during this work. The most important growth parameters that control the growth process will be presented in relation to the work already done at LSPM. Finally, the rest of the chapter will be devoted to point defects in diamond for doping, and more particularly boron doping, as well as extended defects, which constitutes a strong limitation in the quality of diamond. The obstacles that limit its use for power electronics particularly for the development of vertical components will be recalled.

## 1.2 Diamond: An Outstanding material

When you hear the word diamond, it is completely intuitive to think of that precious stone or jewelry. However, we are facing one of the materials that have attracted the most attention in recent years for its exceptional and unexpected properties. Diamond is a metastable allotrope of carbon with incredible physical properties that can be summarized in table I.1.

These properties are the result of the strong bonding between carbon atoms with tetrahedral covalent bonds which involves  $sp^3$ -hybrid orbitals, leading to two possible crystal symmetries: (i) the most common in nature and synthetic, the cubic symmetry and (ii) the very rare hexagonal symmetry.

Property	Diamond
Hardness	Hardest known material (Mohs scale: 10)
Thermal Conductivity	2000 W/mK
Electrical Conductivity	Insulator
Lattice Structure	$Sp^3$ Hybridization, covalent bonds
Melting Point	3500°C (sublime at 4100°C)
Density	3.52 g/cm <sup>3</sup>
Transparency	Transparent
Friction Coefficient	Ultra-low (0.02)
Oxidation resistance	High
Applications	Electronics, quantum sensing, power devices, cutting tools, high-temperature applications, jewelry, bearings, optical windows and lenses, etc.

Table I.1 – Diamond properties

Diamond cubic lattice, outlined in Figure I.1, is formed by two face centered cubic (FCC) lattices superposed and displaced by  $a/4$  along each direction. The C-C bond has a length of  $1.54 \text{ \AA}$  and the unit cell dimension is  $a = \frac{4}{\sqrt{3}}r_{C-C} = 3.56 \text{ \AA}$  containing eight carbon atoms resulting in a density of  $3.515 \text{ g}\cdot\text{cm}^{-3}$ . Pernot et al have described that at room temperature, a maximum electron mobility of around  $1000 \text{ cm}^2\text{V}^{-1}\text{s}^{-1}$  [1] and  $2000 \text{ cm}^2\text{V}^{-1}\text{s}^{-1}$  for holes [2] can be measured.

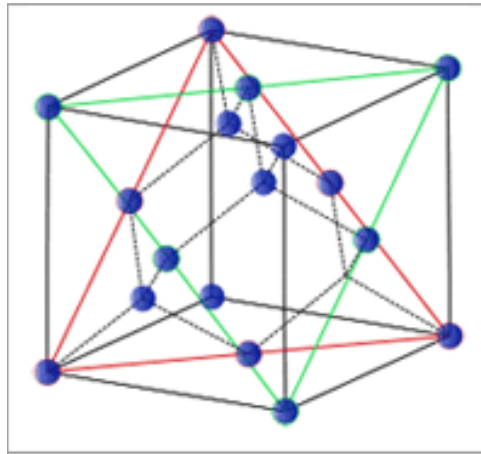


Figure I.1 - Diamond unit cell formed by two superposed FCC networks

In addition, diamond is optically transparent in the ultraviolet, visible, infrared and far infrared regions. It is extremely chemically inert and then not affected by acid and other wet chemical treatments and it is not toxic. These outstanding properties make diamond an extremely versatile material and that's the reason why it has been studied all over the past decades not only for jewelry applications but also to be used for industrial applications such as tribology, power electronic, quantum sensing, biological and medical applications [3-5].

Building on these findings, the next part of this chapter will delve deeper into the classification of diamonds based on their impurities and properties, further emphasizing its versatility as material.

### 1.3 Diamond classification

Based on the nature and impurities quantity, a diamond classification has been established and illustrated in Figure I.2. The main impurities regarding this classification are those with boron and nitrogen. Crystals which contain nitrogen impurities are from class I, while those without are class II. Adding the quantity factor to these two classes, it is possible to define four types of diamond:



- Type Ia: crystals containing nitrogen impurities in aggregates that give them a pale yellow color. (98% of natural diamonds)
- Type Ib: their color ranges from an intense yellow to brown. They contain large amounts of nitrogen (10 to 1000 ppm) in substitutional positions and constitute the majority of HPHT diamonds.
- Type IIa: good purity, they may contain less than 2ppm of nitrogen. They have the biggest thermal conductivity and these types of diamonds are very rare in nature.
- Type IIb: these contain a small amount of nitrogen, but they have also incorporated boron, which gives them a blue coloration and a p- type electronic conductivity.

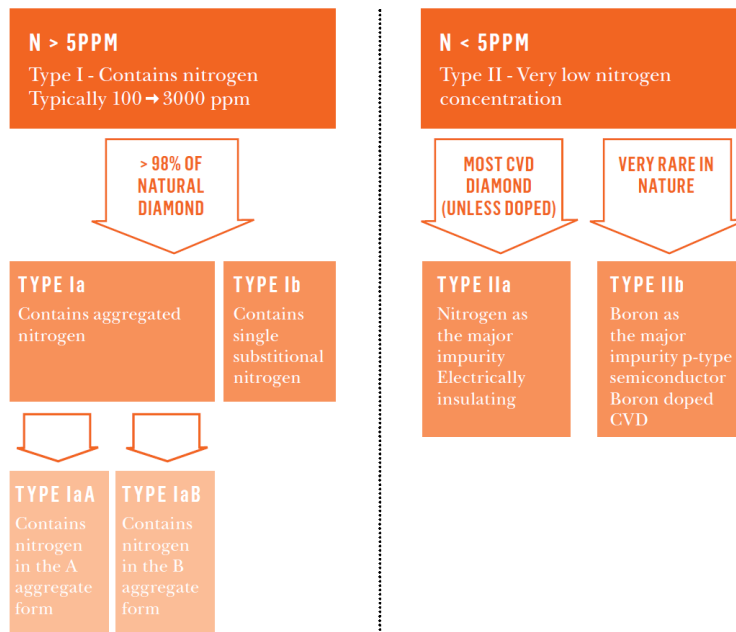


Figure I.2 - General classification of diamond by their nitrogen concentration[6].

Diamond classification based on the nature and quantity of impurities highlights its diversity and high potential. This has led to the development of various diamond synthesis technologies that I will present in the following.

#### 1.4 The diamond synthesis

Henry Moissan in 1893 created the first man-made diamonds, starting from small amounts of carbon subjected to high pressure and high temperature conditions [7]. Then, systematic studies were carried out in the 1910s in Europe [7] but it was only in the 50s that real technologic progresses were made [8, 9].

The starting point of diamond synthesis is the carbon phase diagram presented in Figure I.3. Indeed, diamond is one of the different allotropic forms of the carbon that can evolve, depending on pressure and temperature, to the graphitic allotropic form, which is the most abundant on Earth.

It can be noted that other carbon allotropic forms have been more recently discovered such as graphene, nanotubes and fullerenes but they will not be discussed in this part as my PhD work didn't concern them.

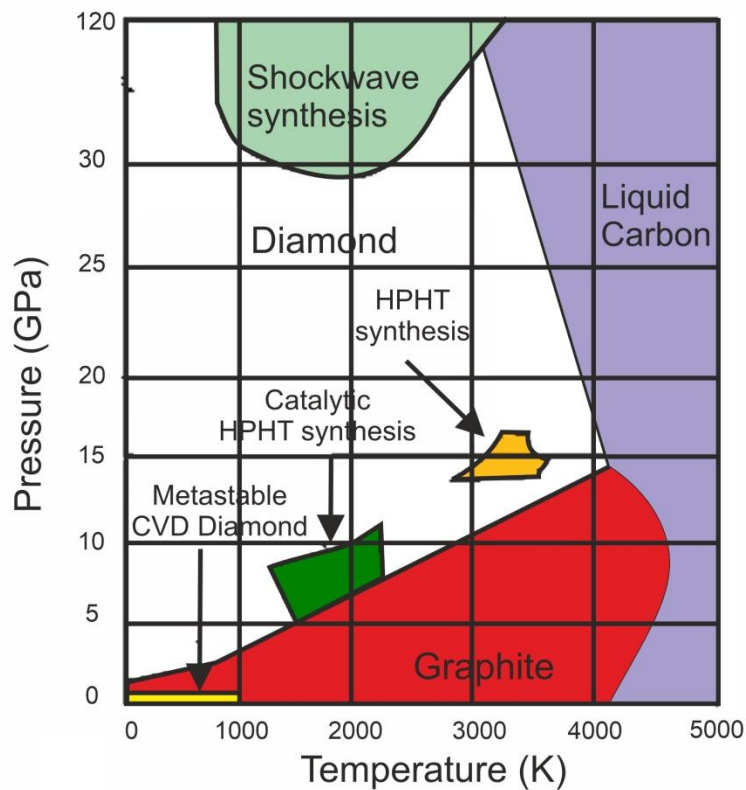


Figure I.3 - Carbon phase diagram [10]

By reading this phase diagram, it is possible to determine the most suitable conditions for the synthesis of diamond. For example, the orange area which is labeled as “HPHT synthesis”, allows transforming graphite into diamond by choosing a suitable pressure/temperature couple.

The values of this couple can be reduced by using a metallic solvent (such as Fe, Co, Ni...) which corresponds in the diagram to the green region called “Catalytic HPHT synthesis”. It can be also noticed in

this diagram that there is a yellow zone labeled as “metastable CVD diamond” in which diamond can be formed under a very low pressure and moderate temperature.

In this area, on the contrary to the HPHT methods (which are thermodynamically controlled), the growth is kinetically controlled and it is what we call the synthesis by CVD.

Even if graphite and diamond are composed of carbon, their properties are completely different. These two allotropic forms do not have the same hardness, optical transparency, electrical behavior, etc. as it is illustrated in table I.2 in which diamond properties are compared with those of graphite.

<b>Property</b>	<b>Diamond</b>	<b>Graphite</b>
Hardness	Hardest known material (Mohs scale: 10)	Soft (Mohs scale: 1-2)
Thermal Conductivity	2000 W/mK	200-500 W/mK
Electrical Conductivity	Insulator	Conductor
Lattice Structure	Sp <sup>3</sup> Hybridization, covalent bonds	Sp <sup>2</sup> Hybridization, weak van der Waals forces
Melting Point	3500°C (sublime at 4100°C)	3650°C
Density	3.52 g/cm <sup>3</sup>	2.2 g/cm <sup>3</sup>
Transparency	Transparent	Opaque
Friction Coefficient	Ultra-low (0.02)	Moderate to high (0.1-0.5)
Oxidation resistance	High	Low
Applications	Electronics, quantum sensing, power devices, cutting tools, high-temperature applications, jewelry, bearings, optical windows and lenses, etc.	Lubricants, batteries, fuel cells, pencils, coatings, refractories, etc.

Table I.2 - Comparative properties of diamond and graphite.

#### 1.4.1 High Pressure – High Temperature (HPHT) Diamond synthesis.

The HPHT process was first developed in 1893 and has been used for diamond synthesis since the mid-twentieth century [9]. The way to proceed is relatively simple: carbon must be exposed to thermodynamically favorable conditions for the formation of diamond, such as in the phase diagram presented in Figure I.3.

In order to limit pressure and temperature, the key is to add carbon (graphite or microcrystal) in a solvent constituted of transition metals (iron, nickel, cobalt) and expose this mixture to a gradient of temperature of few tens of K around 1600 K coupled with high pressures in the order of a few GPa [11]. This process is illustrated in Figure I.4.

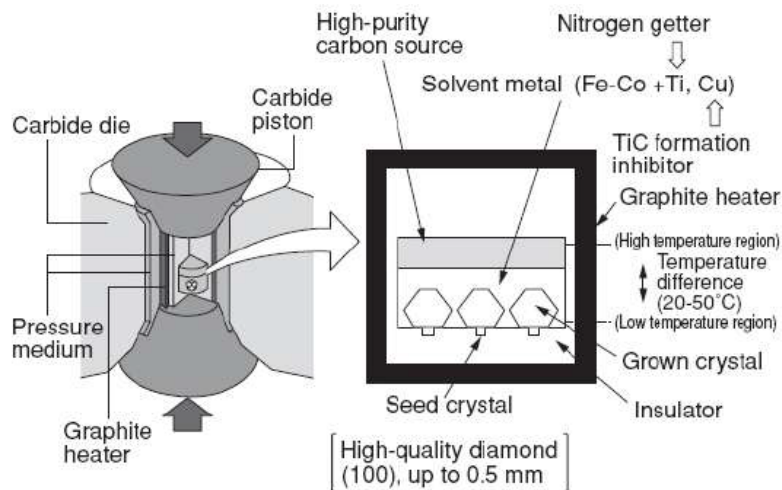


Figure I.4 - HPHT synthesis machinery and process [12]

The resulting crystals synthesized by this technique are in the most cases contaminated by some impurities during the growth. In particular, residual solvents such as Ni or Co can be observed in the grown diamond as well as nitrogen, which is very difficult to eliminate in this process despite the use of Ti getter, leading, as explained in previous paragraphs, to type I diamond.

Recent achievements have shown that it is now possible to also produce high purity diamond with this technique[13, 14] but the availability of such substrates is very limited and the cost is prohibitive for industrial applications since the corresponding market is very often jewelry.

Even if the purity of HPHT diamond substrates is not completely satisfactory, their crystalline quality remains reasonable and it is possible to easily obtain crystals with thicknesses greater than 500  $\mu\text{m}$  and surface areas between 3 x 3 and 5 x 5  $\text{mm}^2$ .

These HPHT diamond plates can then be used as a substrate for another process called CVD, which was developed in the late 1950s, as we will see in the next paragraph. The control of the environment in the CVD process helps to reduce residual impurities and allows for the manufacture of thin films with high quality and purity.

The CVD technique is a powerful method to improve the properties of diamond substrates obtained by HPHT methods and opens the possibility to create devices with improved performances by controlling the environment and the quality of the diamond films.

#### 1.4.2 The Chemical Vapor Deposition (CVD) diamond synthesis

The technique for the manufacture of thin films by CVD was originally developed in the late 1950s and carried out by American and Russian research teams[8, 15], but it was only in 1980s that this technique has acquired more importance thanks to Japanese works[16-19].

Basically, CVD involves the flux of gas precursors into a chamber in which one or more heated substrates to be coated are exposed. The chemical reactions that occur on and near the hot surfaces result into the deposition of a thin film on the substrates.

In addition to this, the production of the chemical gaseous byproducts is extracted out of the chamber along with unreacted precursor gases.

A large variety of materials can be grown using this technique leading to a wide range of applications. There are many CVD variants. The deposition can take place in hot-wall and cold-wall reactors, at sub-Torr total pressures as well as above-atmospheric pressures.

The typical range of temperatures varies from 200 to 1000°C. The gas heating methods allowing activating the gaseous phase can be carried out by different means which can involve the use of plasma, ions, photons, lasers, hot filaments, or combustion reactions to increase depositions rates and/or lower deposition temperatures.

In the specific case of diamond in which molecular hydrogen H<sub>2</sub> and methane CH<sub>4</sub> composed the gas mixture, two principal ways are developed: either by hot filament or microwave electromagnetic source.

The first process is called HFCVD [20] and for it, a tungsten or tantalum filament is placed very close to the substrate. It is heated up to a temperature range of 2300 – 2800 K by electric current circulating allowing molecular hydrogen and carbon precursor to be dissociated and formed essential radicals for diamond growth.

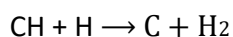
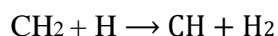
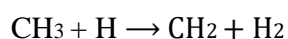
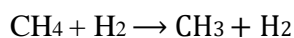
However, in this technique, two main drawbacks exist: first, during the process, some filament particles can be partially vaporized leading to metallic contamination of the diamond film and second, gas temperature is limited by the melting temperature of the filament and then, gas dissociation remains limited. Nevertheless, the method presents some advantages.

In particular, deposition on large surfaces as well as on substrates with complex geometries can be performed which is very useful for some applications in the field of mechanics or electrochemistry for which the diamond film thickness and purity are not crucial parameters.

The gas phase can be also activated by a microwave electromagnetic source. The process is called MPACVD[21] and in this case, much higher gas temperatures can be reached by coupling high microwave power in the plasma[22].

This technique is very well adapted to have a good control of the contamination level in the diamond film and obtain thick films[23]. Figure 1.5 illustrates the general CVD process.

For the diamond growth, the main carbon species involved for carbon atom incorporation in the lattice are methyl radicals  $\text{CH}_3$ . Their production results from the following kinetic scheme:



In this scheme, it is clear that to obtain a high methyl radical density, a large dissociation of molecular hydrogen is required which is obtained for gas temperature above 3000 K in the core of the discharge as it has been demonstrated at LSPM [24-27]. The main interest to use microwave energy rather than hot filament process is then very clear.

Nevertheless, in the same time, methyl radical production requires temperatures below 2200 K [28, 29] to limit their own dissociation to other carbon species such as  $\text{CH}_2$ ,  $\text{CH}$ , etc.

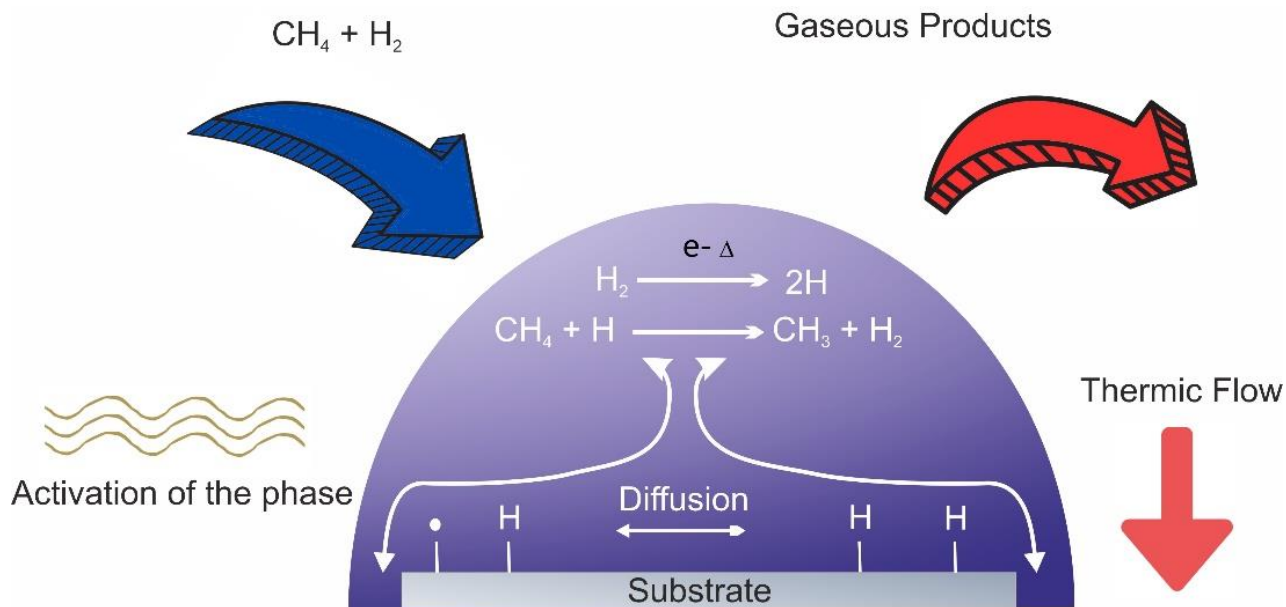


Figure I.5 - Diagram of H<sub>2</sub>/CH<sub>4</sub> microwave plasma with part of the reactions involved during the diamond synthesis in CVD technique.

Fortunately, in this process, the substrate temperature is maintained between 850 and 1000°C, which is much lower than the temperature of the gaseous environment activated by microwave. In these conditions, a phenomenon of heat transfer occurs from the plasma to the surface of the substrate on which the deposition takes place, resulting in a decrease of temperature as well as in the density of atomic hydrogen as illustrated in Figure I.6 (a) and I.6 (b).

During the diffusion process, hydrogen atoms saturate dangling bonds and help to improve the quality of the diamond film by removing the sp<sup>2</sup> graphitic phases. Moreover, the reduction in the temperature of the gas at the plasma/surface interface makes it possible to reach values compatible with the formation of methyl radicals (from 1400 to 2200 K), while maintaining a still high atomic hydrogen density.

This phenomenon results in a high concentration of methyl radicals a few millimeters from the surface (See Figure I.6 (b) near the substrate) [30, 31].

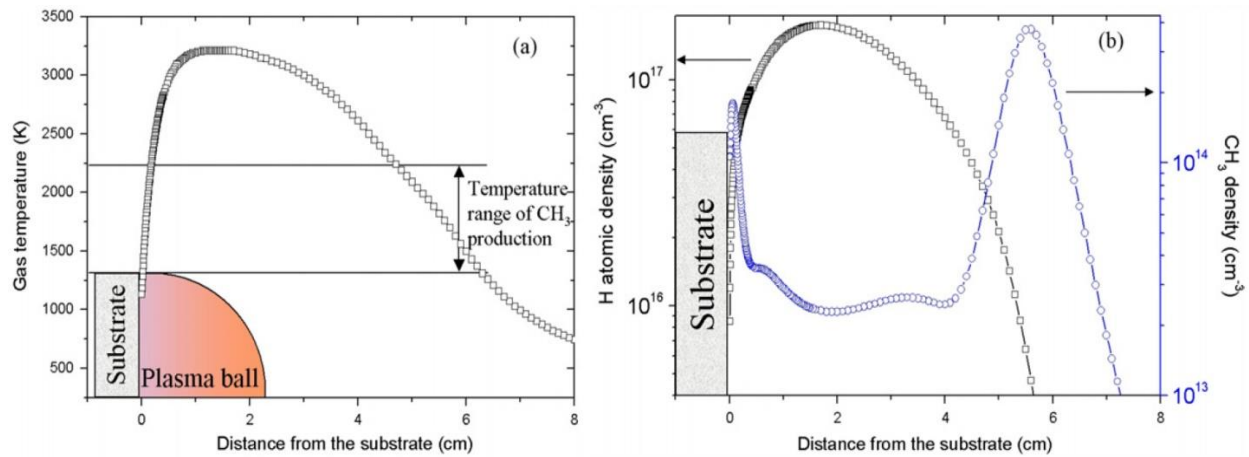


Figure 1.6 - (a) Gas temperature and (b) atomic hydrogen (blue dots) and methyl radical (black squares) concentrations got by calculation with a 1D axial plasma model for MWPD of 1000 Wcm<sup>-3</sup>, 4% of CH<sub>4</sub> in the H<sub>2</sub>/CH<sub>4</sub> gas and a substrate temperature of 1100 K. The substrate is placed at 0 of the X-axes [32]

The main interest and then the main advantage of using high microwave power coupled with a high pressure is that atomic hydrogen and methyl radicals close to the diamond surface are controlled by the temperature gradient of the gas between the plasma core and the plasma-diamond interface.

Therefore, the large atomic hydrogen density induced by the very high temperature plasma lead to H diffusion close to the surface allowing a high CH<sub>3</sub> density very close to the diamond interface. In these conditions , a growth rate close to 70 μm/h has been reached at the LSPM[33] using pressure of 400 mbar without adding any nitrogen to the gas phase, this impurity being very well known to strongly increase the growth rate [34-36].

However, the control of the growth at such extreme conditions remains very difficult particularly in terms of thermal management of the substrate temperature, and more moderate couple pressure-microwave power are usually used, leading to growth rate between 10 and 20 μm/h.

In conclusion, the MPACVD technique proves to be the most efficient way to obtain the best conditions to create the key species for diamond deposition and allowing diamond films synthesis with a very low contamination levels. All the CVD diamond samples fabricated and utilized during this thesis were produced using this technique.

Now that we presented the technique used during this thesis, we will see in the next paragraphs the types of diamond that can be grown. Indeed, depending on the substrate nature and the growth conditions used, polycrystalline, monocrystalline or nanocrystalline diamond can be obtained.



## 1.5 Diamond growth type

The nature of the grown diamond films strongly depends on the nature of the substrate used. Indeed, polycrystalline, and nanocrystalline diamond are obtained when non-diamond substrates are used and monocrystalline diamond is obtained when single crystal diamond is used as substrate.

### 1.5.1 CVD polycrystalline diamond

CVD diamond synthesis requires a special attention in the choice of substrates. Indeed, it is necessary to choose substrate composed of elements having a thermal expansion coefficient compatible with the non-delamination of the film and capable of withstand the harsh deposition conditions.

Before the deposition, a seeding step is required consisting in the formation of diamond nanoparticles on the substrate surface to promote the nucleation, which would be otherwise very weak. Each created nuclei can then grow individually from each other up to the coalescence of the film.

After this step, only faces having the highest growth rate orthogonal to the surface may continue to grow, all of this resulting in a columnar growth with a textured surface (Figure I.7).

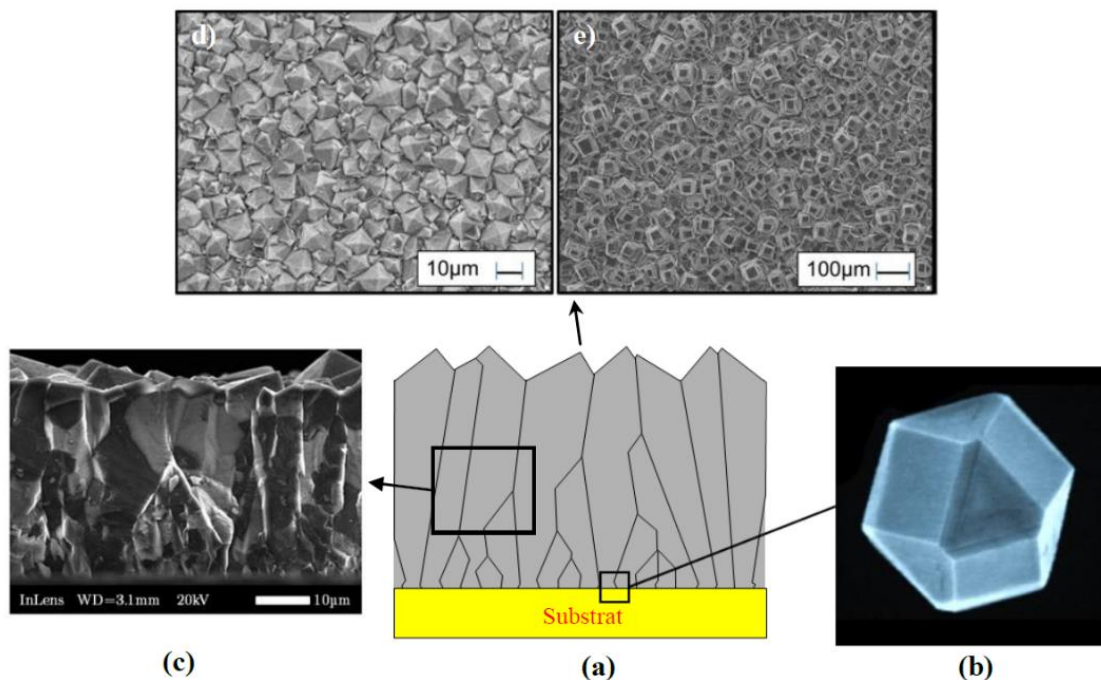


Figure I.7 - Pictures of the growth steps of a CVD polycrystalline diamond film: (b) Diamond crystals at the beginning of the growth step, before coarsening; (a) Sketch showing the columnar growth (Van Der Drift model) [37]; (c) SEM cross section image showing a columnar structure[38]; (d) Textured surface with octahedral crystals and (e) Textured surface with cubooctahedron crystals[39].

One main advantage of this material is the possibility of growing it on relatively large surfaces since we are not limited, as we will see in the next paragraph for single crystal growth, by the size of the substrate.

Using a microwave power excitation at a frequency of 2.45 GHz, it is possible to use substrates with a diameter of two inches, the diameter of the plasma being limited to  $\lambda_g/2$  where  $\lambda_g$  is the wavelength of the microwave. It is the reason why, by using a lower frequency of 915 MHz, it is possible to increase the plasma size and grow polycrystalline diamond on substrates of almost six inches.

Nevertheless, even if this kind of diamond is suitable for several applications such as optical windows, radiation detectors, thermal applications, etc. the presence of grain boundaries is a strong limitation for electronic applications and requires the development of efficient process for single crystal growth.

### 1.5.2 Nanocrystalline diamond

Nanocrystalline diamond (NCD) is a form of diamond that is composed of small diamond crystals, typically with a size less than 100 nanometers. According to a study carried out by O.A. Williams[40], NCD is formed using CVD under specific growth conditions, such as low pressure and high temperature.

This material can be also grown using gas mixture composed of Ar and CH<sub>4</sub> rather than H<sub>2</sub> and CH<sub>4</sub> [41-43]. NCD has unique properties that make it suitable for a wide range of applications, including biotechnology, mechanical engineering, among others [44, 45]. NCD has a high wear resistance and low friction coefficient, which makes it ideal for using in coatings and lubricants. Additionally, the ability to chemically modify NCD to create a range of functionalized forms, such as hydrogen-terminated, oxygen-terminated, and nitrogen-terminated diamond, further expands its potential applications.

Another great advantage of NCD is that the roughness is independent of the film thickness and is limited to a few tens of nanometers. This is not the case for polycrystalline diamond, for which roughness continuously increases with thickness. Therefore, NCD is a promising material for applications that require precise control of surface roughness and low friction coefficient.

### 1.5.3 Heteroepitaxial diamond

Although diamond's exceptional properties make it an attractive material, the limited size of single-crystal diamond samples poses a significant technological challenge for wider applications in the absence of a large substrate.

Polycrystalline diamond, while lacking this limitation, has reduced properties due to the presence of grain boundaries. To achieve good crystalline quality and a large deposition area, researchers have explored and studied the technique of heteroepitaxy for several years.

Like polycrystalline diamond, this technique involves creating carbon seeds on the surface of the specific substrate, called a heterosubstrate, which then grow until they meet and form a diamond film. However, the nature of the heterosubstrate allows controlling the orientation of these seeds so that they are identical for each of them leading to, at the end of the growth, a large single crystal.

It requires Bias-Enhanced Nucleation (BEN), which is the only method available to produce these carbon seeds, and it requires the use of specific heterosubstrates mainly based on the deposition of thin Iridium layer on a specific buffer layer [46-49].

Nevertheless, one of the main drawbacks of heteroepitaxial diamond films is the relatively high dislocation density that is often present in the films. Heteroepitaxial diamond films can be particularly prone to dislocations due to the strain that is often present at the interface between the diamond and the heterosubstrate.

This strain can lead to the formation of misfit dislocations, which are dislocations that form to relax the strain caused by the lattice mismatch between the diamond and the heterosubstrate. These misfit dislocations can then propagate through the diamond film, leading to a high dislocation density.

Nevertheless, Schreck et al have showed that the use of a low-temperature nucleation process with BEN led to a significant reduction in dislocation density in heteroepitaxial diamond films[50]. Despite these advances, the high dislocation density in heteroepitaxial diamond films remains a significant challenge that must be addressed to enable their use in high-performance applications.

#### 1.5.4 CVD monocrystalline diamond

The growth of monocrystalline material requires the use of single crystal diamond substrate and is called homo-epitaxy. After different studies on the deposition of single crystals by CVD, the importance of the quality of the substrate has been widely highlighted. Indeed, the presence of growth sectors or defects such as dislocations which propagate during the growth from the substrate limits significantly the resulting synthesized crystal properties [51-56].

Different types of substrates can be used: natural diamonds, HPHT or even CVD substrates. At the LSPM, different works have been carried out in order to estimate the impact of them on the homoepitaxy [57].

It has been shown that the growth on natural IIa substrate leads to a very high level of stress in the CVD layer due to the high dislocation density initially present in the substrate. On the other hand, the use of Ib HPHT substrate allows growing high quality CVD diamond layer, depending on the substrate preparation.

Indeed, it has been shown that a  $H_2/O_2$  plasma etching is necessary to limit stress in the grown layer and that, it is necessary to start from a substrate presenting a single growth sector [32]. Using HPHT substrates of higher quality (IIa substrates providing by NDT company for example) have been proved to strongly improved the quality of the CVD layer [58].

However, the high cost and low availability of such substrates make their use very limited for homoepitaxy.

## 1.6 CVD single crystal diamond growth control at LSPM

DCM (Diamond and Carbon Materials) team at the LSPM has developed a strong experience allowing the growth of single crystal CVD diamond films with thicknesses up to few millimeters and growth rates adapted for industrial development (growth rates higher than 10  $m\mu/h$ ).

In the following paragraphs, I will present the influence of different important growth parameters (temperature, microwave power, pressure and methane concentration) that have an impact on the final quality of the films and growth rates. The majority of these results have been carried out through the different thesis work performed in the laboratory [57, 59-61].

### 1.6.1 Influence of temperature

In CVD deposition, the increase of temperature plays an important role because it leads to an increase in the mobility of the species at the surface and consequently to an increase in the growth rate that can reach 6 to 7  $\mu m/h$  at  $T= 1000\text{ }^\circ C$ . However, pyramidal defects are generally observed on the surface of the resulting films.

Those defects are often incorporation sites of non-diamond phases leading to the appearance of non-epitaxial crystallites as illustrated on Figure I.8 (a).

At lower temperatures, the mobility of the species is very low which results into a decrease on the growth rate (approximately 2  $\mu m/h$  at  $T= 750\text{ }^\circ C$ ). In addition, the surface of the resulting films has a high roughness and a high concentration of defects (see Figure I.8 (c)).

In the framework of the work thesis performed by C.Findeling-Dufour [60] and A. Tallaire [59], an optimum deposition growth temperature of about 850 °C has been determined. This temperature allows the deposition of single crystal diamond films with a good surface morphology (see Figure I.8 (b)) and growth rates around 4 to 5  $\mu\text{m}/\text{h}$ .

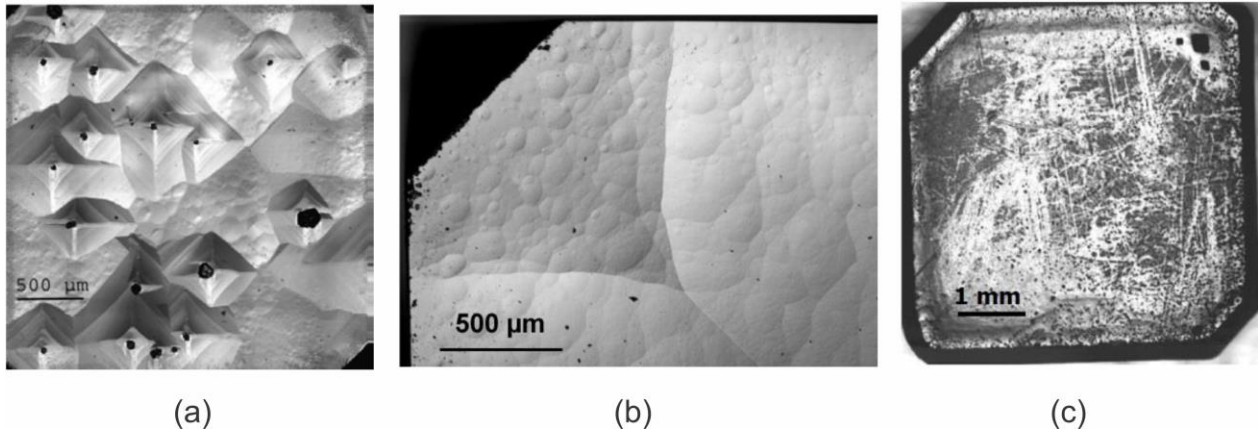


Figure I.8 - Surface morphology of homoepitaxial CVD diamond films synthesized with a couple microwave power/pressure of 3kW and 200 and 4% methane at 1000°C (a), 850°C (b) and 750°C (c).[59]

### 1.6.2 Influence of the methane concentrations

Increasing the growth rates is also possible by increasing the methane concentration. This concentration determines the quantity of carbon precursors in the gas phase and of course plays an important role on the supersaturation of carbon.

Thus, as shown on the graph of Figure I.9, for similar growth conditions in terms of pressure, microwave power and temperature (200mbar, 3kW and 850 °C), the deposition rate rises from 2  $\mu\text{m}/\text{h}$  for a 2% methane concentration to 16  $\mu\text{m}/\text{h}$  for a 7% concentration keeping similar and good surface morphology of the films.

However, above 8% of methane, the saturation of carbon species leads to the formation of soot, which destabilizes the discharges and limits the duration of the deposition.

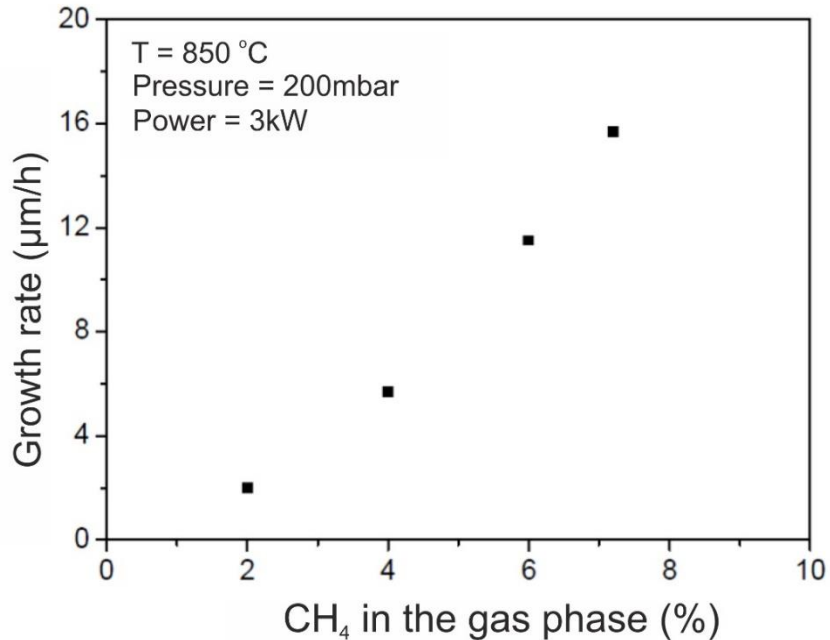


Figure I.9 - Evolution of the growth rate as a function of the methane concentration. Conditions: pressure = 200mbar, power = 3kW and temperature = 850 °C [59].

This highlights the importance of controlling the methane concentration during the CVD process in order to achieve optimal growth rates and film quality.

### 1.6.3 Influence of the couple power and pressure

The gas dissociation and the production of key species for diamond growth (methyl radicals and atomic hydrogen) are governed by the power density coupled to the plasma.

A simultaneous increase of the pressure and microwave power allows keeping a constant plasma volume while leading to an increase of the microwave power density and then of the growth rate (Figure I.10).

Nevertheless, a high power density induces technological difficulties and in particular, the cooling of the reactor elements becomes difficult due to strong heat transfer. A pronounced heating of the waveguides, antenna and deposition chamber usually occurs.

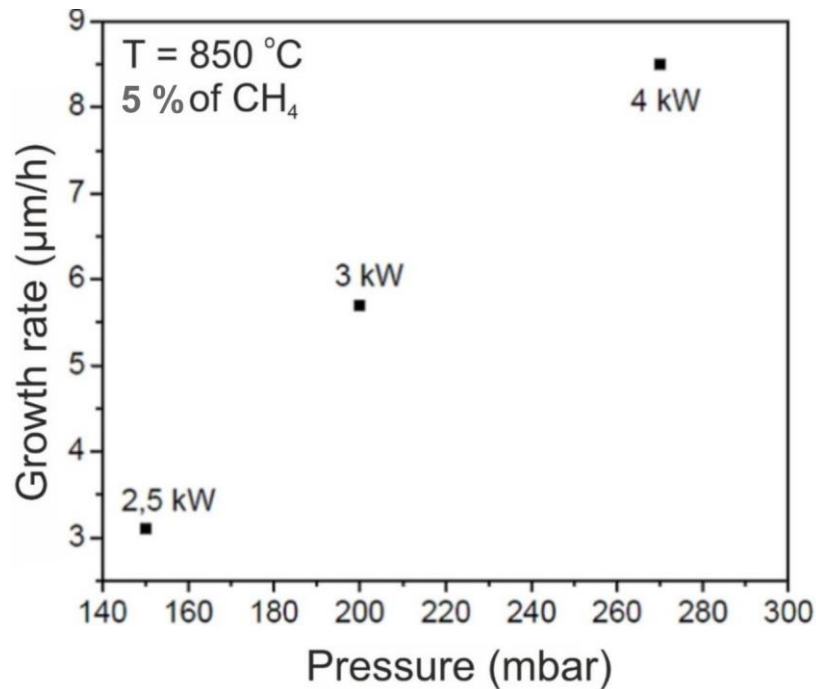


Figure I.10 - Evolution of the growth rate as a function of the injected power density[61].

Taking into account all of these limitations, we can consider that the optimal conditions for CVD intrinsic diamond growth are typically the use of 5% of methane, a substrate temperature of 850 °C, a pressure of 200 mbar and a microwave power of 3kW, the last two parameters allowing preserving a plasma diameter of 5cm. These parameters were utilized during intrinsic CVD diamond growth in some part of my PhD work and were the starting point to optimize the growth rate and the boron doping incorporation in a new reactor dedicated to boron doping.

## 1.7 Defects and purity control in CVD diamond

### 1.7.1 Point defects: doping

Diamond's unique properties make it a promising material for electronic applications. However, to fully utilize diamond's potential, it is essential to control its electrical conductivity through doping. Doping involves introducing impurities into the diamond lattice to create a dopant level in the bandgap, which can produce carriers to the valence or conduction band, depending on whether the dopant is an acceptor or donor of electrons (p-type or n-type doping respectively).

The natural candidates for diamond doping belong to the groups III and V of the periodic table, for p- and n-type respectively. Moreover, the impurities incorporation in the diamond lattice must be by substitution in order to be electrically active. Diamond possesses unique properties, such as a tight lattice structure, high hardness, and low miscibility, which limit the number of possible dopants. Boron is the dopant that can achieve p-type doping in diamond, while phosphorus is the candidate for n-type doping.

The doping of diamond can be carried out in situ during the growth [62, 63] but also by ion implantation [30, 64-67]. But in the latter case, the electrical activity remains very limited [68] and up to now, no clear demonstration have been made on the potentiality of implantation for developing electronic devices. It is the reason why, in situ doping is one of the main technique used to produce doped diamond for device fabrication purposes.

During homoepitaxial diamond growth by Plasma-enhanced chemical vapor deposition (PECVD), boron or phosphorous doping can be achieved by introducing diborane (or trimethylboron) or phosphine (or tertiarybutylphosphine (TBP)[69]), respectively. Notably, in 1998, Yamanaka et al.[70] reported the highest Hall mobility for holes of PECVD boron doped diamond films at 290 K.

In a separate study, Katagiri et al.[71] reported the highest room-temperature Hall mobility for n type doping.

If we take a look on the covalent radius of boron (0.088 nm) and carbon (0.077nm), we can see that they are not so different facilitating its incorporation in substitutional sites.

The activation energy of boron-doped diamond is 0.38 eV[72] and it was largely reported in the literature that this p-type dopant can be incorporated with a very good and high reproducibility [73, 74].

On the contrary, phosphorous has a covalent radius of 0.117 nm, which is much larger than that of carbon, making its incorporation difficult.

The first phosphorous doping has been demonstrated by Koizumi et al. in 1997 [75] on (111)-oriented diamond whereas the first phosphorous doping of (100)-oriented diamond was not achieved until 2005 [76]. The ionization energy for this dopant is 0.57 eV [71, 77]. Figure I.11 displays the diamond energy diagram when phosphorous and boron energetic levels are introduced into the band gap.



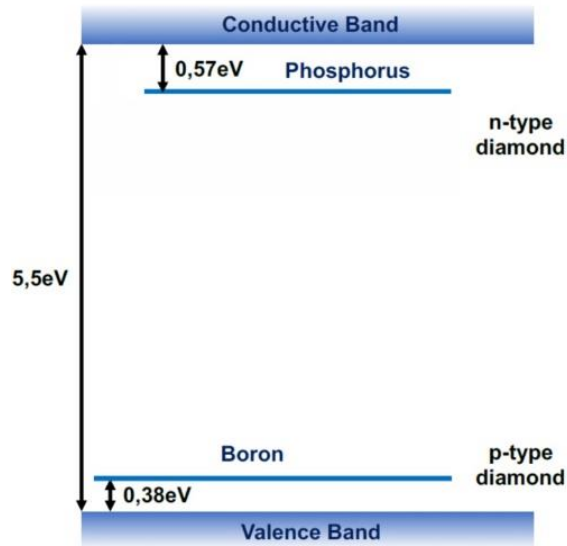


Figure 1.11 – Representation of the energy diagram of selected states in diamond band gap.

In the following, I will only discuss about in situ doping from a gas phase, which remains the only technique for effectively doping of diamond.

#### 1.7.1.1 n-type diamond

##### 1.7.1.1.1 On orientation (111)

The ease of impurity incorporation, which characterizes the (111) orientation, was the main reason for using it for n-type doping of diamond. Unlike the relative ease for p-type doping, n-type conductivity is difficult to achieve.

Nitrogen could be a natural candidate for n-type doping of diamond because it is easily incorporated into substitutional doping sites. However, it creates a level that is too deep (1.7 eV below the conduction band) to make it suitable for electronic devices. Nevertheless, nitrogen doping finds applications in quantum devices such as magnetometry [78, 79].

Phosphorus remains the only chemical element that has proven to be a substitutional efficient dopant for electronic n-type diamond doping even if the ionization energy remains relatively high.

However, n-type doping with phosphorus is only truly effective on the (111) orientation, although promising results have been shown on the (100) orientation[80] as it will be described in the next subsection.

The efficiency of phosphorus incorporation for n-type doping in diamond on the (111) orientation is about 12%, according to Pinault-Thaury et al. [81]. Additionally, a low compensation rate (the ratio between the number of acceptor  $N_a$  and the number of donor  $N_d$ ) was observed to be lower than 10% [82], doping with this impurity remains difficult because even a small amount of hydrogen in diamond forms phosphorus-hydrogen complexes that compensate for substitutional doping.

To date, only six laboratories have mastered this technology, including the NIMS (National Institute for Materials Science), which was the first to achieve this type of doping in 1997 [75] and GEMaC in France (Groupe d'étude de la matière condensée).

The maximum incorporation achieved is about  $5 \times 10^{19} \text{ cm}^{-3}$ . This result has been replicated at the Instituut voor Materiaalonderzoek (IMO) in Belgium on polycrystalline diamond [83] and at the Néel Institute [84].

Additionally, it has also been achieved at the AIST (National Institute of Advanced Industrial Science and Technology) [77], the GEMaC [85], and more recently at the University of Michigan with slightly higher incorporation at  $10^{20} \text{ cm}^{-3}$  [86].

Other candidates for n-type doping have been also studied, such as arsenic, which has a theoretical activation energy value of 0.4 eV. In studies conducted at the GEMaC, although arsenic incorporation was demonstrated via the gas phase, the incorporated atoms were electrically inactive, indicating that arsenic was not incorporated substitutionally but in interstitial sites, or they had formed complexes with hydrogen or other defects present in the material [87].

It was only through implantation in collaboration with IBS (Ion Beam Services) that As was demonstrated to be placed in substitutional sites. A signature of bound excitons in CL was obtained, but no electrical signature was observed. [88]

Other chemical elements have also been studied to evaluate their potential as donors in diamond. For example, sulfur has too low or no doping efficiency according to some studies [89, 90], while lithium and sodium are in interstitial positions in the diamond lattice with a strong tendency toward irreversible graphitization of the diamond layer at high concentrations [91].

As it is well known that the (111) orientation is strongly susceptible to twinning, and that it is very difficult to grow thick films of good quality in this crystal direction, n-type doping studies have been also developed using (100)-oriented diamond substrates.

#### 1.7.1.1.2 On orientation (100)

In 2004, the AIST[92] paved the way by developing n-type doping with phosphorus on (100) oriented diamond. Only three groups (AIST[93], Osaka University[94], and GEMaC[95]) have succeeded so far in obtaining phosphorus donors in diamond on layers a few microns thick with this orientation.

However, to date, despite promising recent results showing improved incorporation of phosphorus at substitutional sites [80], n-type doping on (100) orientation remains difficult.

The main differences between (100) and (111) orientations are: (i) low incorporation efficiency (1000 times lower on (100) than on (111)), (ii) a high compensation rate (50-100% on (100))[93, 96], but this is constantly decreasing. Thus, recently at GEMaC, a compensation rate of 40% was achieved on (100) orientation.

Finally, (iii) a donor fraction (ratio of phosphorus atoms in donor positions to incorporated phosphorus concentration) that is close to 1 on (111) orientation [97] and equal to 0.91 on (100) orientation[80]. Thus, the improvement of the electrical activity of phosphorus confirms its position as the only substitutional site donor with low compensation in diamond.

The successful incorporation of arsenic according to the (111) orientation achieved at GEMaC is one of the avenues explored by researchers. However, despite improved crystalline quality compared to arsenic-doped layers on (111) orientation, no emission of bound excitons has been detected by cathodoluminescence, and the incorporation efficiency of this element is 6500 times lower on (100) orientation compared to (111) orientation[98]. Sulfur has also been studied as a potential donor on (100) orientation. Successful incorporation had been reported by Sakaguchi et al. (1999)[99] as a donor in diamond. However, electrical measurements by Kalish et al. (2000)[100] later reported that these samples were unintentionally doped with boron and showed p-type doping instead.

Nishitani-Gamo et al. (2000)[101] reported observations of n-type doping on (100) orientation, while Garrido et al. (2002)[102] observed no n-type doping except at 0.48 eV above the valence band attributed to complex formation due to the presence of sulfur.

Nakazawa et al. (2003) reported the same conclusion for activation energies of 0.5-0.75 eV[103]. The ambiguity surrounding the reported results and the dispersion of theoretical energy activation values (for sulfur and these complexes)[89, 104, 105] indicates that n-type doping with sulfur is still controversial.

### 1.7.1.2 P-type diamond

#### 1.7.1.2.1 On orientation (111)

On orientation (111), boron is the only p-type dopant that can be efficiently and reproducibly incorporated into diamond at sufficient concentrations for electronic device fabrication. However, growth on this orientation is prone to twinning and crystal defects[106], which further complicates the growth of thick high-quality layers and drastically reduces electronic properties. Additionally, high-quality substrates are scarce.

There is limited research on the growth of boron-doped layers on orientation (111), and available studies mainly focus on films with very low thickness ( $< 2\mu\text{m}$ ) and extremely slow growth rates [107-109]. However, some studies have shown the potential for superconductivity in diamond very heavily doped with boron [110, 111].

Boron incorporation is easier to incorporate in the (111) plane than in the (100) plane[112], and the doping concentration of obtained films varies widely (from  $10^{16}$  to  $10^{22}\text{cm}^{-3}$ )[113].

#### 1.7.1.2.2 On orientation (100)

P-type diamond is an important material for electronic applications, and boron is the most commonly used dopant for p-type doping in diamond. Boron doping has been successfully incorporated into thin films on the (100) orientation with doping ranges from  $10^{15}$  to  $10^{21}\text{cm}^{-3}$  by various teams [114, 115]. The aim of doping in diamond is to produce more charge carriers in the semiconductor in order to reduce the resistivity.

In the case of diamond, values of charge carriers lower than  $10^{19}\text{cm}^{-3}$  lead to a conduction dominated by the free holes which are thermally activated in the valence band. Higher doping concentrations induce variable-range jumps in conduction between the gap states leading to a metal-insulator transition above  $3 \times 10^{20}$  [B] atoms  $\text{cm}^{-3}$ [72, 110, 116, 117].

The resistivity of heavily doped diamond of a (100) orientation can be as low as  $10\text{ m}\Omega\cdot\text{cm}$  at room temperature [72, 118-120] which allows to think to the development of boron doped substrates for fabricating vertical components.

However, producing thick, heavily doped films to obtain a self-supporting layer by separating the CVD layer from the substrate is challenging and has only been accomplished by LSPM [121, 122] and some of these results are shown in Figure I.12.

The resulting doped substrates have high crystal quality and an extremely low compensation rate[123], which is essential for producing vertical unipolar power components [124].

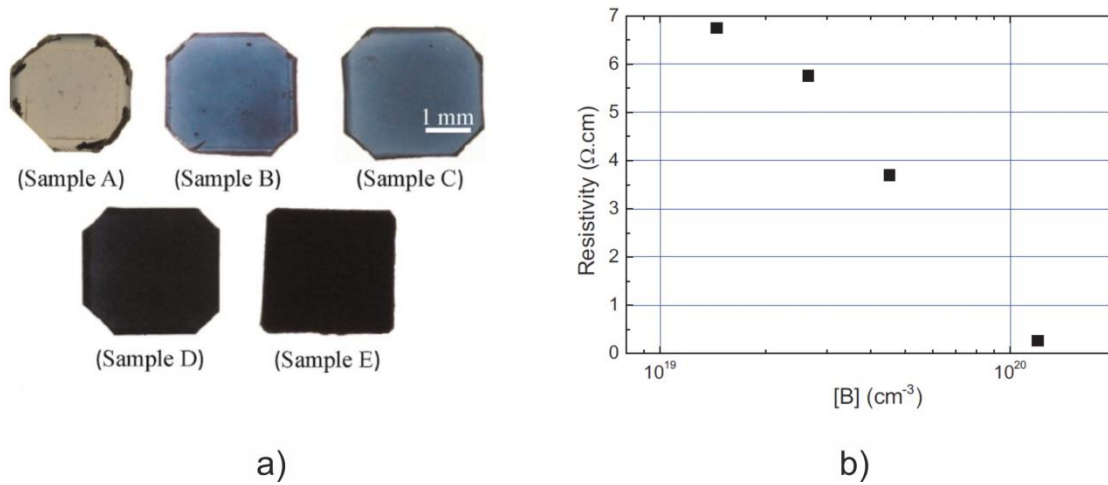


Figure I.12 – a) Optical pictures of the freestanding samples accomplished by LSPM and b) Evolution of the electrical resistivity measured by four probes technique as a function of boron concentration in the film.[125]

Efficient p-type doping in diamond is typically achieved by incorporating boron impurities during the growth. Nevertheless, another type of p-type doping can be obtained by hydrogenation of the surface of intrinsic diamond and exposure to air, a mechanism known as "transfer doping." However, this mechanism will not be discussed in this chapter because it leads only to surface conductivity which is not the subject of this work.

The development of the process for synthesizing heavily boron doped (100) thick films will be developed in more details in the chapter 4 of the manuscript.

### 1.7.2 Extended Defects: dislocations

Dislocations are known to lead to poor electrical properties limiting the use of diamond in power devices. For instance, dislocations can limit the mobility of charge carriers and modify the conduction paths which can cause the degradation and limiting the device performance, particularly under strong electric field conditions [126].

Dislocations in CVD diamond monocrystals can have two origins as illustrated in Figure I.13: (i) they can originate from the core of the HPHT substrate and propagate through the epitaxial CVD layer, known as threading dislocations (primary dislocations), and (ii) they can form at the HPHT-CVD interface due to the presence of surface defects (secondary dislocations).

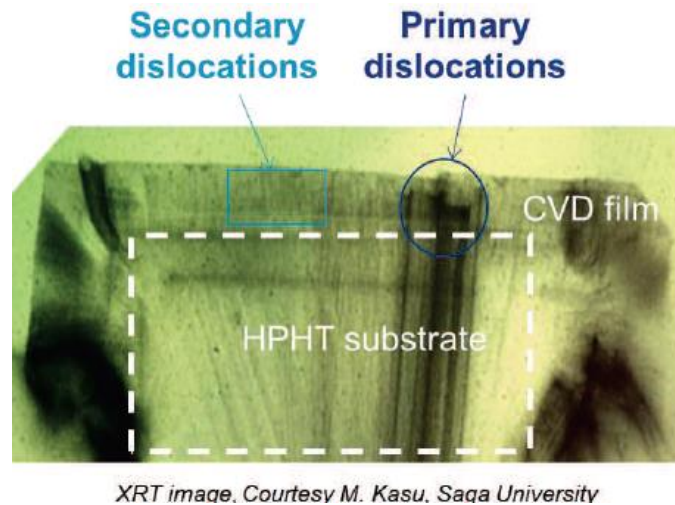


Figure 1.13 - X-ray section topography picture registered on a CVD diamond film. Primary dislocations correspond to the dislocation initially presents in the substrate and the secondary dislocations correspond to the dislocations initiated at the growth resuming.

Therefore, the quality of the HPHT diamond substrate and its surface state are crucial for limiting the density of dislocations present in the CVD layers [56, 127]. Dislocations represent a significant issue to the use of diamond in electronics and, as a result, numerous research endeavors have focused on addressing it. In the following subsection, we will discuss the progress made, particularly at LSPM, for overcoming these issues.

#### 1.7.2.1 Surface treatments before growth

The density of dislocations present in CVD films is systematically higher than that initially present in the HPHT substrate. This difference is attributed to the formation of new dislocations at the HPHT-CVD interface [128] due to the presence of surface defects.

Typically, the substrate is mechanically polished using a "scaife" system in order to obtain the lowest possible surface roughness. However, this polishing step damages the surface of the HPHT substrate and creates a strained layer of a few micrometers in thickness [129] that is responsible for the appearance of new dislocations in homoepitaxial CVD layers.

Thus, various surface treatments to remove the strained layer have been developed. They can be grouped into two categories:

- Dry etching:
  - By  $H_2/O_2$  plasma before growth under plasma conditions identical to those of growth [130].
  - By ECR oxygen plasma (Electron Cyclotron Resonance) [131];

- By RIE plasma (Reactive Ion Etching) [132];
- Wet etching:
  - In a mixture of molten potassium nitrate[133];
  - In a mixture of molten KCl and KOH at 1100°C[134].

At LSPM, the work of Alexandre Tallaire [51] and Ovidiu Brinza [57] has clearly shown that the use of H<sub>2</sub>/O<sub>2</sub> plasma pretreatment eliminates the strained layer as well as the polishing scratches and greatly improves surface morphology during the growth of thick films.

In these very strong etching conditions, an effective etching of the lateral faces of the substrate also occurs, relaxing the stresses present in the HPHT substrate preventing the rupture of the CVD crystal when the thickness exceeds a hundred of micrometers.

However, such a treatment induces the formation of deep etch pits on emerging defects [135] prone to the formation of new dislocations and the incorporation of impurities [127].

In this context, Achard et al. [136] reported the combined use of H<sub>2</sub>/O<sub>2</sub> plasma etching and inductively coupled plasma-reactive ion etching (ICP-RIE) or chemo-mechanical polishing (CMP). The sample preparation process is detailed in Figure I.14 (a).

The first two steps are identical for all three processes. The first step consists of H<sub>2</sub>/(2%)O<sub>2</sub> plasma etching for 1 hour at a microwave power/pressure of 3 kW/200 mbar and a temperature of 850°C.

The etching plasma is used to remove defects induced by polishing on the top surface and prepares the lateral faces. A thickness of 3 to 4 μm corresponding to the strained layer is etched. The second step is a conventional "scaife" polishing to obtain a smooth surface with a roughness of around 3 nm.

For sample A, low-pressure (0.4 Pa) ICP plasma etching is performed using an Ar:O<sub>2</sub> gas mixture optimized to obtain low anisotropy and low roughness. Plasma and polarization powers of 500 and 280 W, respectively, are used.

Regarding sample B, a 45-minute chemo-mechanical polishing is performed using an oxidizing agent (H<sub>2</sub>O<sub>2</sub>) deposited on a polishing disk without adding diamond powder.

The sample C undergoes no further treatment and is used as a reference. Finally, CVD growth is performed on all three samples to grow a 400  $\mu\text{m}$  thick layer (3 kW/200 mbar/850°C/4%  $\text{CH}_4$ ) and the result show that the combination of  $\text{H}_2/\text{O}_2$  plasma and ICP-RIE plasma or the combination of  $\text{H}_2/\text{O}_2$  plasma and CMP leads to a much lower dislocation density than for the reference sample.

The dislocation density is almost equivalent to the dislocations originating from the HPHT substrate. The latter are unfortunately independent of the surface treatments requiring the use of dislocation free substrates or the development of other techniques to block them during growth, as has been done for other semiconductors such as GaN.

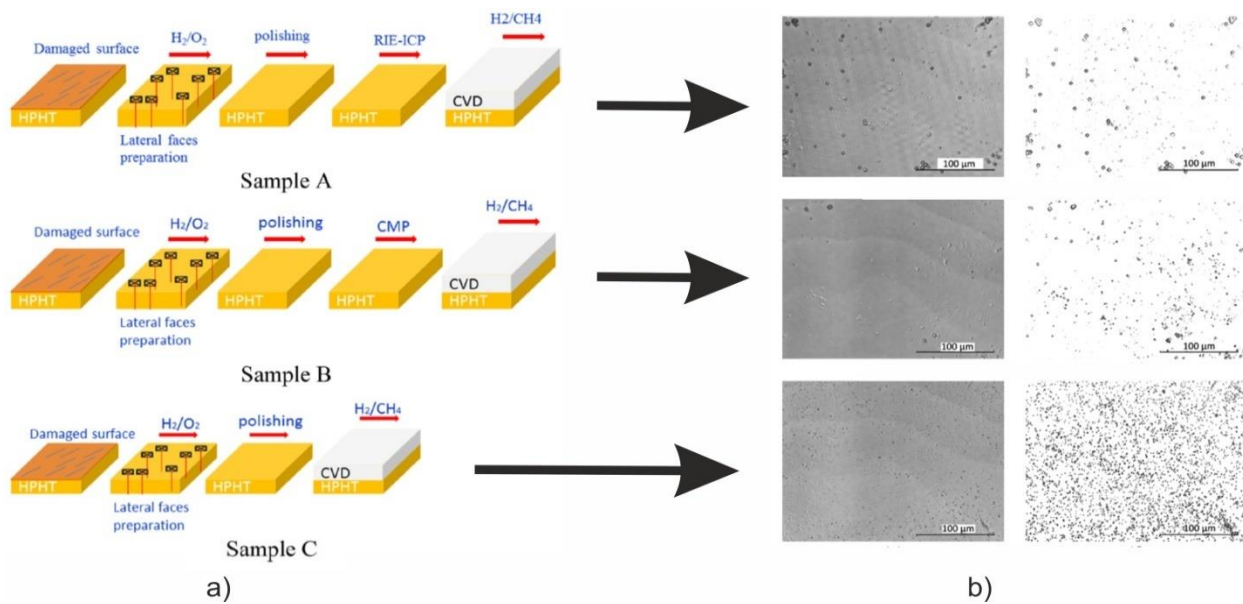


Figure I.14 - (a) Sample preparation process, (b) on the left, surface morphology of CVD layers after ICP plasma etching to reveal etch pits, and on the right, image processing to estimate dislocation density[136].

### 1.7.2.2 Low-Dislocation-Density Substrates

By applying appropriate surface treatments, it is then possible to suppress or at least to strongly limit secondary dislocations. It is then of prime interest to choose appropriate substrate with a low primary dislocation density which are known to affect the material properties[137].

Type IIa HPHT substrates are currently the best candidates for growing high-quality CVD layers. Sumiya et al. [138] reported the growth of crystals with high crystal quality through advanced HPHT process control. The use of an optimal growth temperature (1340-1350°C) allowed producing almost free-dislocation single crystals with (100) faces larger than 10 mm (see Figure I.15).



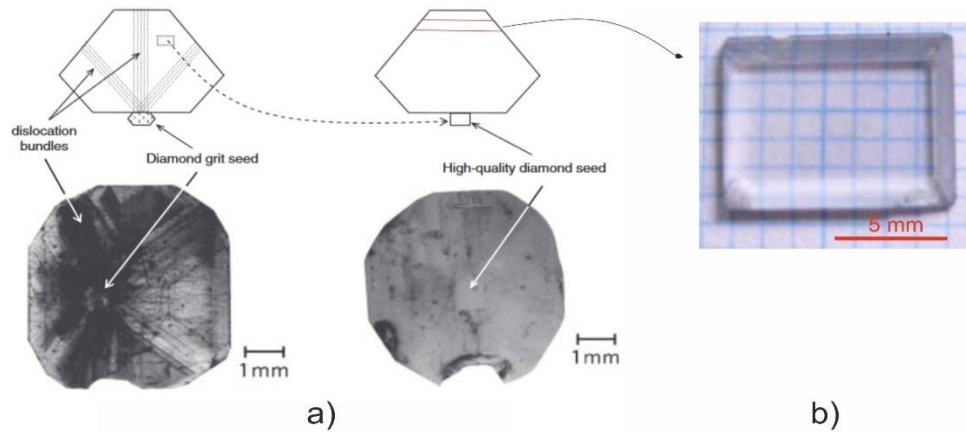


Figure I.15 - (a) X-ray topography image of Ila diamond crystals (100) obtained by HPHT growth from (left) a low-quality Ib seed crystal and (right) a high-quality Ila seed crystal cut from a defect-free zone, (b) High-quality Ila HPHT substrate with high crystalline quality ( $7.5 \times 6 \times 0.7 \text{ mm}^3$ ) obtained by cutting the high region of the single crystal that has the least crystalline face[138].

The photoluminescence imaging analysis conducted under UV excitation (depicted in Figure I.16(b)) reveals low fluorescence, which suggests high purity and low stress levels. However, the blue luminescence detected at the edges of the substrate indicates the presence of small amounts of nitrogen and boron[138].

Mokuno et al. [139] used this substrate for CVD growth, resulting in a high-quality CVD layer (Figure I.16(c)) even if significant stress at the periphery of the layer can be observed (see Figure I.16 (e)). Nevertheless, the Figure I.16(d) clearly shows that the dislocation density was extremely low, estimated to  $400 \text{ cm}^{-2}$  in a  $2.5 \times 2.3 \text{ mm}^2$  zone.

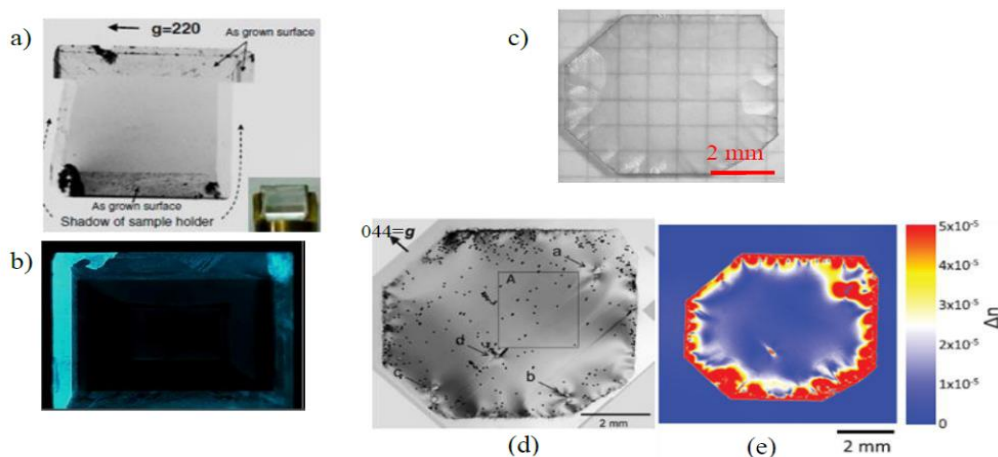


Figure I.16 - (a) X-ray transmission topography image of the Ila HPHT substrate, (b) DiamondView image of the Ila HPHT substrate [219]. (c) Photo of the self-supported layer obtained by CVD growth on the substrate of Figure I.21b (thickness:  $350 \mu\text{m}$ ), (d) X-ray topography image of the self-supported CVD layer showing the presence of a low density of dislocations and (e) Birefringence image of the self-supported CVD layer[139].

Thus, type IIa HPHT substrates with very low dislocation densities appear to be the ideal substrates for CVD growth if, of course, adequate surface preparation before the growth is used. However, their rarity and high cost require the development of techniques allowing reducing or at least limiting the propagation of threading dislocations using the more commonly type Ib (100) substrates.

In this aim, several growth strategies have been developed at LSPM in order to block or bent dislocation during the growth.

### 1.7.2.3 Dislocation blocking

This method has been developed by LSPM and is based on a selective masking by Platinum (Pt) nanoparticles of existing defects revealed at the surface of diamond substrates [56]. After  $H_2/O_2$  etching (step 1 of Figure I.17), a thin layer (30nm) of platinum is deposited by MOCVD (Metal-Organic Chemical Vapor Deposition) (step 2 of Figure I.17).

The choice of the metal used was based on low solubility with carbon (it should not react with diamond during growth), high melting point so as not to degrade during the MPACVD process, and low adhesion to the diamond surface.

This last parameter is necessary for step 3 of dewetting the metal film by thermal annealing at 600 to 900 °C under  $H_2$  plasma which allows the formation of Pt nanoparticles that come to position themselves in the etching figures (step 3 of Figure I.17)) just above emerging defects revealed by plasma etching. After this step, a CVD diamond growth is then performed (step 4 of Figure I.17) followed by an etching plasma allowing revealing dislocations. The procedure has been repeated 3 times and evaluated.

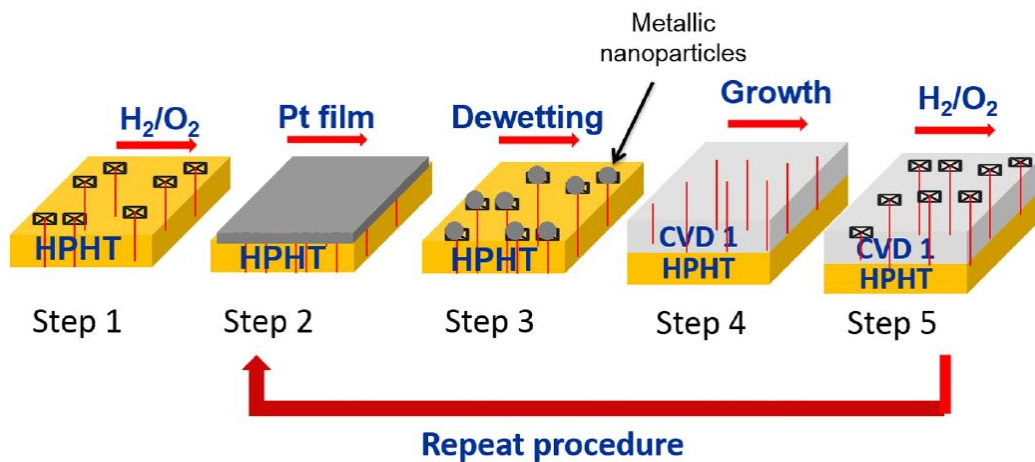


Figure I.17 - Method employed to reduce dislocation density that involves the selective masking of substrate defects using metallic nanoparticles [140]

As presented in Figure I.18, this technique allows dislocation density reduction, but unfortunately its effectiveness is limited as the density of dislocations is only reduced by a factor of 5 to 6. We are well below the performance achieved with GaN, but we should not forget that for the latter, the initial densities of dislocations are much higher, since they are around  $10^9 \text{ cm}^{-2}$  compared to only a few  $10^5$  to  $10^6 \text{ cm}^{-2}$  for diamond. The relative low efficiency of this approach encouraged us to develop other strategies.

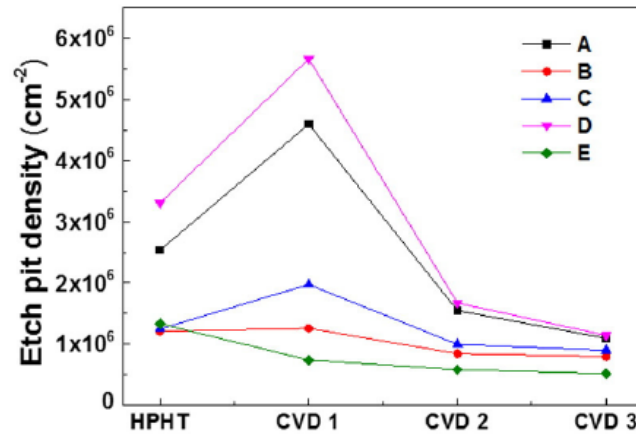


Figure I.18 - Density of etch pits after masking the HPHT substrate and 3 successive CVD growths on samples A to E [140]

#### 1.7.2.4 Dislocation reduction by Lateral growth over a macroscopic hole

The lateral growth or ELOG (Epitaxial Lateral Over-Growth) technique is a dislocation blocking technique applied in the case of GaN and which has been transposed to the diamond case by Alexandre Tallaire et al.[141] at LSPM. It involves the growth of diamond over a macroscopic hole pierced into the substrate presented in Figure I.19(a), which serves as a dislocation sink.

The growth is initiated from the edges of the hole and proceeds laterally across the surface to fill the hole (See Figure I.19(b)). This technique has been shown to reduce the dislocation density in diamond up to two orders of magnitude and values as low as  $10^3 \text{ cm}^{-2}$  have been obtained.

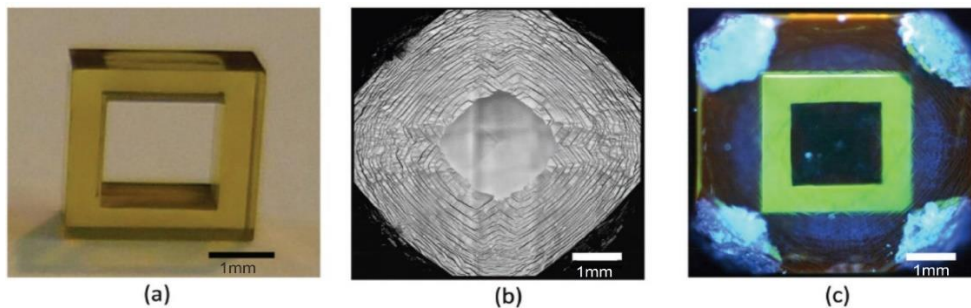


Figure I.19 - Thick CVD diamond layer grown on a pierced HPHT diamond substrate. a) Optical image of the substrate, b) laser microscope, and c) UV photoluminescence images of the sample after CVD growth[141]

This is a significant improvement over other techniques that have already been used to reduce dislocation density in diamond [142] and it opens up new possibilities for improving the quality of diamond substrates.

In particular, this technique has been extended to heteroepitaxial diamond material which presents the advantage of larger surface than single crystal diamond but the drawback of dislocation density larger than  $10^7 \text{ cm}^{-2}$  as previously mentioned in this chapter. For this purpose, a hole array, presented in Figure I.20, having lateral dimension of  $500 \times 500 \mu\text{m}^2$  with a periodicity of 2 mm have been pierced by laser into a commercial heteroepitaxial diamond substrate supplied by Audiatic.

After an optimization of the growth parameters in order to promote lateral growth conditions, all the holes can be filled allowing recovering a quasi-single crystal with a size similar to the initial one as illustrated on Figure I.21 (a)[143].

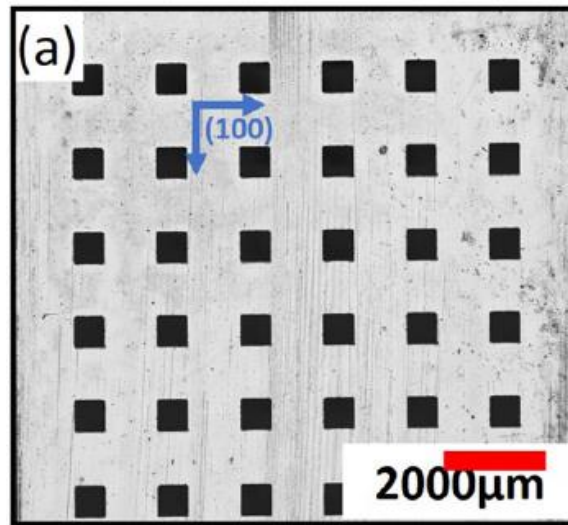


Figure I.20 - Confocal Laser Scanning Microscopy (CLSM) image of the  $500 \times 500 \mu\text{m}^2$  laser-pierced hole array[143]

The efficiency of the growth strategy was evaluated by comparing the dislocation density revealed by  $\text{H}_2/\text{O}_2$  plasma etching and their distribution on different areas of the sample, in particular above and between the initial holes (see Figure I.21(a) and (b)).

In the part of the sample where the holes have been filled, a dislocation density as low as  $10^5 \text{ cm}^{-2}$  have been estimated which is one of the lowest reported in the literature[144].

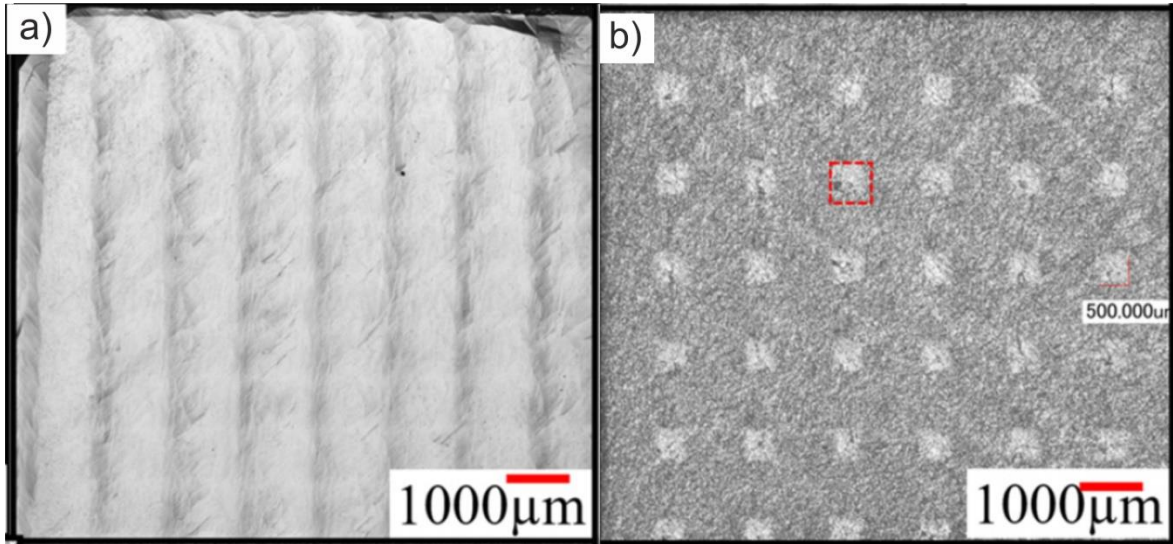


Figure I.21 - (a) Confocal Laser Scanning Microscopy (CLSM) images of the sample after a 600  $\mu\text{m}$  overgrown diamond layer leading to a complete disappearance of the hole array. (b) CLSM image after plasma etching to reveal the dislocation pattern.[143]

Further studies were developed in the framework of this thesis using this technique and they will be presented in chapter 4 with the aim of reducing dislocation density in boron doped diamond.

## 1.8 Electronic applications

The increasingly constraints in power electronics (high voltage, high temperature, high frequency) and the high integration density lead to significant thermal management problems.

In addition, the desire to reduce  $\text{CO}_2$  emissions into the atmosphere for environmental reasons by decreasing the use of fossil fuels in favor of renewable energies such as wind or solar, which require, among other things, the reorganization of energy distribution networks, imposes the development of more efficient switches based on the use of materials with large bandgap capable of withstanding higher voltages and current densities.

Diamond-based devices are promising candidates due to the exceptional characteristics of this material. The possible applications depending on the current and operating voltage as well as the corresponding devices for high-power applications are summarized in Figure I.22.

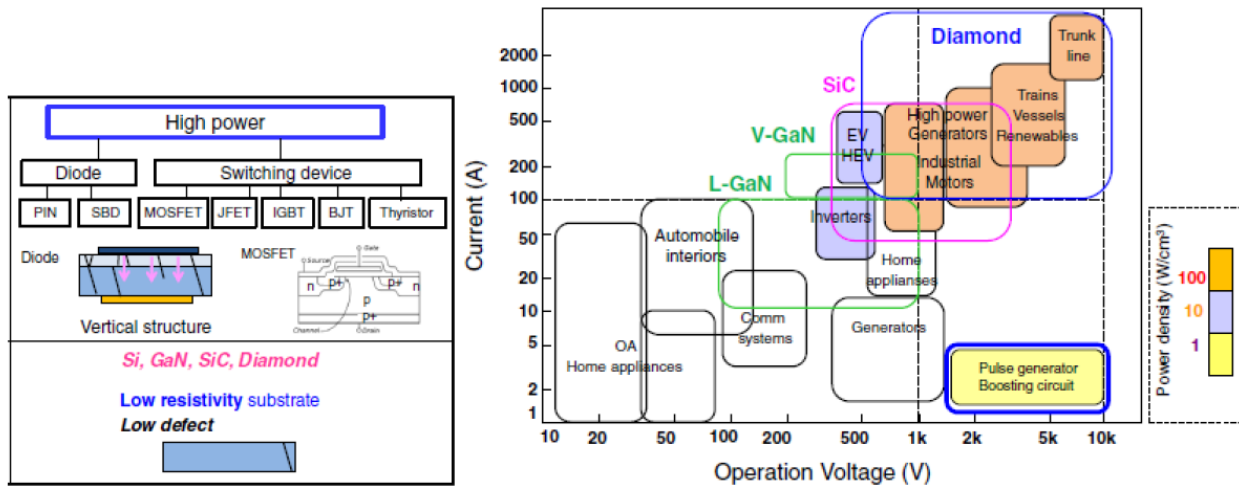


Figure 1.22 - On the left, devices corresponding to high power applications, on the right, possible applications depending on the current and voltage[143]

In this highly competitive and constantly evolving context, my research work aimed to develop processes for producing heavily boron-doped single-crystal diamond substrates with the lowest dislocation density possible to enable the development of vertical components and more specifically, vertical Schottky diodes, which constitutes a building block for more sophisticated power electronic components.

These works were carried out and financed by the ANR MoveToDiam project. It brings together several academic partners (LAAS, GEMaC, Ampère and LSPM) and industrial partners (IBS) and thanks to CONAcYt funding.

## 1.9 Conclusion

This chapter highlights the challenges faced in utilizing diamond for various applications even if its properties are exceptional. The key to take advantage of these properties, particularly for power electronic applications lies in the ability to synthesize high-quality thick diamond material having in mind the dislocation reduction while controlling the dopant concentration. During my thesis, these objectives were at the forefront of my research.

In this chapter, we firstly introduced diamond and its exceptional properties, followed by a discussion of the various methods used for diamond synthesis and the issues encountered during the growth of monocrystalline films. We emphasized the importance of the initial substrate quality, which partly determines the quality of homoepitaxial diamond films.

We then delved into the concept of diamond doping and focused on p-type boron doping on (100) orientation. The improvement of p-type diamond growth on (100) orientation is crucial in developing a technology for vertical bipolar diamond-based components.

The control of high-quality single-crystal growth is intimately connected with extended defects and in particular dislocations. In the last part of this chapter, we revisited the strong impact of the substrate in producing low-dislocation diamond layers, paying special attention to those emerging from the substrate's core.

We outlined pre-growth surface treatments, techniques for masking and blocking dislocations, and culminated with an overview of the overgrowth techniques allowing reducing dislocation density, which constituted a large part of my thesis. Finally, we summarized the possible benefits of diamond in power electronics.

## 1.10 References

1. Pernot, J. and S. Koizumi, *Electron mobility in phosphorous doped {111} homoepitaxial diamond*. Applied Physics Letters, 2008. **93**: p. 052105-052105.
2. Pernot, J., et al., *Hall hole mobility in boron-doped homoepitaxial diamond*. Physical Review B, 2010. **81**(20): p. 205203.
3. Dankerl, M., et al., *Diamond Transistor Array for Extracellular Recording From Electrogenic Cells*. Advanced Functional Materials, 2009. **19**(18): p. 2915-2923.
4. Zhang, Q., et al., *Fluorescent PLLA-nanodiamond composites for bone tissue engineering*. Biomaterials, 2011. **32**(1): p. 87-94.
5. Mochalin, V.N., et al., *The properties and applications of nanodiamonds*. Nature Nanotechnology, 2012. **7**(1): p. 11-23.
6. <https://www.e6.com/>. Elementsix website].
7. Von-bolton, W., *The segregation of carbon in diamond form*. Elektrochemie, 1911. **17**(8): p. 971-972.
8. Eversole, W.G., *Synthesis of diamond* 1958: US.
9. Bundy, F.P., et al., *Man-Made Diamonds*. Nature, 1955. **176**(4471): p. 51-55.
10. Bundy, F.P., *The P, T phase and reaction diagram for elemental carbon, 1979*. Journal of Geophysical Research: Solid Earth, 1980. **85**(B12): p. 6930-6936.
11. Liu, W.Q., et al., *Effects of additive Al on the HPHT diamond synthesis in an Fe–Mn–C system*. Diamond and Related Materials, 2007. **16**(8): p. 1486-1489.
12. laboratories, i.d.; Available from: [http://www.diamondlab.org/80-hpht\\_synthesis.htm](http://www.diamondlab.org/80-hpht_synthesis.htm).
13. H. Sumiya, K.H., K. Tamasaku, *HPHT synthesis and crystalline quality of large high-quality (001) and (111) diamond crystals*. Diam. Relat. Mat, 2015. **58**: p. pp 221–225.
14. B. Deljanin, M.A., A. Peretti, M. Åström, *NDT breaking the 10ct barrier: World Record faceted and gem-quality diamonds investigated*. Contributions to Gemology, 2015. **15**.
15. Spitsyn, B.V., *Origin and Evolution of the Science and Technology of Diamond Synthesis in the USSR*, in *Diamond and Diamond-like Films and Coatings*, R.E. Clausing, et al., Editors. 1991, Springer US: Boston, MA. p. 855-873.
16. Spitsyn, B.V., L.L. Bouilov, and B.V. Derjaguin, *Vapor growth of diamond on diamond and other surfaces*. Journal of Crystal Growth, 1981. **52**: p. 219-226.
17. Builov, S.B.V.a.L.L., *The growth of diamond and diamond like films from a gaz phase*. Proceeding of the Diamond and diamond-like materials synthesis, 1988. **Extended abstract, M.R.S**: p. p. 3-14.
18. B.V., S., *Diamond films : Synthesis, properties and some fields of application*. Proceeding of the Science and Technology of New Diamond, Tokyo, KTK Scientific Publishers, 1990: p. p. 1 - 7.
19. Spitsyn, B.V., *Chemical crystallization of diamond from the activated vapor phase*. Journal of Crystal Growth, 1990. **99**(1, Part 2): p. 1162-1167.
20. Clausing R.E., e.a., *Clausing R.E., et al., Electron microscopy of the growth features and crystal structures of filament assisted CVD diamond films*. Surface and Coatings Technology, 1989: p. p. 199-210.
21. Kamo M., e.a., *Diamond synthesis from gas phase in microwave plasma*. Journal of Crystal Growth 62, 1986: p. p. 642-644.
22. J. Achard, F.S., A. Tallaire, X. Bonnin, G. Lombardi, K. Hassouni, A. Gicquel, *High quality MPACVD diamond single crystal growth: high microwave power density regime*. J. Phys. D, 2007. **40**: p. pp 6175-6188



23. Tallaire, A., et al., *Growth of large size diamond single crystals by plasma assisted chemical vapour deposition: Recent achievements and remaining challenges*. Comptes Rendus Physique, 2013. **14**(2): p. 169-184.
24. Gicquel A., e.a., *CVD diamond films: from growth to applications*. Current Applied Physics 1 (6) 2001, 2001: p. p. 479-496.
25. Gicquel A., e.a., *Validation of actinometry for estimating relative hydrogen atom densities and electron energy evolution in plasma assisted diamond deposition reactors*. Journal of Applied Physics 83 (12), 1998: p. p. 7504-7521.
26. Hassouni K., T.A.G., and A. Gicquel,, *Self-consistent microwave field and plasma discharge simulations for a moderate pressure hydrogen discharge reactor*. Journal of Applied Physics 86 (1), 1999: p. p. 134-151.
27. Hassouni K., F.S.a.A.G., *Modelling of diamond deposition microwave cavity generated plasmas*. Journal of Physics D-Applied Physics 43 (15), 2010: p. p. 153001.
28. Gicquel A., e.a., *Ground state and excited state H-atom temperatures in a microwave plasma diamond deposition reactor*. Journal de physique III 6, 1996: p. p. 1167-1180.
29. Hassouni K., e.a., *Modeling of H<sub>2</sub> and H<sub>2</sub>/CH<sub>4</sub> Moderate-Pressure Microwave Plasma Used for Diamond Deposition*. Plasma Chemistry and Plasma Processing 18 (3), 1998: p. p. 325-362.
30. Uzan-Saguy C., e.a., *Formation of delta-doped, buried conducting layers in diamond, by high-energy, B-ion implantation,*. Diamond and Related Materials 7 (10) 1998, 1998: p. p. 1429-1432.
31. Kalish R., e.a., *Nitrogen doping of diamond by ion implantation*. Diamond and Related Materials 6, 1997: p. p. 516-520.
32. Achard J., e.a., *High quality MPACVD diamond single crystal growth: high microwave power density regime*. Journal of Physics D: Applied Physics 40 (20), 2007: p. p. 6175-6188.
33. Achard J., e.a., *The control of growth parameters in the synthesis of high-quality single crystalline diamond by CVD*. Journal of Crystal Growth 284 (3-4), 2005: p. p. 396-405.
34. Cao G.Z., e.a., *Growth of {100} textured diamond films by the addition of nitrogen*. Journal of Applied Physics 79 (3), 1996: p. p. 1357-64.
35. Jin S. and T.D. Moustakas, *Effect on nitrogen on the growth of diamond films,*. Applied Physics Letters 65 (4), 1994: p. p. 403-405.
36. Tallaire A., e.a., *Characterisation of high-quality thick single-crystal diamond grown by CVD with a low nitrogen addition,*. Diamond and Related Materials 15 (10), 2006: p. p. 1700-1707.
37. van der Drift A., *Evolutionary selection, a principle governing growth orientation in vapour-deposited layers*. Philips Research Reports., 1967: p. p. 267-288.
38. Vaissière N., *Synthèse de films de diamant de haute qualité cristalline pour la réalisation de dosimètres pour la radiothérapie,*. École normale supérieure de Cachan-ENS Cachan,, 2014.
39. Mallik A.K., N.D., and S. Chakraborty, *Characterizations of microwave plasma CVD grown polycrystalline diamond coatings for advanced technological applications*. Processing and Application of Ceramics 8 (2), 2014: p. p. 69-80.
40. Williams, O.A., *Nanocrystalline diamond*. Diamond and Related Materials, 2011. **20**(5): p. 621-640.
41. Gruen, D.M., *NANOCRYSTALLINE DIAMOND FILMS*. Annual Review of Materials Science, 1999. **29**(1): p. 211-259.
42. Baudrillart, B., et al., *Microstructure and growth kinetics of nanocrystalline diamond films deposited in large area/low temperature distributed antenna array microwave-plasma reactor*. physica status solidi (a), 2015. **212**(11): p. 2611-2615.
43. Williams, O.A., et al., *Growth, electronic properties and applications of nanodiamond*. Diamond and Related Materials, 2008. **17**(7): p. 1080-1088.

44. Lions, M., et al., *Ultra-thin nanocrystalline diamond films (<100 nm) with high electrical resistivity*. physica status solidi (RRL) – Rapid Research Letters, 2009. **3**(6): p. 205-207.
45. Stoner, B.R., et al., *Heteroepitaxial Nucleation of Diamond*. MRS Online Proceedings Library, 1995. **416**(1): p. 69-73.
46. Kimura, Y., et al., *Analysis of the correlation between in-situ and ex-situ observations of the initial stages of growth of heteroepitaxial diamond on Ir(001)/MgO(001)*. Journal of Crystal Growth, 2022. **595**: p. 126807.
47. Sawabe, A., et al., *Interface between CVD diamond and iridium films*. Surface Science, 2000. **467**(1): p. L845-L849.
48. Stehl, C., et al., *Efficiency of dislocation density reduction during heteroepitaxial growth of diamond for detector applications*. Applied Physics Letters, 2013. **103**: p. 151905-151905.
49. Achard, J., et al., *The use of CVD diamond for high-power switching using electron beam excitation*. Diamond and Related Materials, 2004. **13**(4-8): p. 876-880.
50. Teraji, T., S. Mitani, and T. Ito., *High rate growth and luminescence properties of highquality homoepitaxial diamond (100) films*. physica status solidi (a),, 2003: p. p. 395-406.
51. Teraji, T., et al.,, *Transport properties of electron-beam and photo excited carriers in high-quality single-crystalline chemical-vapor-deposition diamond films*. Journal of Applied Physics,, 2004: p. p. 7300-7305.
52. Teraji, T., et al.,, *High-quality homoepitaxial diamond (100) films grown under high-rate growth condition*. Diamond and Related Materials,, 2005: p. p. 1747-1752.
53. Yamamoto, M., T. Teraji, and T. Ito, *Improvement in the crystalline quality of homoepitaxial diamond films by oxygen plasma etching of mirror-polished diamond substrates*. Journal of Crystal Growth, 2005: p. p. 130-136.
54. Tavares, C., S. Koizumi, and H. Kanda, *Effects of RIE treatments for {111} diamond substrates on the growth of P-doped diamond thin films*. physica status solidi (a),, 2005: p. p. 2129-2133.
55. Brinza O., *Stratégies pour la croissance de cristaux de diamant par CVD assisté par plasma micro-onde*,, 2009, Université Paris Nord - Paris XIII.
56. Tallaire, A., et al., *Thick CVD diamond films grown on high-quality type IIa HPHT diamond substrates from New Diamond Technology*. Diamond and Related Materials, 2017. **77**: p. 146-152.
57. Tallaire, A. and A. Gicquel, *Croissance de monocristaux de diamant par dépôt chimique en phase vapeur pour des applications en électronique de puissance*. 2005.
58. Findeling-Dufour, C., *De la mosaïque au monocristal centimétrique de diamant : étude d'un procédé de croissance homoépitaxiale par plasma micro-onde*, 1997, Université Paris 13.
59. Issaoui, R., *Elaboration de films épais de diamant monocristallin dopé*, 2011, Université Paris 13.
60. Langer, J., et al., *Manipulation of the In Situ Nitrogen-Vacancy Doping Efficiency in CVD-Grown Diamond*. physica status solidi (a), 2022. **219**(10): p. 2100756.
61. Schwander, M. and F. Vollertsen, *In situ doping of diamond coatings with silicon, aluminum and titanium through a modified laser-based CVD process*. Diamond and Related Materials, 2014. **41**: p. 41-48.
62. Prins, J.F., *Activation of boron-dopant atoms in ion-implanted diamonds*. Physical Review B, 1988. **38**(8): p. 5576-5584.
63. Ueda, K., M. Kasu, and T. Makimoto, *High-pressure and high-temperature annealing as an activation method for ion-implanted dopants in diamond*. Applied Physics Letters, 2007. **90**(12): p. 122102.
64. Tsubouchi, N. and M. Ogura, *Enhancement of Dopant Activation in B-Implanted Diamond by High-Temperature Annealing*. Japanese Journal of Applied Physics, 2008. **47**: p. 7047-7051.

65. Ratnikova, A.K., et al., *Homoepitaxial single crystal diamond grown on natural diamond seeds (type IIa) with boron-implanted layer demonstrating the highest mobility of 1150cm<sup>2</sup>/Vs at 300K for ion-implanted diamond*. *Diamond and Related Materials*, 2011. **20**(8): p. 1243-1245.
66. Johan, F.P., *Ion implantation of diamond for electronic applications*. *Semiconductor Science and Technology*, 2003. **18**(3): p. S27.
67. Pinault-Thaury, M.-A., et al., *Electrical activity of (100) n-type diamond with full donor site incorporation of phosphorus*. *physica status solidi (a)*, 2015. **212**(11): p. 2454-2459.
68. Yamanaka, S., et al., *Junction properties of homoepitaxial diamond films grown by step-flow mode*. *Journal of Applied Physics*, 1998. **84**(11): p. 6095-6099.
69. Katagiri, M., et al., *Lightly phosphorus-doped homoepitaxial diamond films grown by chemical vapor deposition*. *Applied Physics Letters*, 2004. **85**(26): p. 6365-6367.
70. Lagrange, J.P., A. Deneuve, and E. Gheeraert, *Activation energy in low compensated homoepitaxial boron-doped diamond films* Paper presented at the *Diamond 1997 Conference*. *Diamond and Related Materials*, 1998. **7**(9): p. 1390-1393.
71. Boussadi, A., et al., *Thick heavily boron doped CVD diamond films homoepitaxially grown on (111)-oriented substrates*. *Diamond and Related Materials*, 2017. **79**: p. 108-111.
72. Ri, S.-G., et al., *Growth and characterization of boron-doped (111) CVD homoepitaxial diamond films*. *Journal of Crystal Growth*, 2007. **299**(2): p. 235-242.
73. Koizumi, S., et al., *Growth and characterization of phosphorous doped {111} homoepitaxial diamond thin films*. *Applied Physics Letters*, 1997. **71**(8): p. 1065-1067.
74. Makino, T., et al., *Strong Excitonic Emission from (001)-Oriented Diamond<i>P</i>-<i>N</i> Junction*. *Japanese Journal of Applied Physics*, 2005. **44**(No. 38): p. L1190-L1192.
75. Kato, H., S. Yamasaki, and H. Okushi, *Growth and characterization of phosphorus-doped diamond using organophosphorus gases*. *physica status solidi (a)*, 2005. **202**: p. 2122-2128.
76. Michl, J., et al., *Perfect alignment and preferential orientation of nitrogen-vacancy centers during chemical vapor deposition diamond growth on (111) surfaces*. *Applied Physics Letters*, 2014. **104**(10): p. 102407.
77. Neu, E., et al., *Photonic nano-structures on (111)-oriented diamond*. *Applied Physics Letters*, 2014. **104**(15): p. 153108.
78. Pinault-Thaury, M.-A., et al., *High fraction of substitutional phosphorus in a (100) diamond epilayer with low surface roughness*. *Applied Physics Letters*, 2012. **100**.
79. Pinault-Thaury, M.-A., et al., *The n-type doping of diamond: Present status and pending questions*. *Physica B: Condensed Matter*, 2007. **401**: p. 51-56.
80. Pinault-Thaury, M.-A., et al., *N-Type CVD diamond: Epitaxy and doping*. *Materials Science and Engineering B-advanced Functional Solid-state Materials*, 2011. **176**: p. 1401-1408.
81. Nesládek, M., et al., *N-type P-doped polycrystalline diamond*. *physica status solidi (a)*, 2003. **199**(1): p. 77-81.
82. Gheeraert, E., et al., *n-Type Doping of Diamond by Sulfur and Phosphorus*. *Diamond and Related Materials*, 2002. **11**: p. 289-295.
83. Kociniewski, T., et al., *n-type CVD diamond doped with phosphorus using the MOCVD technology for dopant incorporation*. *physica status solidi (a)*, 2006. **203**(12): p. 3136-3141.
84. Grotjohn, T.A., et al., *Heavy phosphorus doping by epitaxial growth on the (111) diamond surface*. *Diamond and Related Materials*, 2014. **44**: p. 129-133.
85. Frangieh, G., et al., *Incorporation of arsenic in diamond grown by chemical vapor deposition*. *physica status solidi (a)*, 2008. **205**(9): p. 2207-2210.
86. Barjon, J., F. Jomard, and S. Morata, *Arsenic-bound excitons in diamond*. *Physical Review B*, 2014. **89**(4): p. 045201.

87. Miyazaki, T. and H. Okushi, *A theoretical study of a sulfur impurity in diamond*. Diamond and Related Materials, 2001. **10**: p. 449-452.
88. Nishitani-Gamo, M., et al., *Homoepitaxial diamond growth with sulfur-doping by microwave plasma-assisted chemical vapor deposition*. Thin Solid Films, 2001. **382**: p. 113-123.
89. S.A. Kajihara, A.A., and J. Bernholc, *Impurity incorporation and doping of diamond*. Phys. B Cond. Mater, 1993. **185**: p. 144.
90. Kato, H., S. Yamasaki, and H. Okushi, *n-type doping of (001)-oriented single-crystalline diamond by phosphorus*. Applied Physics Letters, 2005. **86**(22): p. 222111.
91. Kato, H., et al., *Electrical activity of doped phosphorus atoms in (001) n-type diamond*. physica status solidi (a), 2008. **205**: p. 2195-2199.
92. Nakai, T., O. Maida, and T. Ito, *Characterization of phosphorus-doped homoepitaxial (100) diamond films grown using high-power-density MWPCVD method with a conventional quartz-tube chamber*. Applied Surface Science, 2008. **254**(19): p. 6281-6284.
93. Frangieh, G., et al., *Phosphorus incorporation and activity in (100)-oriented homoepitaxial diamond layers*. physica status solidi (a), 2009. **206**(9): p. 2000-2003.
94. Pinault-Thaury, M.-A., et al., *Phosphorus donor incorporation in (1 0 0) homoepitaxial diamond: Role of the lateral growth*. Journal of Crystal Growth - J CRYST GROWTH, 2011. **335**: p. 31-36.
95. Hasegawa, M., T. Teraji, and S. Koizumi, *Lattice location of phosphorus in n-type homoepitaxial diamond films grown by chemical-vapor deposition*. Applied Physics Letters, 2001. **79**(19): p. 3068-3070.
96. Pinault-Thaury, M.A., et al., *n-Type CVD diamond: Epitaxy and doping*. Materials Science and Engineering: B, 2011. **176**(17): p. 1401-1408.
97. Sakaguchi, I., et al., *Sulfur: A donor dopant for n-type diamond semiconductors*. Physical Review B, 1999. **60**(4): p. R2139-R2141.
98. Kalish, R., et al., *Is sulfur a donor in diamond?* Applied Physics Letters, 2000. **76**(6): p. 757-759.
99. Nishitani-Gamo, M., et al., *Sulfur-doped homoepitaxial (001) diamond with n-type semiconductive properties*. Diamond and Related Materials, 2000. **9**(3): p. 941-947.
100. Garrido, J.A., et al., *Electrical and optical measurements of CVD diamond doped with sulfur*. Physical Review B, 2002. **65**(16): p. 165409.
101. Nakazawa, K., et al., *Cathodoluminescence and Hall-effect measurements in sulfur-doped chemical-vapor-deposited diamond*. Applied Physics Letters, 2003. **82**(13): p. 2074-2076.
102. Zhou, H., et al., *Quantum Chemical Calculations of Sulfur Doping Reactions in Diamond CVD*. Japanese Journal of Applied Physics, 2001. **40**(4S): p. 2830.
103. Katayama-Yoshida, H., et al., *Codoping method for the fabrication of low-resistivity wide band-gap semiconductors in p-type GaN, p-type AlN and n-type diamond: prediction versus experiment*. Journal of Physics: Condensed Matter, 2001. **13**(40): p. 8901.
104. Kasu, M., et al., *Formation of stacking faults containing microtwins in (111) chemical-vapor-deposited diamond homoepitaxial layers*. Applied Physics Letters, 2003. **83**(17): p. 3465-3467.
105. Lazea, A., et al., *High quality p-type chemical vapor deposited {111}-oriented diamonds: Growth and fabrication of related electrical devices*. physica status solidi (a), 2012. **209**(10): p. 1978-1981.
106. Mermoux, M., et al., *Raman characterization of boron-doped {111} homoepitaxial diamond layers*. Diamond and Related Materials, 2006. **15**(4): p. 572-576.
107. Sato, K., et al., *Fabrication of diamond lateral p-n junction diodes on (111) substrates*. physica status solidi (a), 2015. **212**(11): p. 2548-2552.
108. Ekimov, E., et al., *Superconductivity in Diamond*. Nature, 2004. **428**: p. 542-5.
109. Klein, T., et al., *Metal-insulator transition and superconductivity in boron-doped diamond*. Physical Review B, 2007. **75**(16): p. 165313.

110. Ushizawa, K., et al., *Boron concentration dependence of Raman spectra on {100} and {111} facets of B-doped CVD diamond*. *Diamond and Related Materials*, 1998: p. p. 1719-1722.
111. Ghodbane, S., F. Omnès, and C. Agnès, *A cathodoluminescence study of boron doped {111}-homoepitaxial diamond films*. *Diamond and Related Materials*, 2010. **19**(4): p. 273-278.
112. Deneuille, A., et al., *Highly and heavily boron doped diamond films*. *Diamond and Related Materials*, 2007. **16**(4): p. 915-920.
113. Demlow, S.N., R. Rechenberg, and T. Grotjohn, *The effect of substrate temperature and growth rate on the doping efficiency of single crystal boron doped diamond*. *Diamond and Related Materials*, 2014. **49**: p. 19-24.
114. Yokoya, T., et al., *Origin of the metallic properties of heavily boron-doped superconducting diamond*. *Nature*, 2005. **438**(7068): p. 647-650.
115. Bustarret, E., *Superconducting diamond: an introduction*. *physica status solidi (a)*, 2008. **205**(5): p. 997-1008.
116. Tokuda, N., et al., *Hillock-Free Heavily Boron-Doped Homoepitaxial Diamond Films on Misoriented (001) Substrates*. *Japanese Journal of Applied Physics*, 2007. **46**(4A): p. 1469-1470.
117. Tokuda, N., et al., *Hillock-Free Heavily Boron-Doped Homoepitaxial Diamond Films on Misoriented (001) Substrates*. *Japanese Journal of Applied Physics*, 2007. **46**: p. 1469-1470.
118. Tokuda, N., et al., *Surface roughening of diamond (001) films during homoepitaxial growth in heavy boron doping*. *Diamond and Related Materials*, 2007. **16**(4): p. 767-770.
119. Achard, J., et al., *Thick boron doped diamond single crystals for high power electronics*. *Diamond and Related Materials*, 2011. **20**(2): p. 145-152.
120. Issaoui, R., et al., *Growth of thick heavily boron-doped diamond single crystals: Effect of microwave power density*. *Applied Physics Letters*, 2010. **97**(18): p. 182101.
121. Barjon, J., et al., *Homoepitaxial boron-doped diamond with very low compensation*. *physica status solidi (a)*, 2012. **209**(9): p. 1750-1753.
122. Monflier, R., et al., *Diamond Schottky diodes operating at 473 K*. *EPE Journal*, 2017. **27**(3): p. 118-124.
123. Achard, J., et al., *Freestanding CVD boron doped diamond single crystals: A substrate for vertical power electronic devices?* *physica status solidi (a)*, 2012. **209**(9): p. 1651-1658.
124. Umezawa, H., Y. Kato, and S.-i. Shikata, *1  $\Omega$  On-Resistance Diamond Vertical-Schottky Barrier Diode Operated at 250 °C*. *Applied Physics Express*, 2013. **6**(1): p. 011302.
125. Tallaire, A., et al., *Dislocations and impurities introduced from etch-pits at the epitaxial growth resumption of diamond*. *Diamond and Related Materials*, 2011. **20**(7): p. 875-881.
126. Martineau, P.M., et al., *High crystalline quality single crystal chemical vapour deposition diamond*. *Journal of Physics: Condensed Matter*, 2009. **21**(36): p. 364205.
127. Volpe P.-N., e.a., *Defect analysis and excitons diffusion in undoped homoepitaxial diamond films after polishing and oxygen plasma etching*. *Diamond and Related Materials* **18** (10), 2009: p. p. 1205-1210.
128. Achard, J., et al., *Identification of etch-pit crystallographic faces induced on diamond surface by H<sub>2</sub>/O<sub>2</sub> etching plasma treatment*. *physica status solidi (a)*, 2009. **206**(9): p. 1949-1954.
129. Bernard, M., et al., *Electron cyclotron resonance oxygen plasma etching of diamond*. *Diamond and Related Materials*, 2004. **13**(2): p. 287-291.
130. Lee, C.L., et al., *Etching and micro-optics fabrication in diamond using chlorine-based inductively-coupled plasma*. *Diamond and Related Materials*, 2008. **17**(7): p. 1292-1296.
131. de Theije, F., et al., *Oxidative etching of diamond*. *Diamond and Related Materials*, 2000. **9**: p. 929-934.

132. Yao, Y., et al., *Fast removal of surface damage layer from single crystal diamond by using chemical etching in molten KCl+KOH solution*. *Diamond and Related Materials*, 2016. **63**: p. 86-90.
133. Ichikawa, K., et al., *Dislocation in heteroepitaxial diamond visualized by hydrogen plasma etching*. *Thin Solid Films*, 2016. **600**: p. 142-145.
134. Achard, J., et al., *Improvement of dislocation density in thick CVD single crystal diamond films by coupling H<sub>2</sub>/O<sub>2</sub> plasma etching and chemo-mechanical or ICP treatment of HPHT substrates*. *physica status solidi (a)*, 2014. **211**(10): p. 2264-2267.
135. P.M. Martineau, S.C.L., A.J. Taylor, S.J. Quinn, D.J. Evans, M.J. Crowder, *Identification of synthetic diamond grown using chemical vapor deposition (CVD)*. *Gems & Gemology*, 2004. **40**: p. 2-25.
136. Sumiya, H. and K. Tamasaku, *Large Defect-Free Synthetic Type IIa Diamond Crystals Synthesized via High Pressure and High Temperature*. *Japanese Journal of Applied Physics*, 2012. **51**(9R): p. 090102.
137. Mokuno, Y., et al., *A nitrogen doped low-dislocation density free-standing single crystal diamond plate fabricated by a lift-off process*. *Applied Physics Letters*, 2014. **104**(25): p. 252109.
138. Naamoun M., e.a., *Reduction of dislocation densities in single crystal CVD diamond by using self-assembled metallic masks*. *Diamond and Related Materials* 58, 2015: p. 62-68.
139. Tallaire, A., et al., *Reduction of Dislocations in Single Crystal Diamond by Lateral Growth over a Macroscopic Hole*. *Advanced Materials*, 2017. **29**(16): p. 1604823.
140. Boussadi, A., et al., *Reduction of dislocation densities in single crystal CVD diamond by confinement in the lateral sector*. *Diamond and Related Materials*, 2018. **83**: p. 162-169.
141. Mehmel, L., et al., *Dislocation density reduction using overgrowth on hole arrays made in heteroepitaxial diamond substrates*. *Applied Physics Letters*, 2021. **118**(6): p. 061901.
142. Wang, W.-h., et al., *Recent progress on controlling dislocation density and behavior during heteroepitaxial single crystal diamond growth*. *New Carbon Materials*, 2021. **36**(6): p. 1034-1045.
143. Shikata, S., *Single crystal diamond wafers for high power electronics*. *Diamond and Related Materials*, 2016. **65**: p. 168-175.

# **Chapter II: Instrumentation for the sample manufacturing and characterization**

## Summary

2	Chapter II: Instrumentation for the sample manufacturing and characterization .....	51
2.1	Introduction.....	53
2.2	HPHT substrate treatment before growth .....	53
2.2.1	Diamond substrate cleaning.....	53
2.2.2	Choosing the correct side for the growth process .....	54
2.2.3	Surface treatment .....	55
2.3	CVD growth reactors .....	55
2.4	Characterization techniques.....	59
2.4.1	DiamondView™ .....	59
2.4.2	Confocal Laser Scanning Microscopy .....	60
2.4.3	Raman spectroscopy .....	62
2.4.4	Cathodoluminescence spectroscopy.....	67
2.4.5	Secondary Ion mass spectrometry (SIMS).....	75
2.5	Conclusions.....	79
2.6	References.....	80



## 2.1 Introduction

The main focus of this chapter is to present the experimental growth setup and characterization techniques used during this work. In the first part, I will describe the substrate pretreatments carried out before each growth and will give some explanations about the main and key points about the diamond growth.

I will also present two MWPACVD reactors: the boron doped reactor in which just the boron doped layers are deposited and the intrinsic one, a *Bell Jar* type reactor, dedicated only to intrinsic diamond layer deposition

I will finish this chapter by presenting different characterization techniques that were utilized.

## 2.2 HPHT substrate treatment before growth

A crucial point for the growth of CVD diamond layers is to have good quality substrates. During this work, the CVD monocrystalline diamond growth was performed on commercial (100) oriented Ib HPHT diamond substrates provided by Sumitomo company [1].

Typically, these substrates have nitrogen impurities with concentrations close to  $10^{19}$  atoms/cm<sup>3</sup> (100ppm) and dimensions of 3 x 3 x 1.5 mm<sup>3</sup>. Before each growth, some pre-treatments are required to remove any impurities on the substrate surface and also to avoid the defects generation during the growth process.

### 2.2.1 Diamond substrate cleaning

As described in the first chapter, HPHT substrates are produced under high pressure and high temperature in the presence solvents such as nickel or cobalt. The crystal obtained is laser cut along (100) direction in order to obtain half-cubic substrate with 6 (100)-oriented faces before being polished.

Such processes, operated by the manufacturer of substrates, leads to damaged surfaces with possible metal inclusions that are not suitable to start a CVD growth. The first step of the cleaning process is to remove these metallic particles by acid cleaning using the following procedure:

1. Chemical etching for 60 minutes at 100 °C with a solution composed by HCl (37 %) and HNO<sub>3</sub> (65%) (3:1).
2. Cleaning with distilled water (at least two baths)
3. 5 minutes ultrasonic bath in acetone
4. 5 minutes ultrasonic bath in isopropanol

### 2.2.2 Choosing the correct side for the growth process

One of the characteristics of HPHT growth process is that the obtained crystals have multiple growth sectors. In fact, the crystal grows along the crystalline directions (100), (111), (113) and (110) and when the resulting crystal is sliced for producing a (100)-oriented plate, it intercepts the planes (111), (113) and (110) which lead to the appearance of what are called the growth sectors as illustrated in figure II.1. Depending on the position where the cut is made, these growth sectors are more or less important in size.

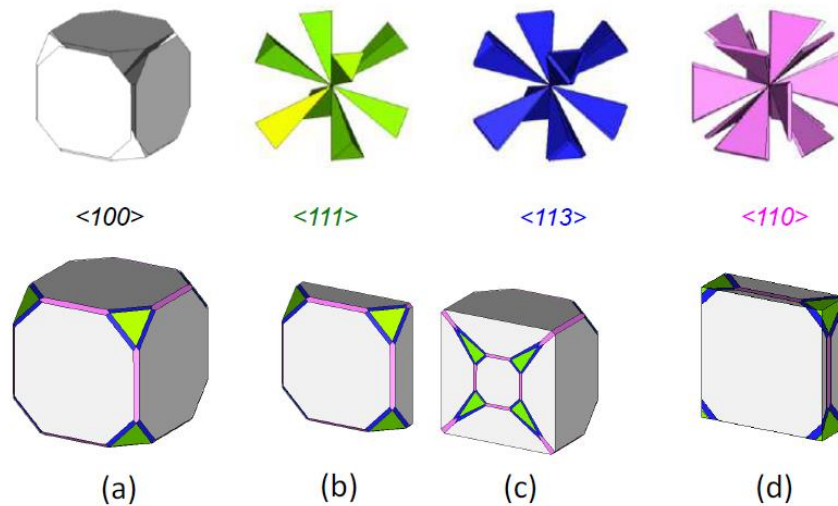


Figure II.1 – Illustration of the growth of a HPHT diamond crystal through a schematic diagram. (a) As the crystal grows, it expands along the (100), (111), (113), and (110) crystal directions. (b) The final crystal comprises of all these elementary growths. (c) When the crystal is cut in a specific crystalline orientation (100), it intersects the planes (111), (113), and (110), resulting in the formation of growth sectors. The prominence of these growth sectors varies depending on the location where the cutting takes place.

As the incorporation of defects and impurities during the growth strongly depends on the crystalline orientation, it result in strong inhomogeneity which can lead to significant internal stresses [2]. This specific point is illustrated in Figure II.2, which shows the result of the growth of two CVD films obtained for one, on an HPHT substrate having only one growth sector (100) and for the other, on a substrate having several growth sectors.

The CVD layers were separated from their substrates by laser cutting then polished and analyzed by birefringence (see Figure II.2 (b) and II.2 (d)). It is thus shown that the sample produced on multi-growth sectors presents stresses clearly localized around the growth sectors. It is therefore absolutely necessary to select substrates consisting mainly of a single growth sector.

A stage of identification of the deposition face is now carried out systematically before each deposition using the DiamondView, which allows revealing luminescent defects in the sample as shown in Figure II.2 (a) and II.2 (c). This device will be described in more details further.

The single growth sector face corresponds to a homogeneous luminescence image, while an inhomogeneous luminescence image corresponds to a multi-growth sectors face.

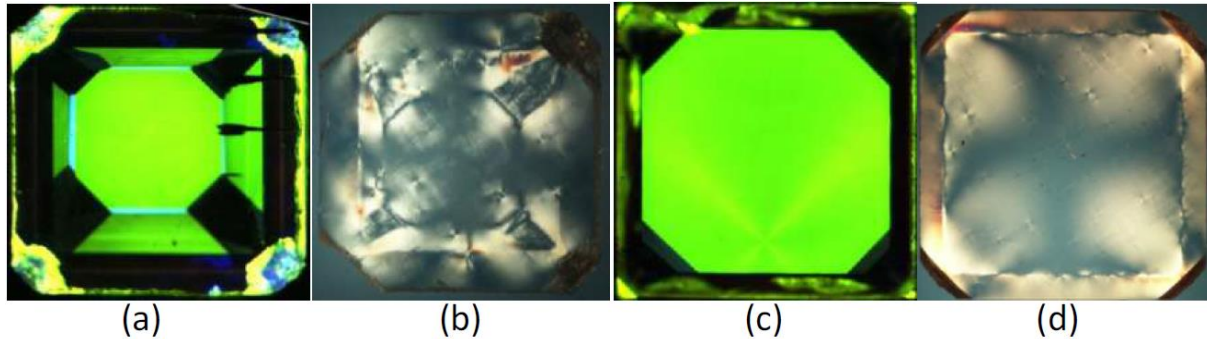


Figure II.2 - Images obtained by DiamondView (a and c), and birefringence photograph (b and d). The DiamondView images show the face formed by multiple growth sectors (a) and the one formed by a single sector (c). The birefringence photographs depict the stresses in the crystals, which are formed around the growth sectors (b). In the case where the deposit is made on the face with a single growth sector, the layer does not present any stresses (d).

### 2.2.3 Surface treatment

Once the good face is identified, the last treatment must be carried out on the HPHT diamond substrate just before starting the homo-epitaxial growth. It consists in a plasma etching with a gas mixture of  $H_2/O_2$  (with 2% of oxygen) during 30 minutes performed at the same pressure and microwave power than for the diamond growth [3]. The aim is to remove the damaged layer induced by the polishing and that can extend up to  $1 \mu m$  below the surface [2, 4].

## 2.3 CVD growth reactors

The diamond growths carried out during this PhD thesis were performed in two different MPACVD reactors. The first one, called SDR 150, was dedicated to boron doping. The second one, called BJS 150, was used only for intrinsic layers. Both reactors are commercially available and manufactured by Plassys Company for the growth of high crystalline quality CVD diamond films [5, 6]

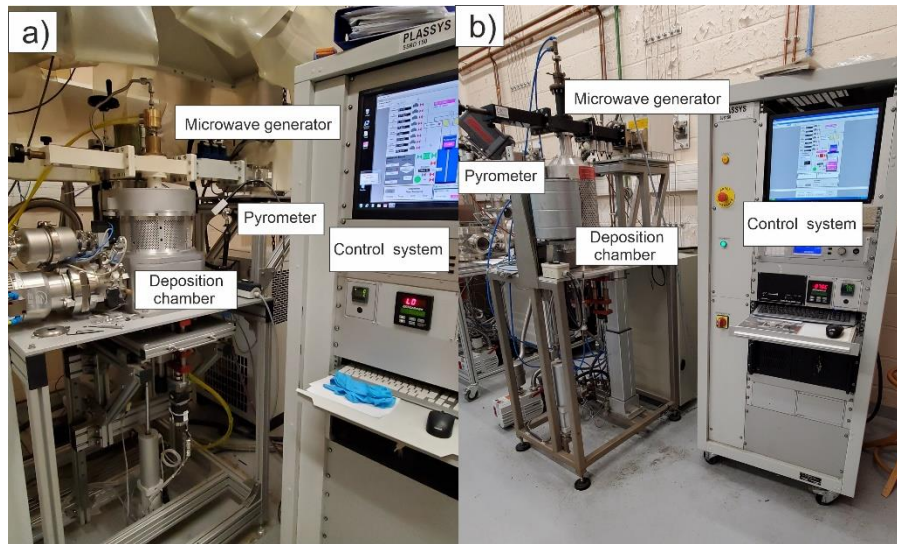


Figure II.3 - Pictures of the SSRR and the BJS150 intrinsic reactors (a) dedicated to boron-doped diamonds, (b) dedicated to intrinsic diamond layers.

Indeed, the BJS150 and SSRR can be used with high microwave power which can lead to high growth rate keeping good quality[7]. Both machines are equipped with a cooled substrate holder, which allows decoupling the substrate temperature from the plasma characteristics and adjusting the appropriate temperature during growth.

The 2 inches substrate holder position can be varied during the growth along the vertical direction allowing a careful adjustment of the substrate position regarding the plasma. These systems are very accessible by the lower flange, making it comfortable the load and unload operations.

An illustrating scheme showing its different elements is reported on Figure II.4. The machines can be controlled with a computer that allows the use of recipes prepared by the operator.

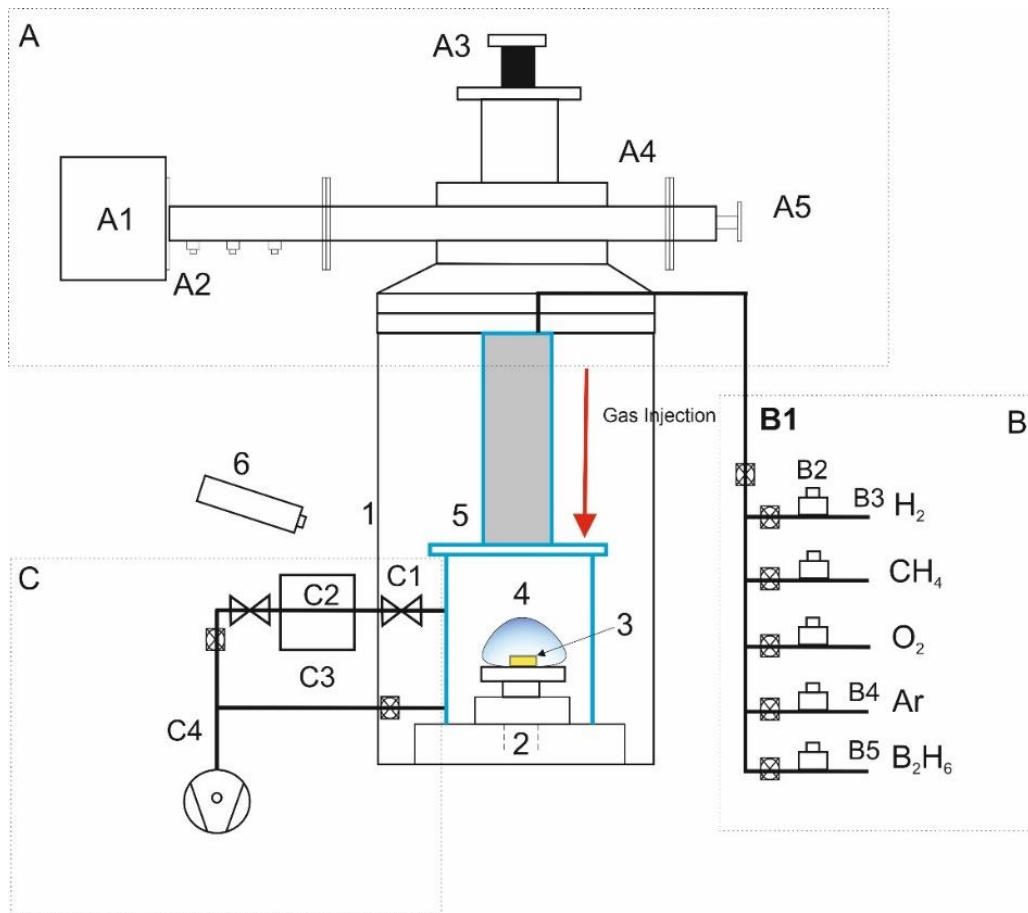


Figure II.4 - Diagram of the intrinsic reactor and a list of the various elements that comprise

1. Resonant aluminum cavity
2. Water-cooled and height-adjustable sample holder
3. Diamond substrate
4. Plasma
5. Cylinder quartz chamber
6. Dichromatic pyrometer

#### A microwave coupling device

- A1. 2.45 GHz magnetron head powered by a pulsed generator (Sairem 6kW)
- A2. Impedance adapters
- A3. Water cooled coupling antenna
- A4. Wave Guide A5. Piston of short circuit

#### B. Gas panel

- B1. Access of gases by pneumatic valves
- B2. Mass flow meters
- B3. Hydrogen purified by a palladium diffuser
- B4. Argon gas
- B5. Diborane gas

#### C. Pumping system

- C1. Gate valve
- C2. Turbomolecular pump
- C3. Pressure control by solenoid valve
- C4. Primary pump

Microwave generators working at 2.45 GHz with a maximum power of 6 kW are used to activate the gas phase. The main difference between the two systems is the geometry of the deposition chamber which consists in a bell jar system [8] for the BJS150. The main drawback of this machine is related to high boron doping which leads to soot formation that damages the top of the bell jar as shown by the LPSM [9].

It is the reason why Plassys updated the geometry of the machines and replace the bell jar by a quartz cylinder with water cooled antenna directly fixed on the top of the cylinder.

Such geometry is supposed to avoid the damages of the quartz when high boron concentration in the gas phase is required.

The gas mixture used for intrinsic diamond is composed of  $H_2$ ,  $CH_4$  while in the case of boron doping, diborane ( $B_2H_6$ ) and  $O_2$  is added. All the gas concentrations with the corresponding growth experimental parameters will be described in more details in chapter III.

## 2.4 Characterization techniques

Different techniques of characterization were performed during this work for each CVD diamond layer deposited in order to validate the sample manufacturing and the reliability of the process. These experimental setups are presented below.

### 2.4.1 DiamondView™

This is a photoluminescence imaging device developed by the Diamond Trading Company (DTC). This enables the analysis and characterization of luminescence in single-crystal diamonds. Upon UV excitation of the sample, a filter allows only wavelengths below 230 nm to pass.

This means that photons with energies at least equal to the bandgap of diamond will pass through. Under this excitation energy, the luminescent defects present in the material can emit photons, which will be collected by a CCD camera. A photography of the device is shown in Figure II.5.

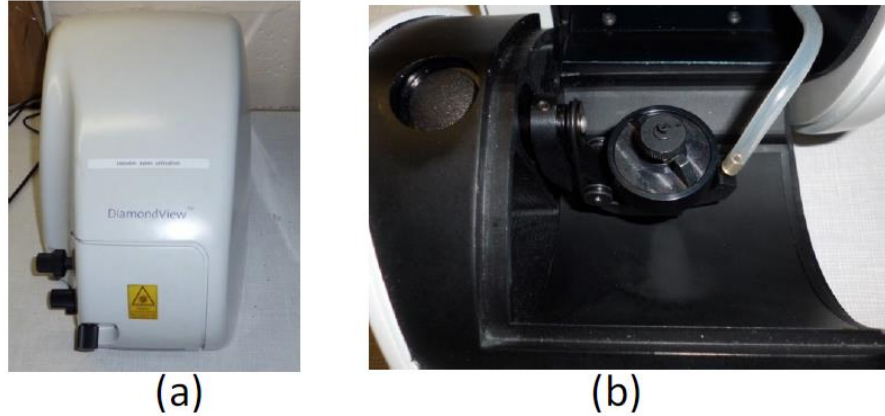


Figure II.5 - (a) DiamondView™ instrument photography, (b) substrate holder inside the device for the analysis by a pumping system.

It is then possible to map the luminescence of a sample. This device is very useful to observe preferential nitrogen incorporation (orange luminescence) or areas with dislocations leading to blue luminescence or determine single growth sector substrate.

#### 2.4.2 Confocal Laser Scanning Microscopy

A confocal microscope is an optical microscope that has the property of producing images with a very shallow depth of field called "optical sectioning". By positioning the focal plane of the objective at different heights of the sample, it is possible to make a set of images from which a three-dimensional representation of the object can be obtained as shown in Figure II.6.

The principle of the confocal microscope was described by Marvin Minsky in 1953, but it is only in the late 1980s that commercial models appeared, making this technique accessible to many laboratories.

This device uses a laser diode as the light source explaining why we talk about Confocal Laser Microscope (CLSM). The main purpose of the laser is to provide a monochromatic light easier to control even if a white light is also available for basic illumination of the sample.

The main components of the CLSM are shown in Figure II.6. The sample surface is scanned in the XY directions by a laser beam. Then, the objective lens is moved in the Z direction and the scanning of the sample is performed again. This process is repeated until the entire desired depth scale has been covered.

By this mean only the photons coming from the focal plane pass the pinhole and participate to the formation of the image of the focal plane. By varying this plane in depth, we can obtain a succession of several sections giving clear and precise information in the three dimensions of the observed object.

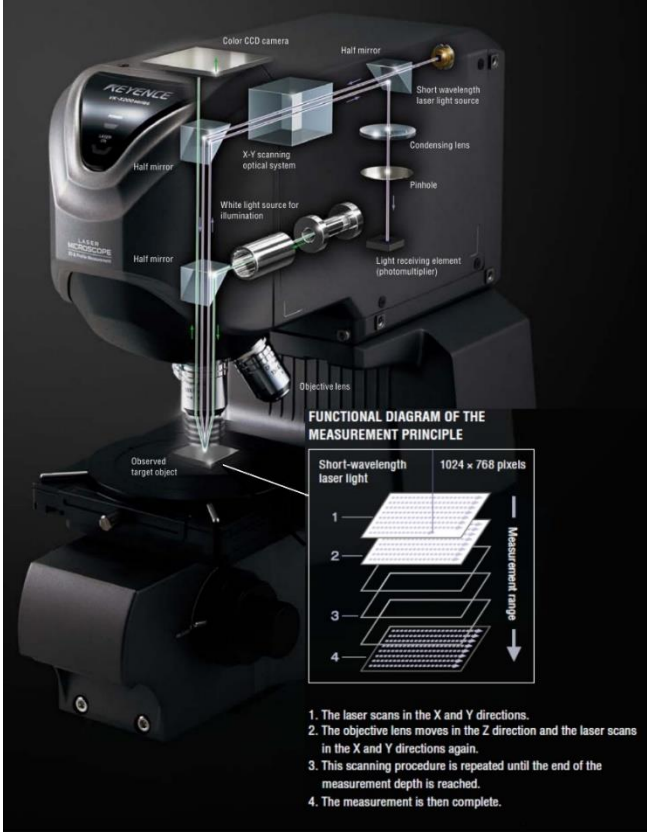


Figure II.6 - Confocal Laser Scanning Microscopy (Keyence, VK 9700) illustration with its optical sections and the functional diagram of measurement principle[10]

The scanning field observed by laser is done thanks to two orthogonal galvanic mirrors which are very fast (between 200 Hz and 2kHz) that scan in X, followed by a mirror that scans in Y. The positioning of the depth of the sample is generally obtained by moving the objective in the Z direction with piezoelectric quartz in successive steps of 200-300 nm.



The detectors used are photomultiplier tubes and a high sensitive CCD camera. The amount of light produced by the laser is measured and converted into digital signals based on the sample position, which creates digital images. The apparatus used during this work and implanted at LSPM was a CLSM type VK 9700 supplied by Keyence Company.

### 2.4.3 Raman spectroscopy

The Raman spectroscopy analysis is generally used in our team to identify the different carbon phases present in the layers deposited. For monocrystalline diamond we are more particularly interested in the full width at half maximum (FWHM) of the Raman diamond peak which gives information about the quality of the crystal. Its characteristic and shape can also give information on the doping rate of the films as we will see below.

#### 2.4.3.1 Principle of Raman spectroscopy

Raman spectroscopy is mainly based in the interaction between laser excitation and matter. When the photons interact with the material, they are either absorbed or scattered and under the effect of the electromagnetic field the scattered photons can disturb the electronic cloud (due change in the polarization of molecules) which will induce the transition of the molecules system into a virtual excitation level. There are three types of process that could happen during this effect, which are illustrated in Figure II.7:

- Rayleigh scattering: this is an elastic scattering without change of energy. During this diffusion process, the incident photon induces the transition from the vibrational state of the molecule to a virtual state with higher energy. Thereafter the molecule de-excites to the same initial state. ( $\nu$ )
- Raman Stokes scattering: this is an inelastic scattering. In this case the material absorbs part of the photon energy and then de-excites to a level with higher energy level ( $\nu+\nu_1$ )
- Raman anti-Stokes scattering: this is also an inelastic scattering. For this case the material gives energy to the photon, and then it de-excites at level ( $\nu-\nu_1$ ).

These last two scattering processes are Raman scattering processes which represent a characteristic of the material.

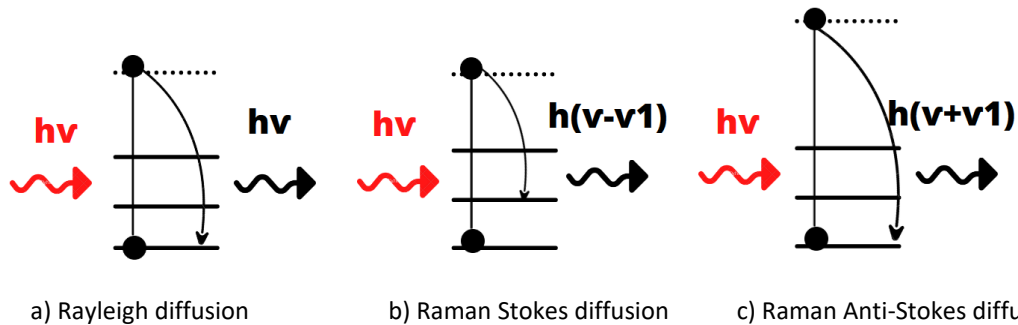


Figure II.7 - Illustration of the different vibrational transitions involved in the photon-matter interaction (Raman effect)

#### 2.4.3.2 Instrumentation available at the LSPM

A Raman spectrometer device is generally constituted by different elements.

- The excitation source which is a laser.
- A motorized stage for imaging.
- Optical elements to collect the signal, which is generally an optical microscope that allows the laser to be focused on the surface of the sample. The spectrometer can also be equipped with a confocal system that makes it possible to limit the volume analyzed. After excitation, a notch filter is used to cut the Rayleigh emission (most intense emission, whose wavelength is that of the excitation laser).
- A grating that separates the different components of the light scattered by the sample.
- A CCD detector with a low noise level and working at low temperature.
- An electronic acquisition system that records and processes data.

At the LSPM we have a high-resolution Jobin-Yvon steup (HR800). It is equipped with a motorized X-Y stage for imaging and a system of confocal slots with adjustable aperture. The micro analysis system (10x, 20x, 100x and 40xUV objectives) associated with a CCD detector cooled by a Pelletier allows high sensitivity and good flexibility of use. The Rayleigh frequency is cut thanks to notch filters. The available excitation wavelengths are 473 nm and 633 nm. A photography of the device used during this work is presented in Figure II.8.



Figure II.8 - Photograph of the Jobin-Yvon HR800 Raman device at LSPM

#### 2.4.3.3 Raman spectroscopy in diamond

Raman spectroscopy analysis on diamond leads to the appearance of a diamond peak around  $1332.5 \text{ cm}^{-1}$  (the most intense peak) which is due a triple degenerate single photon in the region of the optical center. When the films have an excellent quality, the second or even the third peak order can be observed. Moreover, the lower the width at half height of this peak the better is the crystal quality [11]. It is of the order of  $1.5 \text{ cm}^{-1}$  for natural or CVD single crystals of exceptional quality [12].

It is also possible to have information about mechanical stresses from the offset of this peak with respect to its theoretical position. If it is positive the film is under compression and if it is negative the film is in tension [13]. Bergman et al [14] indicated that a Raman peak shift of  $1.9 \text{ cm}^{-1}$  corresponds to a stress of 1 Gpa. Other components can be observed on the Raman spectra carried out on diamond films. They can be attributed to defects or non-diamond phases.

Position (cm <sup>-1</sup> )	FWHM (cm <sup>-1</sup> )	Origin
500	214-261	Observed in highly boron-doped films (>10,000 ppm). B-C vibration
1150	30-100	Trans-polyacetylene
1225 and 1280	100-200 and 30-50	Observed in highly boron-doped films (>10,000 ppm). B-C vibration
1332	1.5-40	First-order diamond Raman peak
1350	80-400	Band D: Graphite
1480	20-150	Trans-polyacetylene
1500	350-500	Band I: amorphous carbon a-C. Low quality PCD films.
1570	40-200	G band: graphite
2459	500	Second order Raman peak

Table II.1 - Principle Raman peaks and bands.

#### 2.4.3.4 Boron doping characterization by Raman spectroscopy

##### 2.4.3.4.1 The Fano effect

When boron is incorporated into a silicon matrix, there are localized vibrations that take place and this phenomenon is called Fano effect[15]. It also exists in diamond.

Thus, in addition to the information about the quality of the diamond film, Raman spectroscopy can also give some information about boron incorporation in diamond. In the Raman spectrum, the Fano effect is characterized by the appearance of a baseline asymmetry together with a decrease in intensity and a shift in the position towards lower frequencies of the characteristic diamond peak.

The comparison of two CVD diamond spectrum is shown on Figure II.9 and there we can notice the distortion of the spectrum with the Fano effect which is a consequence of the interaction between a discrete state and a continuum one. It is important to note that in the case of boron doping, this phenomenon has a threshold concentration below which it cannot be observed (some  $10^{19}$  atoms  $B.cm^{-3}$ ).

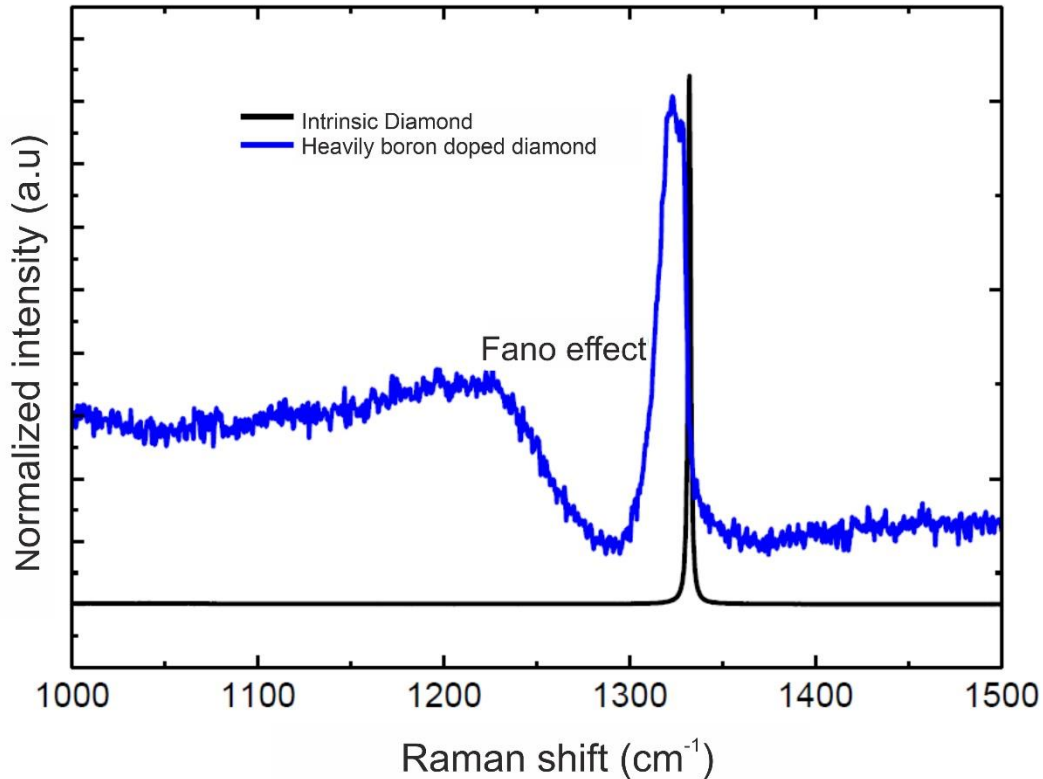


Figure II.9 - Fano effect due to a high boron concentration incorporated in the film

The determination of the boron concentration from obtained Raman spectrum is possible [16] but SIMS (Secondary Ion Mass Spectroscopy) measurement is essential for calibration [17].

#### 2.4.3.4.2 Boron contribution on Raman spectra

In addition to the appearance of the Fano effect on the characteristic diamond peak at  $1332.5\text{ cm}^{-1}$ , there are other signatures that can be attributed to boron. For instance, a band at  $550\text{ cm}^{-1}$  is generally observed in diamond films with high doping ( $> 10^{19}\text{ cm}^{-3}$ ); in some cases, a shift of the band towards lower wavelength may indicate an increase of doping levels.

Some authors attribute this band to the activation of a phonon in the diamond band due to the relaxation of the selection rules related to the strong presence of boron [18]. It can be attributed to a vibration of a pair of boron atoms [18]. There is also a band located at  $1225\text{ cm}^{-1}$  that can be seen on highly doped films.

#### 2.4.4 Cathodoluminescence spectroscopy

Cathodoluminescence (CL) technique consists in observing the light emissions produced under the action of an electronic beam. The interaction produced between the electron beam of several thousand of eV and the semiconductor material generates electron-hole pairs in the conduction and valence bands creating local non-equilibrium state[19]. The de-excitation phase of those excited electronic levels can take place in different ways and is illustrated in Figure II.10.

- (I) First case (Figure II.10 (a)) is a band to band radiative transition which is called fundamental transition leading to the emission of a photon with an energy  $h\nu$  equal to the band gap energy (BGE) ;
- (II) When intermediate levels induced by structural defects or impurities are presents in the band gap, the de-excitation can occur in a radiative way by a donor or acceptor levels (Figure II.10 (b)). In this case, a luminescence characteristic is produced with an energy  $h\nu'$  lower than the BGE.
- (III) The last one is when the de-excitation is non radiative and coupled with a significant production of phonons (lattice vibrations). It leads to a localized temperature increase in the sample (Figure II.10 (c)) and in this case there is no luminescence produced. The transition cannot be observed in CL.

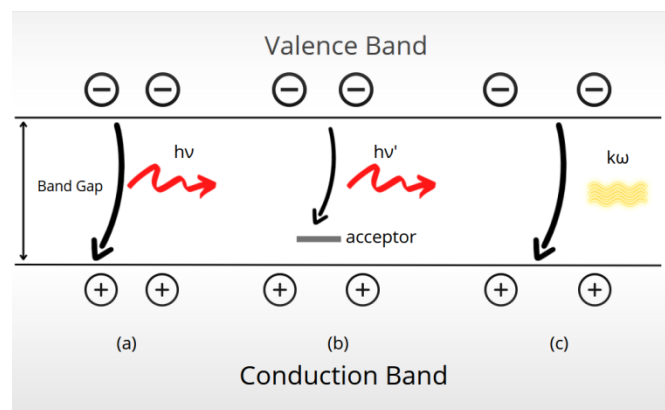


Figure II.10 - Illustration of the recombination process after excitation by an electronic beam, (a) direct radiative transition band-to-band, (b) radiation transition with a localized acceptor level and (c) non radiative transition with phonon assistance.

The principle we have described is very simplified. Indeed, diamond is a semiconductor material with an indirect band gap. This means that, in the band diagram (in which we represent energy  $E$  as a function of the moment  $P$  of the electron), an electron cannot shift from the highest-energy state in the valence band to the lowest-energy state in the conduction band without a change in momentum.

Therefore, it is then impossible to see a direct band-to-band transition. Thus, the transition must be done in two stages: the emission of a photon that provides almost all the energy required and the production of a phonon (lattice vibration) which allows preserving the momentum. The energy of this phonon (a few meV) is negligible compared to that of the light emission (at least in the case of diamond).

Moreover, we cannot consider that the electron-hole pairs produced by the interaction with the incident electron beam is completely free. They attract each other and form a bound state, called free exciton (FE). The energy involved is of a few meV and it is as if the emitted electron from the valence band was in an energy level slightly lower than the energy of the conduction band.

Finally, the recombination of these free excitons across the band gap generates a light emission of energy ( $E$ ) close to the BGE, which is given by the following relation:

$$E = h\nu = BGE - E_{phonon} - E_{exciton} \quad \text{Eq. 1}$$

In which  $E_{exciton}$  correspond to the bounding energy of the electron-hole pair (80 meV for diamond) and  $E_{phonon}$  is the energy of the conservation from the phonon momentum. This description can be associated to the intrinsic diamond but in the case of phosphorus or boron doping, excitons localized in the donor and acceptor levels are also observed. These are called bound excitons (BE). They have a recombination mechanism similar to the FE and they can also be observed in a close region to the band gap energy when the material is of good quality[20, 21]

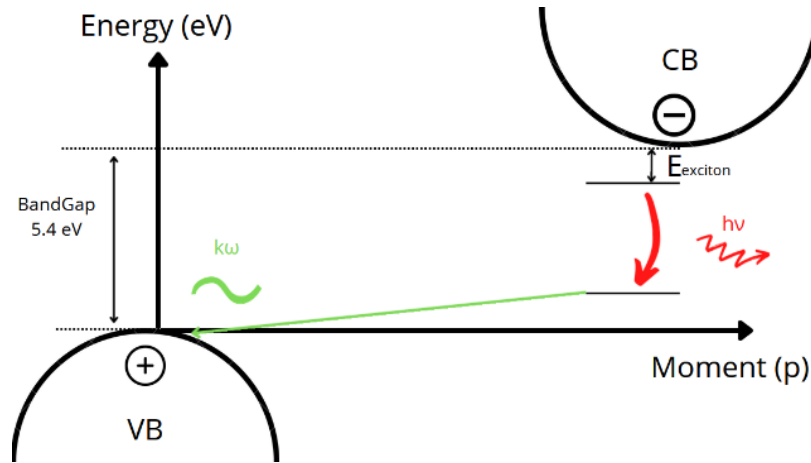


Figure II.11 - Diagram of the band structure of diamond, a material with an indirect band gap. The transition is made from the exciton level to the valence band via the simultaneous emission of a photon and a phonon.

We can see here that CL is a very powerful tool giving relevant information in the region close of the BGE about the quality of a single crystal diamond and the nature and concentration of the doping impurities. In Figure II.12 is presented an example of CL spectrum of a boron-doped homoepitaxial diamond film in which the luminescence from FE and BE are visible with the involvement of the various phonon types.

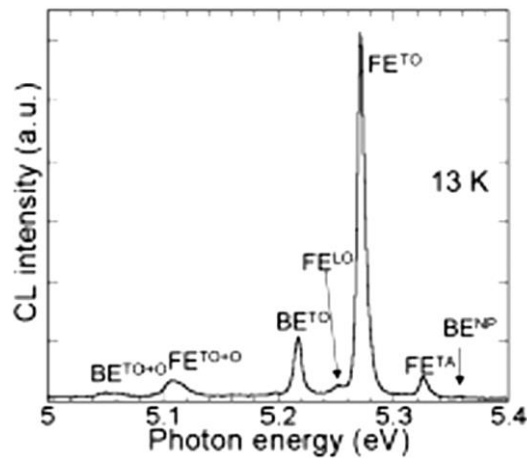


Figure II.12 - CL spectra at 13K in the UV region of a high quality boron doped diamond film in which is possible to observe the free excitons related to different phonons (LO, TO and TA). Excitons bound to the boron acceptor level are also noticeable: BETO and BENP for non-assisted phonon recombination[20].



#### 2.4.4.4 The boron effect on CL measurements

Quantitative estimation of the boron concentration on diamond films can be performed by CL [22-24]. Barjon et al. performed some important and relevant investigations related to the emission of CVD monocrystalline boron doped diamond layers with different doping levels ( $10^{16} - 10^{18} \text{ cm}^{-3}$ ) by Secondary Ion Mass Spectroscopy (SIMS) and CL in order to correlate the exciton recombination emission with the boron concentration [24].

SIMS measurements give fairly accurate values of the total amount of boron concentration in the films as it will be presented in the last part of the chapter. CL is sensitive to substitutional boron acceptors onto which the excitons are generated due the interaction with the incident electron beam.

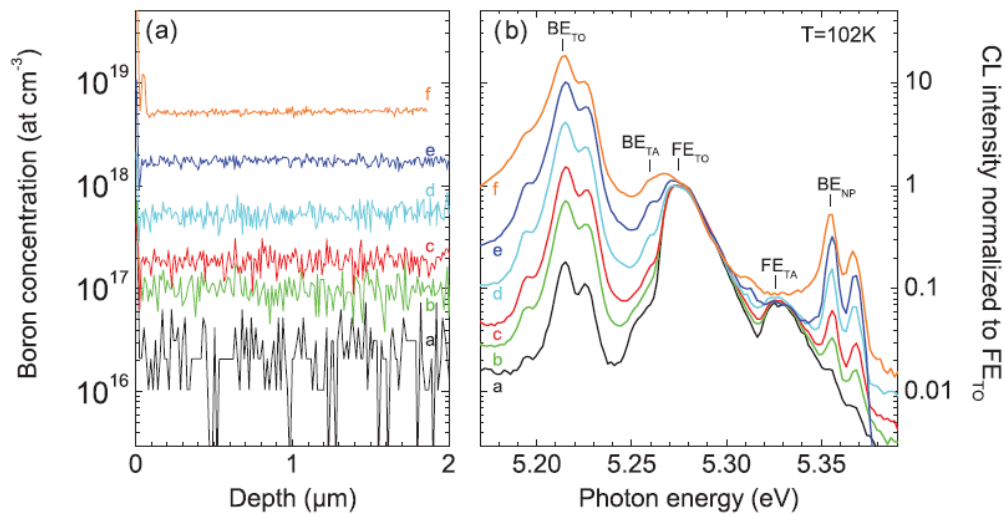


Figure II.13 - SIMS profile and CL spectra of a set of boron doped diamond layers with different doping levels[24].

In Figure II.13 (a) is presented the SIMS analysis of different doped layers and boron concentration as a function of the depth. For CL curves presented in Figure II.13 (b), different emissions related to the BE and FE recombination assisted by transverse optical (TO) or acoustic (TA) phonons are observed as well as the BE without phonon participation (NP).

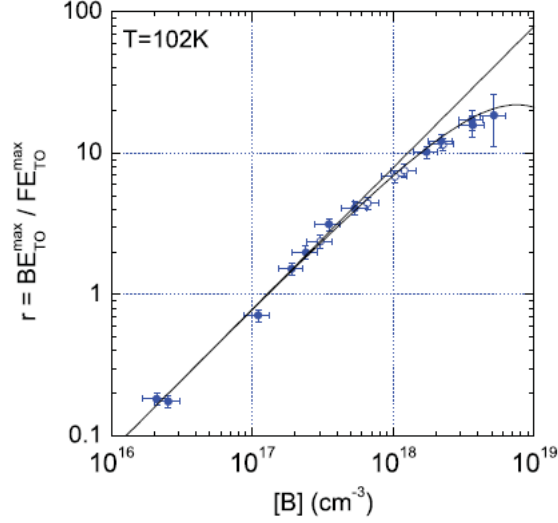


Figure II.14 - Plot of the intensity ratio  $BE_{TO}/FE_{TO}$  versus the boron concentration. The interpolation of the data by linear fit had proved to be in agreement with boron concentration until  $[B] \approx 6 \times 10^{17} \text{ cm}^{-3}$ , and then it is fit by an exponential fit above this boron concentration[24]

The Figure II.14 shows the intensity ratio  $BE_{TO}/FE_{TO}$  as a function of the boron concentration measured by SIMS. Fitting data are also reported showing that the evolution of the ratio is almost linear up to a Boron concentration of about  $6 \times 10^{17} \text{ cm}^{-3}$  (Eq. 2), and that above this value, a deviation from a simple linear relation is observed, but it can be estimated using an exponential fit up to almost  $10^{19} \text{ cm}^{-3}$  (Eq. 3).

$$\frac{BE_{TO}}{FE_{TO}} = A \cdot [B] \quad \text{Eq. 2}$$

$$\frac{BE_{TO}}{FE_{TO}} = A \cdot [B] \cdot e^{(-1.32 \cdot 10^{-19} [B])} \quad \text{Eq. 3}$$

The  $BE_{TO}/FE_{TO}$  ratio comes from the measurement of the CL spectra, meanwhile the boron concentration  $[B]$  was measured by SIMS, and  $A$  is an empirical coefficient equal to  $7.9 \times 10^{-18}$ .

The FE excitons become more quenched on heavily doping layers and cannot be observed anymore. Therefore previous equations cannot be used. However, it is possible to get an estimation of the doping level using BE peaks which become enlarged and shifted to lower energies.

This can be seen on Figure II.15 in which Baron et al. [21] presented  $BE_{TO}$  position as a function of doping measurements by SIMS. This is consistent with the fact that at high boron doping, B atoms do not behave as isolated acceptors but form an impurity band with reduced ionization activation energy that can even lead to a metallic transition, which is typically around  $3 \times 10^{20} \text{ cm}^{-3}$ . This Phenomenon can be described by the following equation:

$$E(eV) = 5.211 - 0.112 \log([B]/1.5 \cdot 10^{19}) \quad \text{Eq. 4}$$

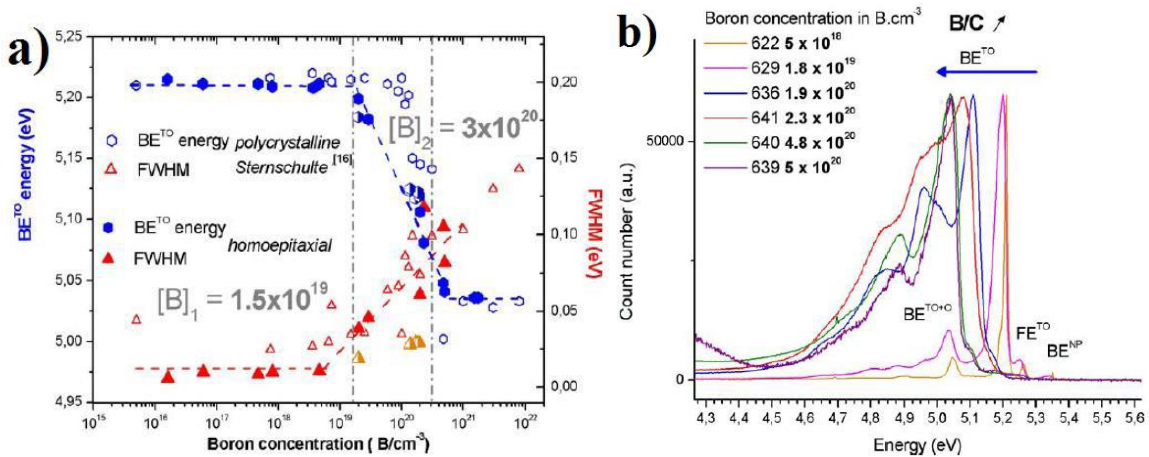


Figure II.15 - (a) Evolution of the  $BE_{TO}$  peak (left axes) and FWHM (right axes) versus the boron concentration, different diamond samples with different boron doping level[164]. (b) Cathodoluminescence spectra on CVD monocrystalline boron doped diamond with different doping levels[22]

#### 2.4.4.5 Dislocations in diamond observed by Cathodoluminescence

Cathodoluminescence technique also allows observing the dislocation propagation in the homoepitaxial overgrown layers. This can be done thanks to the excitonic recombination of the electron-hole pairs induced by the electronic beam excitation which produces a luminescent emission that can be imaged by integrating the FE intensity. Dislocation presence quenches FE and a contrast on the image can be obtained as illustrated in Figure II.16 in which dislocation propagation from a HPHT substrate among two CVD layers can be observed.

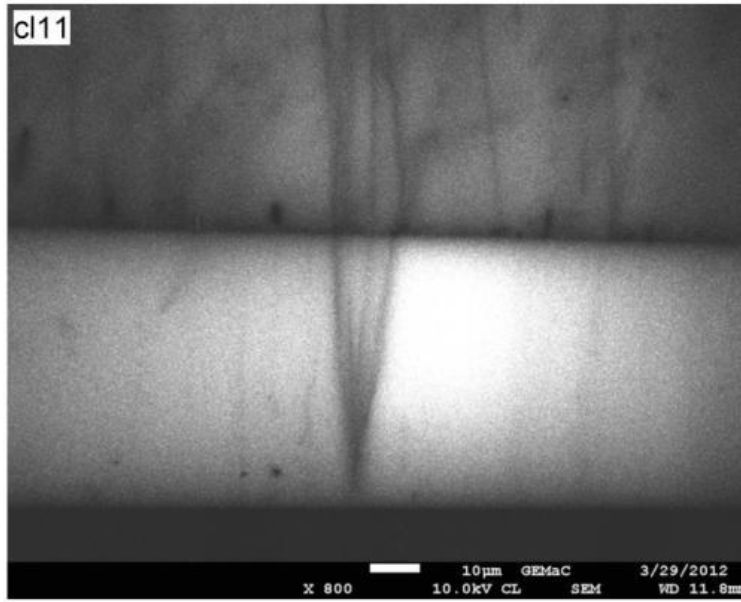


Figure II.16 - Dislocation propagation (shaded lines) among successive CVD layers.[25]

#### 2.4.4.6 Instrumentation used for Cathodoluminescence measurements

CL technique uses a scanning electronic microscope (SEM) in which the primary electron beam serves as an excitation source. The way to produce images on this technique is based on the scanning of a sample by the focused electron beam and the synchronized detection of the resulting secondary (or backscattered) electrons. There are numerous emission (Auger electrons, X-ray photons, etc.) and among all of them the Cathodoluminescence emission.

The setup used during this PhD was a MEB ZEISS EVO MA-15 with a LaB<sub>6</sub> filament coupled with a Horiba-Jobin-Yvon Cathodoluminescence system. It is presented in Figure II.17. Its characteristics are the following:

- Electron accelerator: 2keV to 45 keV
- Cryogenics: 80k -300k
- Beam current: from pA to µA
- Image resolution: 50 nm

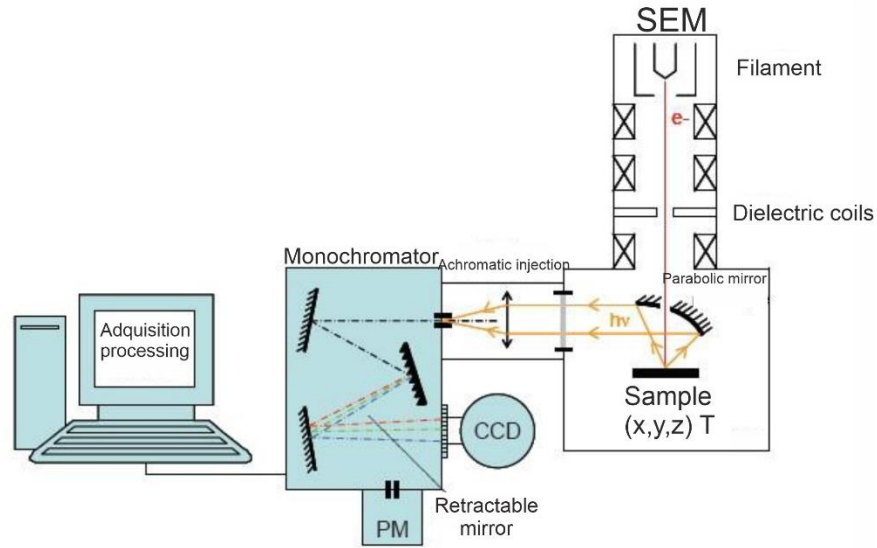


Figure II.17 - Schema of the CL System used at LSPM.

The emitted photons are collected by a pierced parabolic mirror that allows the incident electrons to pass. Photon beam is collimated towards the optical output of the microscope as soon as the photons emitting zone is at the focus of the collecting mirror.

The achromatic injection box positioned at the exit of the system makes possible to refocus the beam on the entrance slit of the monochromator. This achromatic adaptation ensures the collection of photons at any wavelength and thus offers the possibility to quantitatively compare the band edge emission to the defect bands.

A monochromator (TRIA550) is used for the spectral analysis. In order to separate the different wavelengths, a reflection grating is used. The resolution level increases with the number of lines per mm (600 or 1800) and this spectral resolution also depends on the aperture of the input slits.

A typical resolution of 0.07 nm with the grating 1800 lines/mm and slits of 0.075 mm is obtained. A total spectral range from 190 nm to 1100 nm can be covered.

The light scattered by the monochromator is analyzed using a CCD camera with photodetectors. The CCD camera is cooled with liquid nitrogen to decrease electronic noise and thus increase the signal-to-noise ratio. The sample can be mounted on a cryogenic stage that can be cooled up to 80 K.



Figure II.18 - CL spectrometer picture available at LSPM. A liquid nitrogen bottle is used to decrease the temperature to 80K.

#### 2.4.5 Secondary Ion mass spectrometry (SIMS)

Quantify carefully the concentrations of impurities in diamond, in particular boron, is really important in our work. That's why our samples were characterized by secondary ion mass spectrometry (SIMS). It essentially allows detecting and measuring low concentrations of minority elements (atom, neutral molecules, ions...) present in a material with a sensitivity that can reach the ppm.

This analysis can detect virtually all the elements in the periodic table, including hydrogen, with detection limits well below the ppm range. Nearly all elements of the periodic table, from hydrogen to uranium, can be quantitatively analyzed by SIMS technique. Only the noble gases are difficult to measure because they don't form secondary ions.

The typical concentration range that can be measured is from  $10^{16}$  to  $10^{22}$  cm<sup>-3</sup>. This technique can also be used to determine concentration profiles of the species in depth that means that it can be also used to determine the thickness of thin films.

#### 2.4.5.4 Principle

SIMS technique is based on the detection of secondary ions produced under the effect of a bombardment of incident primary ions as illustrated in Figure II.19. An ion or an aggregate of ions with energy of a few keV impacts a surface, and then it produces the erosion and emission of radiation and particles (secondary beam) of different natures and characteristics of the sample: photons, secondary electrons, neutral particles (atoms and molecules), positive and negative secondary ions.

In SIMS, those negative secondary ions are the ones to be extracted, analyzed and selected by a mass spectrometer according to their mass to charge ratio ( $m/q$ ), and returned to an ion counting device.

Thus, it should be noted that this technique is destructive since its principle is based on the damage of the surfaced caused by the bombardment.

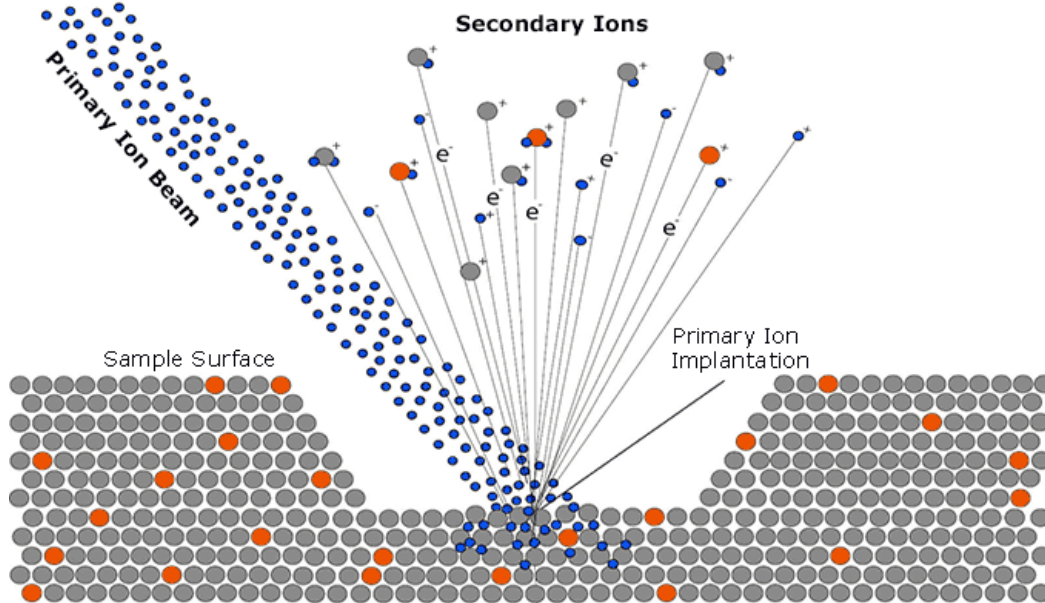


Figure II.19 - Sputtering scheme by ion analysis.

#### 2.4.5.5 Equipment used

The measurements performed during this work were carried out on a CAMECA IMS4f ionic analyzer available at GEMaC. The schematic of the equipment is shown in Figure II.20. The primary ions used are Caesium or Oxygen ions. The primary ion beam is focused into a spot of 100 nm diameters for Cs<sup>+</sup> ions and 1 μm for O<sub>2</sub> ions.

At the end the size of the crater formed will be determined by the scan area of the primary beam. It is typically on the order of 1 to 500 μm in side. The analyzed area has a circular shape, and the diameter of the circle is determined by the optical transfer and is limited to discrete values.

In diamond, the etching rate is in the range of 0.2 to 1 μm/h. We can therefore analyze very thin layers of the order of tens of nanometers (secondary ions originate from at the most three atomic planes below the surface).

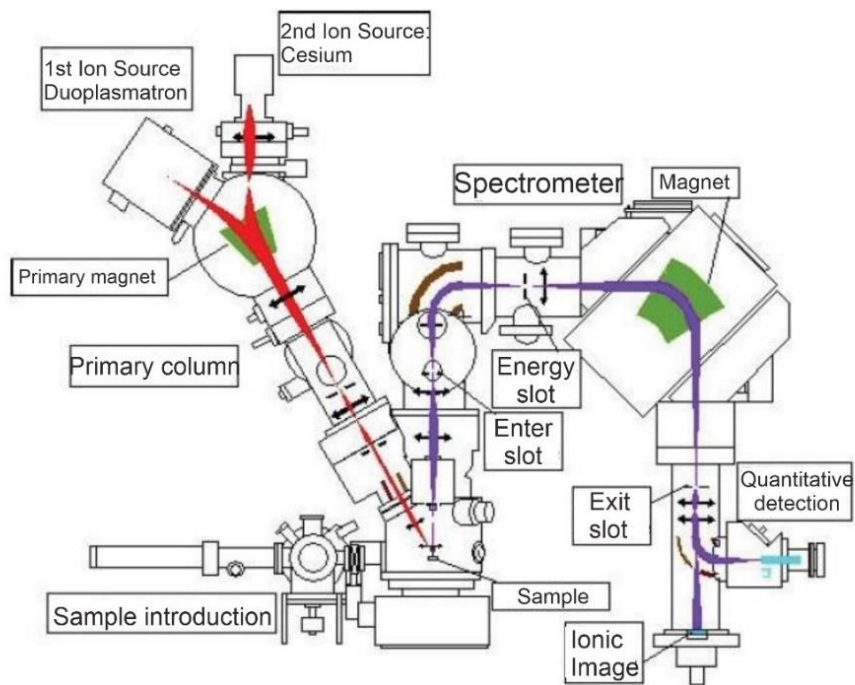


Figure II.20 - Diagram of the CAMECA IMS4f ion analyzer.



For our work, the 10 keV Cs<sup>+</sup> source was used to analyze elements that are easily detectable as negative secondary ions such as hydrogen (H), nitrogen (N), boron (B) or phosphorus (P) in diamond. Indeed, bombardment by Cs<sup>+</sup> ions exalts the secondary ionic emission of electronegative elements (halogens, phosphorus, carbon, oxygen, nitrogen...).

The Cs<sup>+</sup> ions are generated by a solid compound: cesium carbonate. At the exit of the source, a magnetic filtering ensures the purity of the beam. Then, the column which contains a system of electrostatic lenses and deflectors focuses positions and scans the beam on the sample. The secondary column sorts the secondary ions extracted from the sample before detection and counting.

## 2.5 Conclusions

The boron doped samples grown during this PhD have been prepared in the SDR 150 machine supplied by Plassys which has been described at the beginning of this chapter. Pretreatments of the substrates before the growth and the instrumentation required in order to assess the quality and doping rate of the layers produced have been also presented. Indeed, the characterization of diamond samples is a critical step and various characterization techniques are needed, each of them having their own strengths and weaknesses.

The choice of the appropriate technique will depend on the specific properties of the sample and the level of accuracy required. In summary, the combination of several of these characterization techniques can provide a comprehensive understanding of the properties of diamond samples.

## 2.6 References

1. <https://www.sumitomotoool.com/>. Available from: <http://www.sumitomotoool.com>.
2. Tallaire, A. and A. Gicquel, *Croissance de monocristaux de diamant par dépôt chimique en phase vapeur pour des applications en électronique de puissance*. 2005.
3. Naamoun, M., et al., *Etch-pit formation mechanism induced on HPHT and CVD diamond single crystals by H<sub>2</sub>/O<sub>2</sub> plasma etching treatment*. *physica status solidi (a)*, 2012. **209**(9): p. 1715-1720.
4. Tallaire, A., et al., *Oxygen plasma pre-treatments for high quality homoepitaxial CVD diamond deposition*. *physica status solidi (a)*, 2004. **201**(11): p. 2419-2424.
5. Barjon, J., et al., *Homoepitaxial boron-doped diamond with very low compensation*. *physica status solidi (a)*, 2012. **209**(9): p. 1750-1753.
6. Issaoui, R., et al., *Evaluation of freestanding boron-doped diamond grown by chemical vapour deposition as substrates for vertical power electronic devices*. *Applied Physics Letters*, 2012. **100**(12): p. 122109.
7. Achard J., e.a., *High quality MPACVD diamond single crystal growth: high microwave power density regime*. *Journal of Physics D: Applied Physics* 40 (20), 2007: p. p. 6175-6188.
8. Issaoui, R., *Elaboration de films épais de diamant monocristallin dopé au bore par MPAVCD pour la réalisation de substrats de diamant P +*. 2011, Paris XIII.
9. Achard, J., et al., *Freestanding CVD boron doped diamond single crystals: A substrate for vertical power electronic devices?* *physica status solidi (a)*, 2012. **209**(9): p. 1651-1658.
10. <https://www.keyence.com/downloads/?mode=ma&q=>, K.C.V.-S.U.s.M.K.C.
11. Harris, S.J., et al., *Diamond film quality: Effects of gas phase concentrations on the Raman spectra*. *Journal of Applied Physics*, 1996. **80**(4): p. 2187-2194.
12. Bauer, T., et al., *High growth rate homoepitaxial diamond deposition on off-axis substrates*. *Diamond and Related Materials*, 2005. **14**(3-7): p. 266-271.
13. Vlasov, I.I., et al., *Stress mapping of chemical-vapor-deposited diamond film surface by micro-Raman spectroscopy*. *Applied Physics Letters*, 1997. **71**(13): p. 1789-1791.
14. Bergman, L. and R.J. Nemanich, *Raman and photoluminescence analysis of stress state and impurity distribution in diamond thin films*. *Journal of Applied Physics*, 1995. **78**(11): p. 6709-6719.
15. Fano, U., *Effects of Configuration Interaction on Intensities and Phase Shifts*. *Physical Review*, 1961. **124**(6): p. 1866-1878.
16. Bernard, M., A. Deneuve, and P. Muret, *Non-destructive determination of the boron concentration of heavily doped metallic diamond thin films from Raman spectroscopy*. *Diamond and Related Materials*, 2003. **13**: p. 282-286.
17. Pinault-Thaury, M.A., et al., *Front and back side SIMS analysis of boron-doped delta-layer in diamond*. *Applied Surface Science*, 2017. **410**: p. 464-469.
18. Gheeraert, E., et al., *Effect of boron incorporation on the "quality" of MPCVD diamond films*. *Diamond and Related Materials*, 1993: p. p. 742-745.
19. M. Ali Omar, « *Elementary solid state physics* », published by Adison-Wesley, (1974), Chapter 6 : *Semiconductors theory*, page 254.
20. Kasu, M., et al., *Influence of epitaxy on the surface conduction of diamond film*. *Diamond and Related Materials*, 2004. **13**(2): p. 226-232.
21. Gheeraert, E., *Défauts de structure et impuretés dans les couches minces de diamant élaborées par dépôt chimique en phase vapeur*, 1992, Université Joseph Fourier, : Grenoble.
22. Baron, C., et al., *Cathodoluminescence of highly and heavily boron doped (100) homoepitaxial diamond films*. *Diamond and Related Materials*, 2006. **15**(4-8): p. 597-601.

23. Omnès, F., et al., *Study of boron doping in MPCVD grown homoepitaxial diamond layers based on cathodoluminescence spectroscopy, secondary ion mass spectroscopy and capacitance–voltage measurements*. *Diamond and Related Materials*, 2011. **20**: p. 912–916.
24. Barjon, J., et al., *Boron acceptor concentration in diamond from excitonic recombination intensities*. *Physical Review B*, 2011. **83**(7).
25. Naamoun M., *Mécanismes de formation et de propagation des dislocations au sein de diamant CVD monocristallin et développement de stratégies visant à réduire leur densité*.

**Chapter III: Growth Parameters  
Optimization for Boron Doped CVD  
Diamond Growth and Stacking  
Layer Dislocation Study**

## Summary

3	Chapter III: Growth Parameters Optimization for Boron Doped CVD Diamond Growth and Stacking Layer Dislocation Study	82
3.1	Introduction .....	84
3.2	Growth parameters optimization for boron doped CVD diamond growth .....	85
3.2.1	Influence of sample position in the plasma .....	85
3.2.2	Influence of microwave power density .....	87
3.2.3	Influence of methane .....	92
3.2.4	Microwave power and $(B/C)_{gas}$ reduction.....	95
3.2.5	Measurements techniques for boron doping concentration.....	102
3.3	Exploring the Feasibility of Vertical Schottky Diodes with Diamond Layers: Investigations and Future Prospects .....	104
3.3.1	Stacking layer study.....	105
3.3.2	Interface analysis.....	113
3.4	Conclusions .....	119
3.5	References.....	120

### 3.1 Introduction

This chapter is focused on the monocrystalline (100)-oriented boron-doped diamond layers. The target is to develop high quality boron doped layers with different boron doping levels. Thus, we will present doping and thickening solutions for the realization of stacking layers with the aim of improving Schottky diode performances.

In the frame of this work, we acquired a new boron-doped diamond growth machine built by PLASSYS Company (SSDR 150) and the first step was to validate its reliability for developing highly and lightly boron-doped layers. Subsequently, we investigated the interaction between the sample and the plasma to gain a better understanding of its impact on the quality of the grown layers. The final objective of this chapter was to study the feasibility of implementing stacking layers as a means to reduce dislocations propagation and improve the development of Schottky diodes. We pay a particular attention to lightly boron-doped layers as they constitute the active layer of the device.

Indeed, the optimization of growth parameters for boron-doped CVD diamond layer is crucial for obtaining high-quality diamond films with the desired electrical and optical properties. Although boron doping has been shown to significantly enhance the electrical conductivity of diamond films, the determination of the correct parameters to achieve the desired conditions remains challenging due to the complex interaction between the plasma and the substrate. Additionally, achieving dislocation-free or low-density boron-doped CVD diamond films remains ongoing challenges.

In this chapter, we will start with reporting on the effect of different plasma contact modes on the growth of boron doped CVD diamond films. Then we will also proceed to several experiments in order to find the optimal conditions leading to the growth of high quality boron doped films. Finally, we will focus on the study of stacking layers to highlight the behavior of dislocations propagation among different layers. Understanding the formation mechanisms of the dislocations and finding ways to minimize their formation is essential for the improvement of the quality of CVD diamond films.

To achieve our objectives, we will employ various characterization techniques such as Raman and cathodoluminescence (CL) spectroscopy to measure the structural and optical properties of the boron doped CVD diamond films and obtain evidence of any dislocations that may emerge. Another essential tool in the characterization of our samples is the Confocal Laser Scanning Microscopy (CLSM), because it provides a non-destructive method to image the diamond film morphology, including the distribution of defects after plasma etching induced by dislocation. This information is of main interest to determine the quality of the diamond film.

## 3.2 Growth parameters optimization for boron doped CVD diamond growth

### 3.2.1 Influence of sample position in the plasma

The position of the substrate in the plasma is crucial for the growth of high-quality diamond films during the chemical vapor deposition (CVD) process since it has a strong impact on its temperature and the species that contribute to its growth. It affects the growth rate and the overall quality of the films [1-4].

In our boron-doped cylindrical quartz tube reaction chamber (SSDR 150 reactor), we can modify the sample's position with respect to the plasma ball region without any modification on the microwave cavity and then by keeping plasma ball at the same position.

The SSDR machine allows for vertical motion of the sample with micrometric step movement during the growth. This provides an extra degree of freedom compared to other MWPCVD reactors and allows for better thermal control over the substrate during long growth durations. In this context, we will briefly discuss and provide some examples of the interaction between the plasma and the samples.

#### 3.2.1.1 Description of plasma/sample contact modes.

Three different positions were tried during this thesis and we will briefly discuss about them with respect to the distance between the sample and the plasma.



- Inside plasma mode (Figure III.1 (a)): in this case the sample is immersed almost completely inside the plasma and highly exposed to the species produced in the core of the plasma. The growth temperature is higher leading to a higher growth rate the formation of defects which deteriorate the diamond quality [5] as presented on Figure III.1 (d).
- Direct plasma contact mode (Figure III.1 (b)): in this case, the surface of the sample is positioned at the contact of the plasma "ball". In this configuration, the distribution of the plasma species at the surface is probably less homogenous during the process and for longer growth time, the surface morphology is affected as it can be seen in Figure III.1 (e).
- Indirect plasma contact mode (Figure III.1 (c)): in this case, a better control of the growth environment can be achieved as the sample is positioned further away from the plasma "ball". This allows for a better control of the surface morphology (Figure III.1 (f)) even if a slower growth rates is obtained (Figure III.1 (f)).

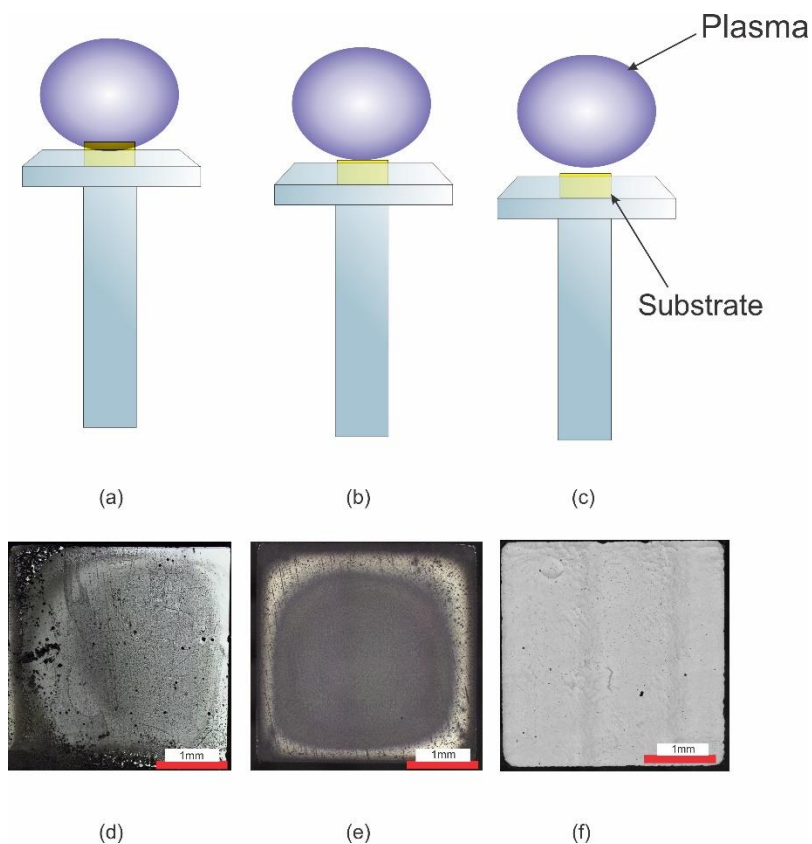


Figure III.1 – Different positions of the sample with respect to the plasma ball and some examples of corresponding surface morphologies; (a) inside the plasma mode, (b) direct contact mode, (c) indirect contact mode, (d) inside the plasma mode surface morphology, (e) direct contact surface morphology and (f) indirect contact surface morphology

It is important to note that, beyond the aspect of surface morphology, the choice of plasma contact mode may have a significant impact on the other properties of the diamond films such as growth rate, crystalline quality and boron doping concentration. Understanding and controlling the plasma contact mode is then crucial for the optimization of diamond film growth.

However, for the purpose of this thesis, we decided to not extensively discuss the intricacies of the different contact modes. Instead, we present findings from the indirect plasma contact mode, which is considered as the most appropriate for producing high-quality films for long growth deposition durations. Consequently, we concentrate our efforts on other critical factors, such as microwave power density,  $(B/C)_{\text{gas}}$  ratio and addition of oxygen in the gas phase and methane concentrations, which will be discussed in more detail in the ensuing paragraphs.

### 3.2.2 Influence of microwave power density

As presented before in the manuscript, one of the aims of this work was to optimize the growth conditions of boron-doped diamond films in order to obtain thick and high-quality layers. High microwave power density is generally accepted to be a favorable condition for reaching high growth rate and preserving high-quality crystal [6].

However, the boron doping efficiency is reduced and high amount of boron must be injected in the gas phase to reach high boron doping [7]. Unfortunately, it results in soot formation that requires stopping the deposition process to avoid damages to the reactor. To overcome this limitation, a low amount of oxygen (0.25%) was also added in order to delay soot formation promoted by diborane gas, nevertheless, it is necessary to modify the standard process by adjusting the pressure and microwave power density during deposition.

However, even after several adjustments it was shown at LSPM that using a bell jar machine, the growth of thick and heavily boron doped films remains very difficult because, after few days of deposition, it was impossible to totally avoid soot formation at the top of the bell jar which strongly absorb microwave energy and requires, for safety reasons, to stop the process.

This is the main reason why Plassys designed the new SDR 150 machine described in the chapter 2, which was delivered at the beginning of my PhD thesis, and the first part of my work was to test this new machine, particularly in high power density conditions. The first set of growth parameters used is detailed in table III.1 and the growth duration was 6h starting from (100)-oriented HPHT substrates.

The growth rate was determined from the difference in film thickness before and after deposition and the surface morphology was studied using CLSM microscopy.

1 <sup>st</sup> set of growth parameters	
Substrate	HPHT – 1b <100>
Pressure	250 mbar
MW Power	3.5 kW
Total gas flux	200 sccm
CH <sub>4</sub>	5%
O <sub>2</sub>	0.25%
Temperature of the sample	850 °C ± 30 °C
(B/C) <sub>gas</sub>	20,000 ppm
Precursor gas	Diborane
Thickness deposited	30 μm
Growth rate	5 μm/h

Table III.1 – Growth conditions used during the first experimental growth optimization

To assess the quality of the deposited film, Raman spectroscopy was performed. Pronounced peaks were observed nearby the 500-600 cm<sup>-1</sup> suggesting high boron doping levels. The diamond peak was observed at 1328 cm<sup>-1</sup> with a FWHM of 5 cm<sup>-1</sup>, indicating a shift to lower values compared to the characteristic diamond peak usually localized at 1332.5 cm<sup>-1</sup> which corresponds to what is expected for high boron doping level [7].

In his thesis work, R. Issaoui reported [8] that for boron doping values below 10<sup>19</sup> cm<sup>-3</sup>, the position of the Raman peak remains comparable to that of intrinsic material in the case of homoepitaxy. In our study, the Raman peak position decreased by 4.5 cm<sup>-1</sup>, which may suggest boron doping levels higher than 10<sup>19</sup> cm<sup>-3</sup>. Indeed, higher boron concentration leads to higher strain in the diamond cell

which can be observed with a shift of the diamond Raman peak to lower values. Moreover, the large FWHM enhances this explanation and can be attributed to higher strain.

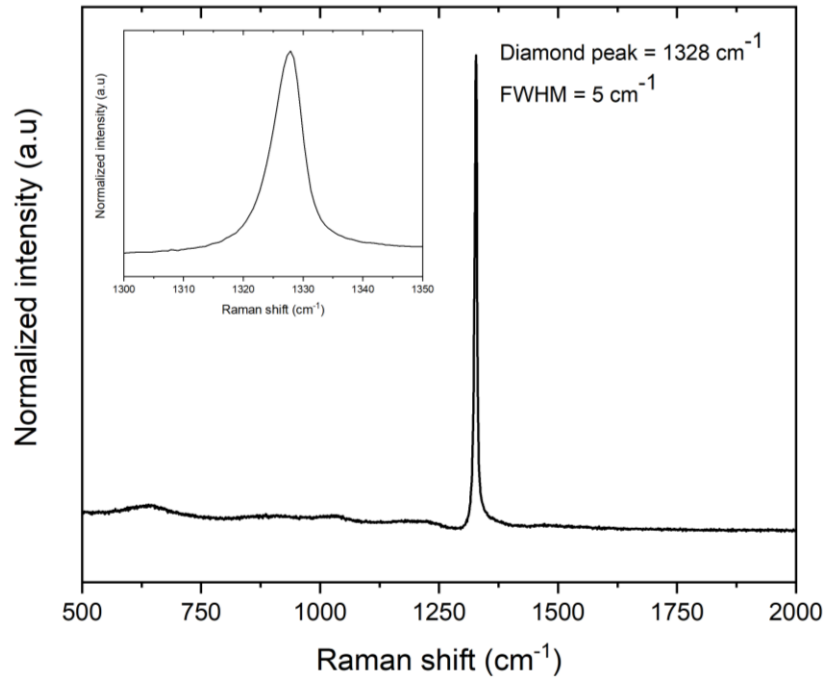


Figure III.2 – Raman spectrum of the grown sample with the first growth conditions

The FWHM of 5 cm<sup>-1</sup> of the sample could be attributed to the doping-induced disorder in heavily boron-doped diamond films, in accordance with the Fano effect [9-12]. This broadening makes it difficult to assess the crystalline quality of the film based solely on the FWHM.

To estimate the boron concentration in the sample, a Raman web tool was employed[13]. It was developed by Ing. M. Lamac, Msc. L. Iwanikov, and Dr. V. Mortet from the Department of Functional Materials at the Institute of Physics of the Czech Academy of Sciences and provides advanced analysis capabilities for Raman spectra. It is specifically dedicated to boron-doped materials and has been used as a reference for assessing the boron doping level in our samples. The boron concentration in this sample was estimated to be approximately  $1 \times 10^{20}$  at cm<sup>-3</sup>.

Nevertheless, SIMS analysis should be also performed to validate the estimation using the Raman web tool and the value determined here must be considered as a reference rather than as an absolute measure of the boron concentration in the film.

Although the growth rate was relatively high (approximately 5  $\mu\text{m}/\text{h}$ ), the first try to obtain thick and highly boron-doped layers using these growth conditions showed random patterns on the surface. Figure III.3 shows a picture obtained with the CLSM revealing the presence of etch pits at the surface of the sample. Thus, even if a high boron concentration can be obtained, the surface morphology of the samples was not uniform further optimization of the growth conditions is required to obtain high-quality boron doped films.

The presence of etch pits after the growth is not usual because they are basically obtained only after an etching step used to reveal threading dislocations and performed with  $\text{H}_2/\text{O}_2$  plasma [14, 15]. In our case we attributed such behavior to two possible causes: i) the growth rate of the faces of the etch pits is lower than that of the (100) face, ii) the high  $(\text{B}/\text{C})_{\text{gas}}$  values in the gas phase used for the growth could lead to local etching phenomenon already observed in the literature and not very well understood at the moment [7, 16].

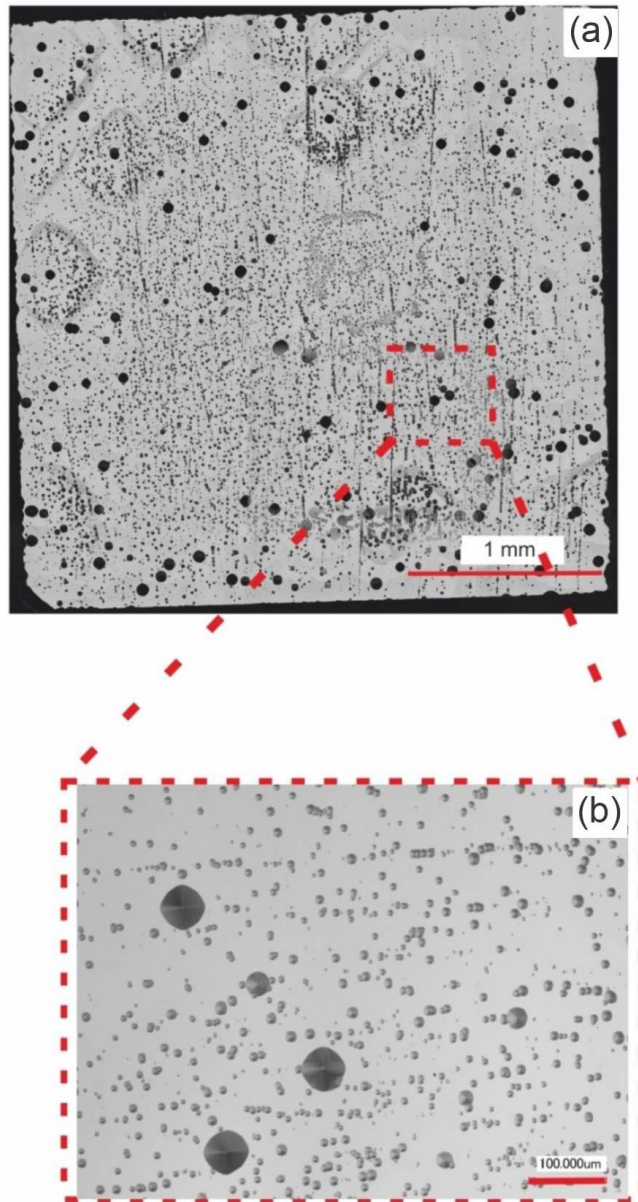


Figure III.3 - CLSM Images of the first recipe tested and a magnification Zone; (a) CLSM image of the full surface, (b) Magnified view of the dislocations in the first sample

In order to determine what the main cause is responsible of the etch pits, we decided to modify the growth conditions and in particular the methane concentration in the gas mixture. The main aim is to change the growth rate and limit the possible cause i).

### 3.2.3 Influence of methane

The specific parameters used are presented in Table III.2.

2 <sup>nd</sup> set of growth parameters	
Substrate	HPHT – 1b <100>
Pressure	250 mbar
MW Power	3.5 kW
Total gas flux	200 sccm
CH <sub>4</sub>	6%
O <sub>2</sub>	0.25%
Temperature of the sample	850 °C ± 30 °C
(B/C) <sub>gas</sub>	20,000 ppm
Precursor gas	Diborane
Thickness deposited	30 μm
Growth rate	5.5 μm/h

Table III.2 - Fixed conditions during the second experimental growth optimization

In this set of experiments, boron-doped diamond film was grown with a slight increase in methane concentration (6%) while maintaining the other process conditions. Raman spectroscopy was also performed with a diamond peak observed at 1327 cm<sup>-1</sup>, which is similar to the tendency observed for the previous sample with a shift to lower values.

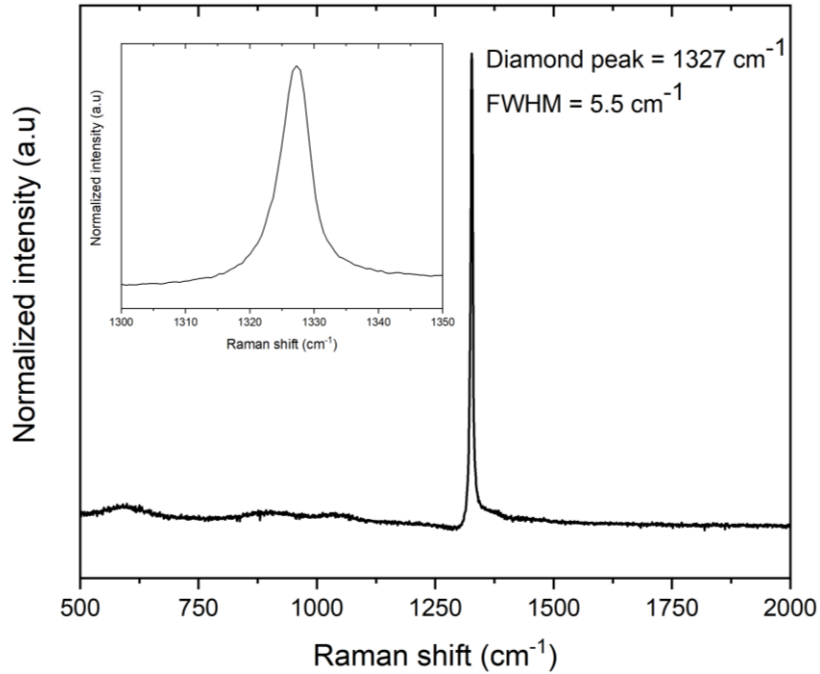


Figure III.4 – Raman spectrum of the sample

The full width at half maximum (FWHM) of the sample was 5.5 cm<sup>-1</sup>, which is a slightly higher than the FWHM of the previous sample. Pronounced peaks were observed nearby the 500-600 cm<sup>-1</sup> range as with the previous sample, which suggests that these samples are also highly doped. Indeed, we observe a slightly increase in the growth rate, which can be attributed to the increase in methane, as well as it may be an increase in boron incorporation [17]. This behavior is likely due to the variation in the concentration of CH<sub>3</sub> and atomic hydrogen at the diamond surface[18, 19]. Finally, according to the Raman web tool, the value for boron doping in the samples is approximately 2x10<sup>20</sup> at cm<sup>-3</sup>.



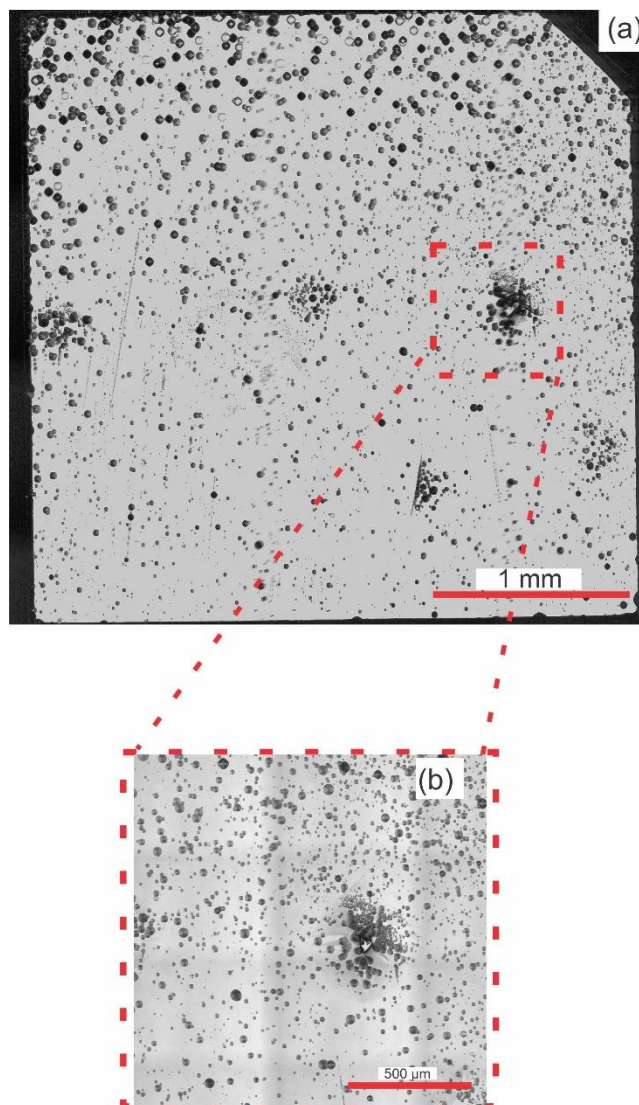


Figure III.5 - Confocal laser microscope images of the second recipe tried after deposition with its respective magnification

Nevertheless, despite the increase of the methane concentration in the gas phase, random patterns were still observed on the sample surface, as observed by CLSM microscopy (Figure III.5). The surface morphology still presents some etch pits as already observed. Even if the Raman analysis indicated relatively high boron doping in the sample, the surface remained non-uniform. These results suggest that solely increasing the methane concentration was not sufficient to achieve thick, highly boron-doped layers without etch pits.

As previously mentioned, the observed etch pits on the surface of the diamond samples could be also attributed to the high  $(B/C)_{gas}$  ratio in the gas phase during the deposition process which could result in etching [16]. Thus we decided to use conditions with lower  $(B/C)_{gas}$  but as it leads to a decrease of boron doping level, we decided in the same time to also reduce the microwave power density which is known to affect the boron doping efficiency [20].

### 3.2.4 Microwave power and $(B/C)_{gas}$ reduction

The microwave power density (MWPD) was reduced, by decreasing both microwave power and pressure in order to keep the same plasma volume. We also reduced the  $(B/C)_{gas}$  ratio in the gas phase as explained at the end of the previous paragraph. Two different samples have been grown: sample A with a  $(B/C)_{gas}$  of 15,000 ppm and sample B with 12,000 ppm. The new set of parameters is presented in the table III.3.

3 <sup>rd</sup> set of growth parameters	
Substrate	HPHT – 1b <100>
Pressure	150 mbar
MW Power	2.5 kW
Total gas flux	200 sccm
CH <sub>4</sub>	6%
O <sub>2</sub>	0.25%
Temperature of the sample	850 °C ± 30 °C
$(B/C)_{gas}$	Sample A with 15,000 ppm and Sample B with 12,000
Precursor gas	Diborane
Thickness deposited	≈ 60 μm for both samples
Growth rate	≈ 2.5 μm/h

Table III.3 - Fixed conditions during the third experimental growth optimization

As expected, by reducing the microwave power density, the growth rate has been decreased to about 2.5 μm/h, leading to a total growth thickness of approximately 60 μm after 24 hours of deposition, whatever the diborane concentration in the gas phase.

In this set of experiments, the Raman spectra analysis exhibited a diamond peak at  $1326\text{ cm}^{-1}$  for the sample A and  $1327.9\text{ cm}^{-1}$  for the sample B that again indicates a shift to lower values with respect to the typical diamond peak at  $1332.5\text{ cm}^{-1}$ . The analysis also revealed a more pronounced asymmetry of the diamond peak due the Fano effect, with a FWHM of  $6.5\text{ cm}^{-1}$  for sample A and  $6\text{ cm}^{-1}$  for sample B.

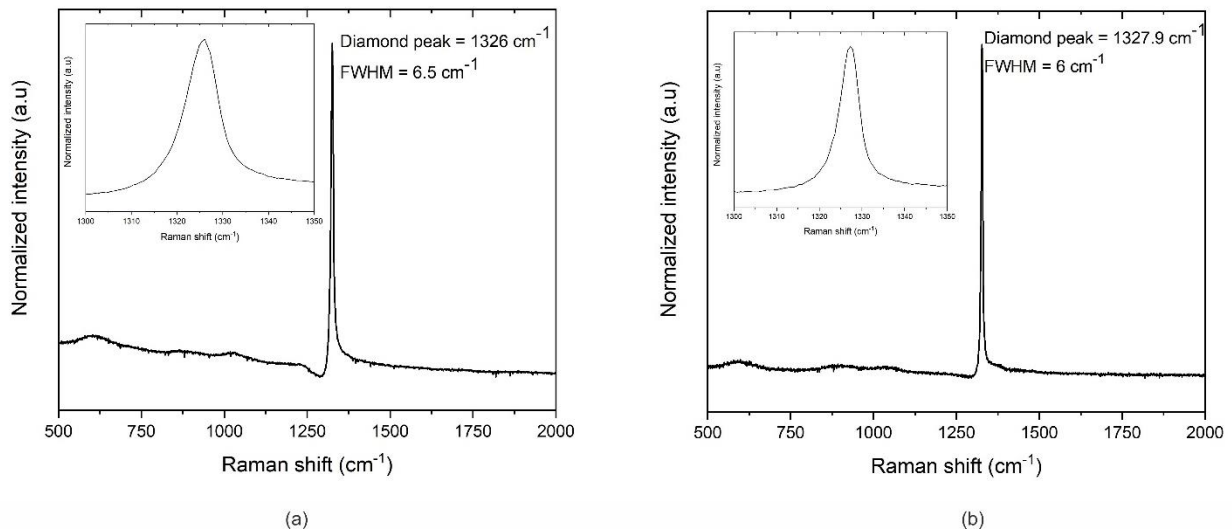


Figure III.6 - Raman analysis of (a) sample A (15,000 ppm) and (b) sample B (12,000 ppm)

Interestingly, there were also pronounced peaks nearby the  $500\text{-}600\text{ cm}^{-1}$  range, indicating that these samples should have similar doping level compared to the previous set of experiments, which has been confirmed using Raman Web tool. A boron doping concentration of approximately  $2 \times 10^{20}$  at  $\text{cm}^{-3}$  has been estimated.

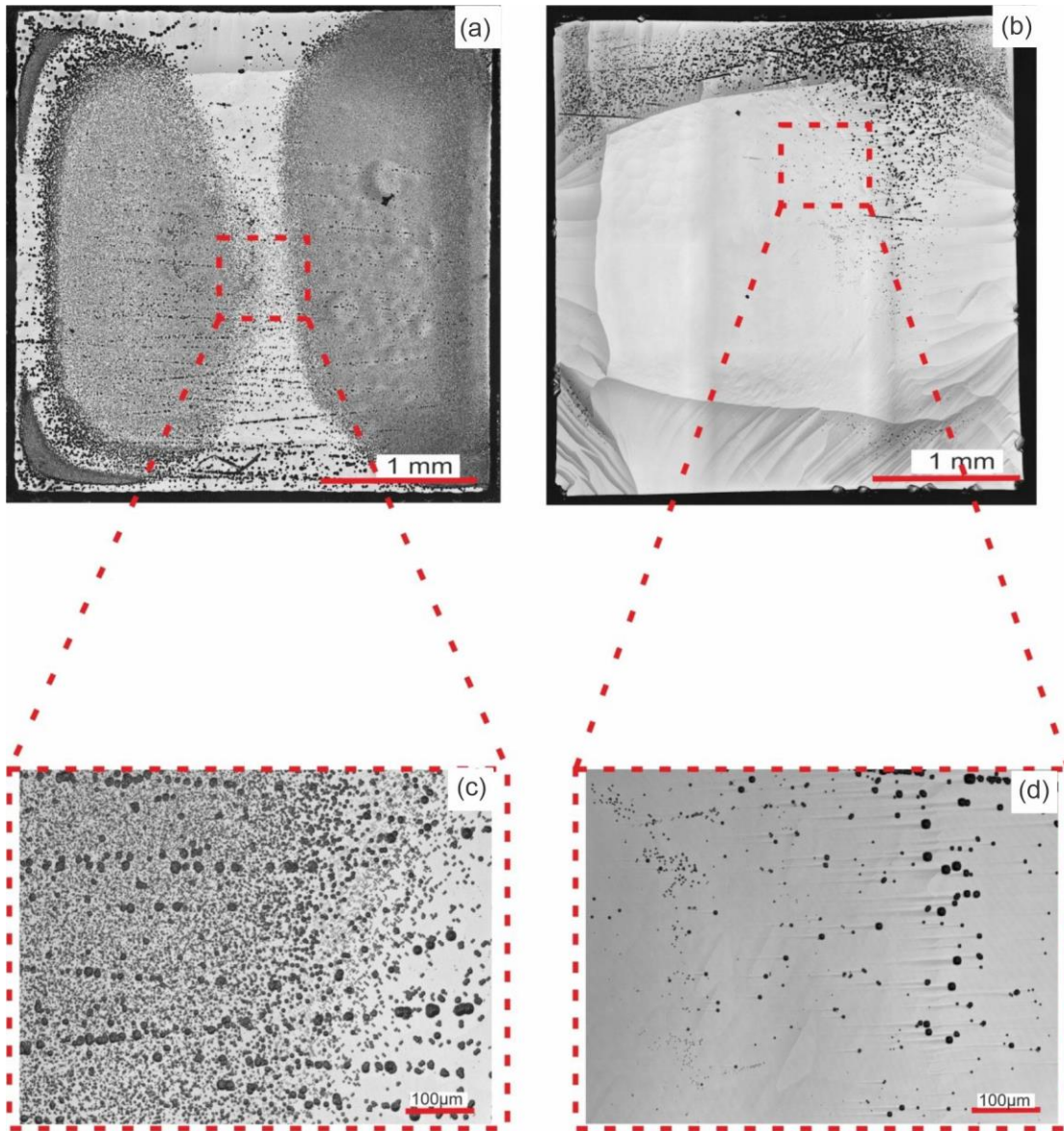


Figure III.7 - Confocal Laser Microscopy (CLSM) Images of the sample A and B grown using the third recipe; (a) CLSM image of sample A, (b) CLSM image of sample B, (c) Magnified view of the dislocations in Sample A, (d) Magnified view of the dislocations in sample B.

After reducing power, pressure, and  $(B/C)_{\text{gas}}$  ratio, the layers that were obtained showed better results in terms of surface morphology, as shown in Figure III.7, even if the appearance of etch pits in some areas of the samples are still observed. It is also interesting to note that the sample grown with a lower  $(B/C)_{\text{gas}}$  ratio leads to a better surface morphology.

This indicated that the influence of  $(B/C)_{\text{gas}}$  ratio is strong and a last set of growth conditions was performed by strongly reducing the  $(B/C)_{\text{gas}}$  ratio to 6,000 and 5,000 ppm. Table III.4 shows the last conditions used in the optimization process.

4 <sup>th</sup> set of growth parameters	
Substrate	HPHT – 1b <100>
Pressure	150 mbar
MW Power	2.5 kW
Total gas flux	200 sccm
CH <sub>4</sub>	6%
O <sub>2</sub>	0.25%
Temperature of the sample	850 °C ± 30 °C
$(B/C)_{\text{gas}}$	Sample C with 6,000 ppm and Sample D with 5,000
Precursor gas	Diborane
Thickness deposited	≈ 50 μm for both samples
Growth rate	≈ 2 μm/h

Table III.4 - Fixed conditions during the last experimental growth optimization

In this final round, the Raman spectra analysis revealed that the diamond peaks were located at 1330 cm<sup>-1</sup> for sample C and 1328 cm<sup>-1</sup> for sample D, respectively. These results are consistent with our previous results in which a shift to lower wavenumbers is observed.

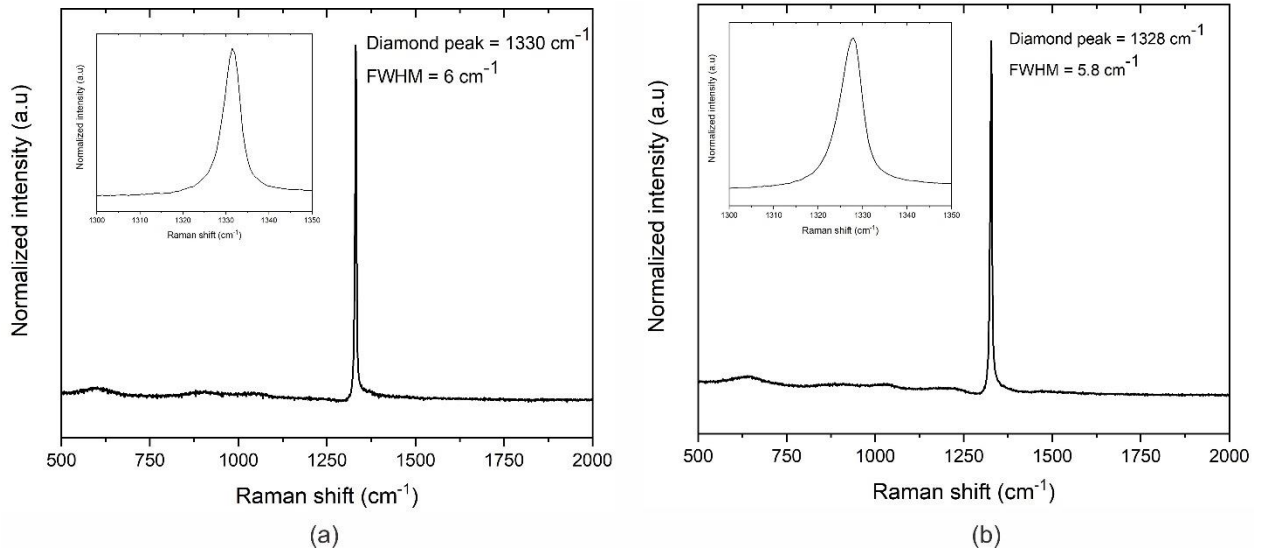


Figure III.8 – Raman analysis of (a) sample C (6000ppm) and (b) sample D (5000 ppm)

Once again, Raman spectra demonstrated a notable asymmetry in the Fano effect, affecting the full width at half-maximum (FWHM) values, which were 6 cm<sup>-1</sup> and 5.8 cm<sup>-1</sup> for sample C and D, respectively. Additionally, the pronounced peaks around the 500-600 cm<sup>-1</sup> range may suggest high levels of boron doping. Values determined using the Raman web tool was approximately  $4 \times 10^{20}$  at cm<sup>-3</sup> and  $2.2 \times 10^{20}$  at cm<sup>-3</sup> respectively.

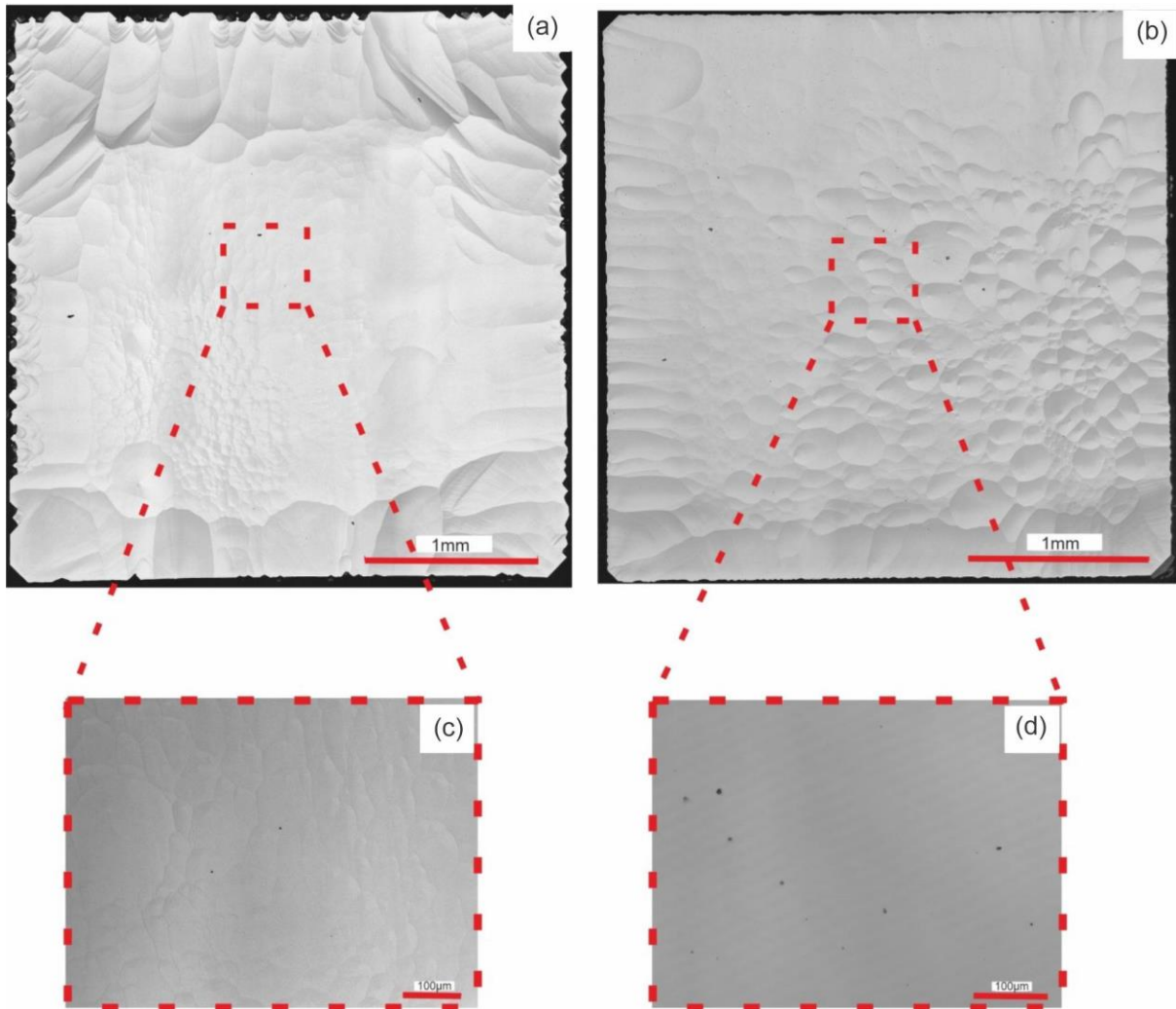


Figure III.9 - (CLSM) Images of the first recipe tested and magnification zones of the samples performed with the last recipe improvement; a) Sample C (6000 ppm) and b) Sample D (5000 ppm), (c) Magnified view of sample C, (d) Magnified view of sample D.

Figure III.9 shows the surface morphologies of diamond samples obtained for the last set of samples and we can clearly see a strong improvement of the surface morphology since no etch pits and a very smooth surface is observed. Moreover, we can see that the morphology of the 2 samples is very similar. Although the growth rate was not as fast as we would desire (approximately  $2 \mu\text{m/h}$ ) the reduction of the  $(B/C)_{\text{gas}}$  ratio below 6,000 ppm allows keeping a good surface morphology with a high doping level since, the sample surfaces are now smooth and free of etch pits, indicating that the optimization efforts were successful.

It must be noticed that similar boron concentration for different  $(B/C)_{gas}$  have been obtained. It could be due to the fact that the concentration of boron atoms incorporated into the diamond lattice may have reached a saturation point, where adding more diborane may not result in a significant increase in boron incorporation.

Overall, it is likely that multiple factors are at play in determining the boron incorporation levels and Raman spectra of the diamond films. Further experimentation and analysis would be needed to fully understand the underlying mechanisms.

The Figure III.10 summarizes our work and the different steps a), b), c) and d) in finding the optimal conditions for producing heavily boron-doped diamond samples with good surface morphology. Although the growth rate is not as fast as desired, we decided to accept this compromise of growing layers slower to ensure good quality by using the recipe d).

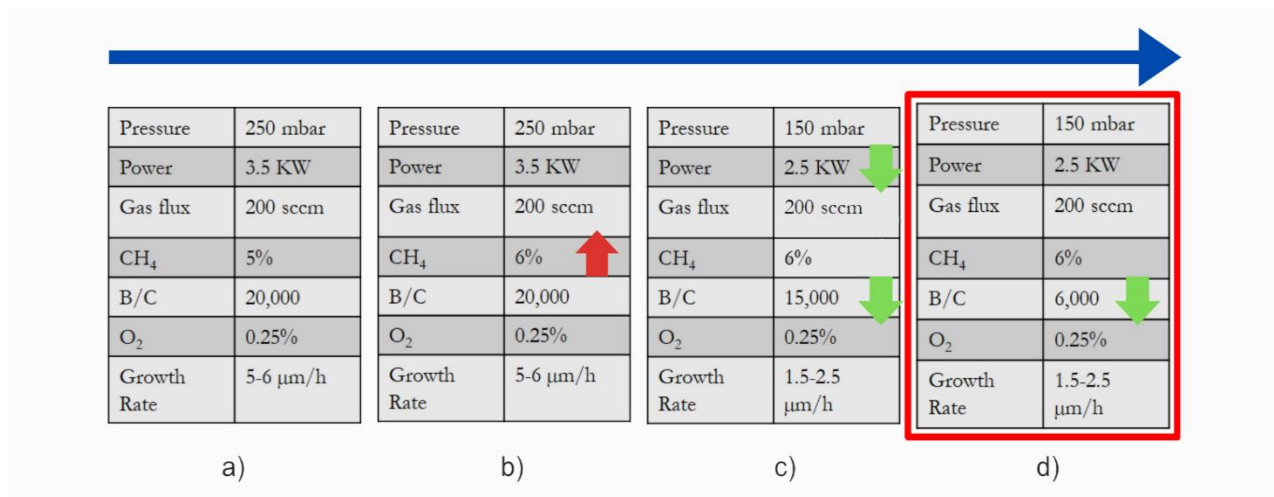


Figure III.10 – Comparative recipes used in our optimization process highlighting d) as the best compromise in terms of surface morphology and growth rate

As previously stated, boron concentration has been only estimated starting from Raman spectroscopy requiring a more quantitative method to precisely determine the level of doping in our samples. It is the main purpose of the next paragraph.



### 3.2.5 Measurements techniques for boron doping concentration

As presented in more details in chapter 2, secondary ions mass spectrometry (SIMS) is one of the most relevant techniques to quantify boron concentration particularly for heavily boron doped samples even if cathodoluminescence (CL) can be a complementary technique. The main objective of this part is to finalize the optimization of the growth process by modifying very slightly the boron concentration in the films and  $(B/C)_{\text{gas}}$  ratio and have a more precise evaluation of the boron doping.

Three samples have been grown in the experimental conditions presented in Table III.5. The only parameters that have been slightly changed are methane concentrations (5% and 6%) and  $(B/C)_{\text{gas}}$  ratio in the gas phase (6000 and 5000 ppm).

Sample	KCR202022	KCR202023	KCR202030
Pressure (mbar)	150	150	150
MW Power (kW)	2.5	2.5	2.5
Gas Flux (sccm)	200	200	200
CH <sub>4</sub>	6%	6%	5%
O <sub>2</sub>	0.25%	0.25%	0.25%
T (°C)	850	850	850
$(B/C)_{\text{gas}}$ (ppm)	6000	5000	6000
Time (h)	24	24	24
$[B]_{\text{film}}$ (at/cm <sup>3</sup> )	$1.5 \times 10^{20}$	$1 \times 10^{20}$	$4.6 \times 10^{19}$

Table III.5 – Samples growth conditions with their respective boron concentration estimated by SIMS measurements

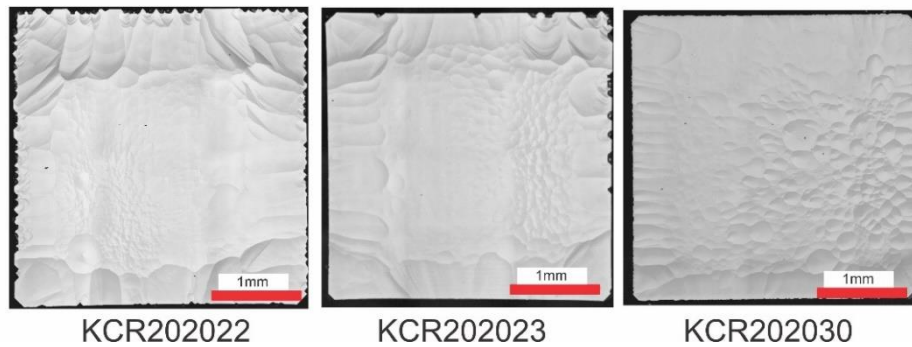
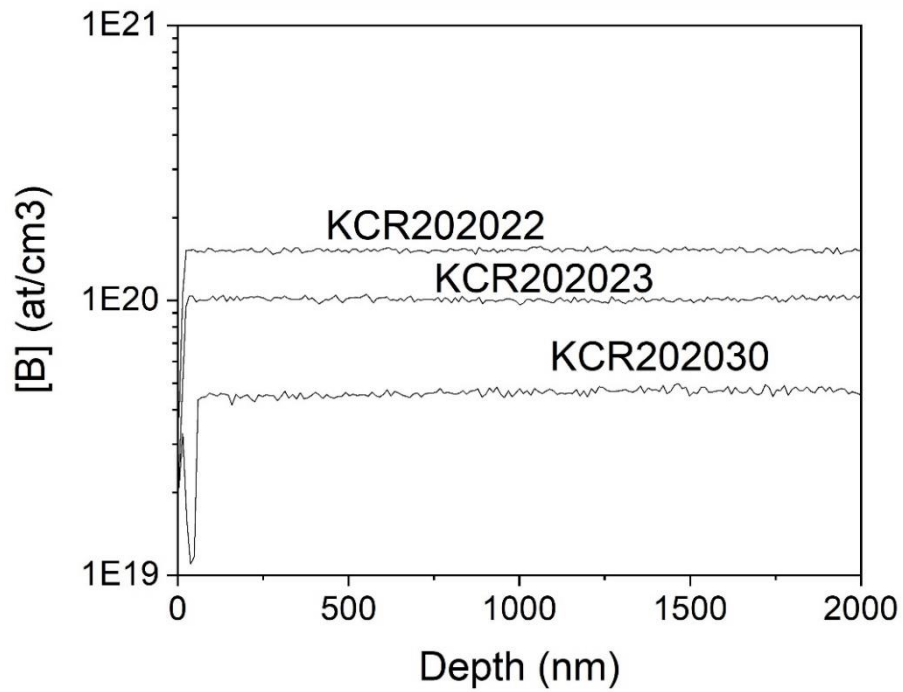


Figure III.11 – SIMS profile of the first 2  $\mu\text{m}$  of the boron-doped layers grown with different methane concentrations and the corresponding surface morphology.

Figure III.11 shows the profiles of boron concentration determined by SIMS in the last 2  $\mu\text{m}$  of the grown samples. Although a small decrease of the boron concentration at the top of the sample is observed, boron incorporation presents a good homogeneity for all the three samples. This indicates favorable doping efficiency, satisfying the prerequisites for optimal Schottky diode performance since the doping is very close, at least for 2 samples, to the metal transition.

We can also note an important point in these results. For similar boron concentration in the gas phase, the methane concentration can be a supplementary degree of freedom to increase boron doping level in the film. Indeed, an increase of methane concentration from 5 to 6% for a similar  $(B/C)_{\text{gas}}$  ratio allows to multiply the doping level by a factor of 2.

This increase in doping with methane concentration is in agreement with the results of Okushi et al, (2001)[21] and Baron et al. [22]. It may be associated with an increase in film growth rate. Indeed, it has been reported that an adsorbed boron impurity adsorbed on the diamond surface has a high probability of desorption[23] and therefore an increased growth rate, in the case of an increase in methane content, may allow boron to be rapidly incorporated into the crystal lattice before it can be desorbed. We attribute the variation in incorporated boron to the increased methane concentration in the gas phase, which may contribute to a change in adsorption/desorption probabilities and coverage rate.

As a conclusion, SIMS measurements confirm the high boron concentrations in our samples initially estimated by the Raman web tool.

Optimal growth conditions have been determined and are highlighted in Table III.5. It corresponds to a microwave power of 2.5 kW, a pressure of 250 mbar, 6% of  $\text{CH}_4$ , a  $(B/C)_{\text{gas}}$  ratio of 6000 ppm and 0.25%  $\text{O}_2$ . These conditions have shown to consistently produce high-quality layers with high boron incorporation (a few  $10^{20}$  B/cm<sup>3</sup>) and good morphology.

Based on the success of our optimized reactor parameters to produce heavily boron doped layers with good-quality, the next step was now to investigate different stacking layer configurations with the aim to optimize the performance of a Schottky diode by limiting as much as possible dislocations in the active p<sup>-</sup> layer. We propose four different configurations and will explore the advantages and disadvantages of each configuration for practical applications.

### 3.3 Exploring the Feasibility of Vertical Schottky Diodes with Diamond Layers: Investigations and Future Prospects

Diamond-based vertical Schottky diodes remain highly challenging and promising devices for the future development of high-power applications. Current research efforts are dedicated to uncovering their potential in high-frequency transistors and targeted power electronics applications [24, 25]. However, the development of these devices requires a precise control of the doping, with particular emphasis on minimizing defect density in the diamond layers.

One main point of the vertical Schottky diode design is the association of a  $p^+$  layer and a  $p^-$  layer. The  $p^+$  layer is heavily boron doped and creates a highly conductive contact layer for an ohmic contact on the backside. The  $p^-$  layer, on the other hand, is lightly doped with boron and constitutes the active layer of the diode. The thickness, the doping level and defect density of the  $p^-$  layer are critical factors for the performance of the device, as they affect the breakdown voltage, leakage current, and series resistance in the on-state [24].

Therefore, it is crucial to optimize the growth conditions and geometry of the diamond layers to achieve low defect densities in the  $p^-$  layer in order to improve the performances and reliability of diamond-based vertical Schottky diodes.

This is the main purpose of the following paragraphs in which we have carried out a stacking layer study with the aim to determine the optimal approach to improve vertical Schottky diode performances.

**3.3.1 Stacking layer study**

In this section, we will describe the investigation of four different stacking layer configurations that are described in Figure III.12. Our objective is to identify the best one that leads to a  $p^-$  layer exhibiting a high quality with a low dislocation density.

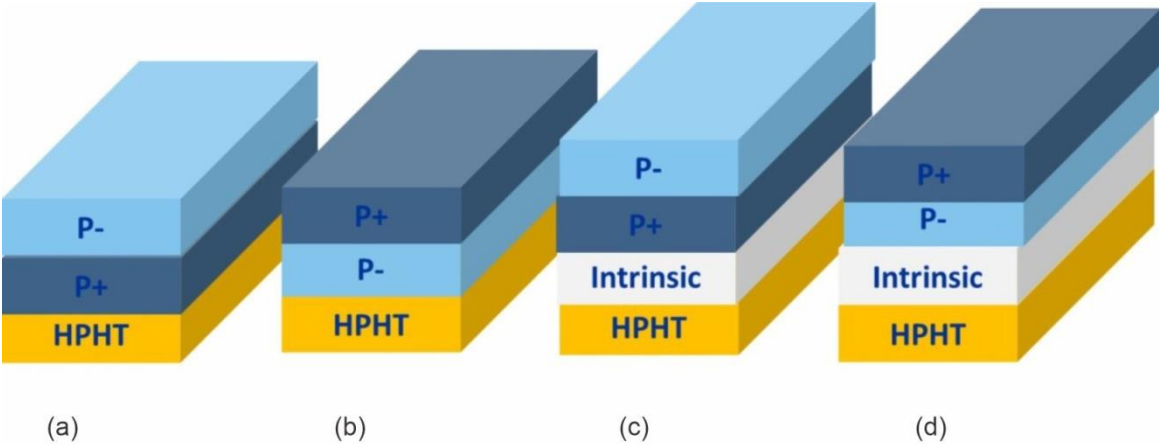


Figure III.12 – Different stacking layers proposed; (a) standard configuration, (b) inversed configuration, (c) standard configuration with a buffer layer and (d) inversed configuration with a buffer layer.

### 3.3.1.1 Sample preparation

To ensure consistency of our study, four (100)-HPHT commercially available substrates with similar characteristics were selected. In particular, we paid attention to have substrates with similar thicknesses, crystalline quality as it can be qualified by Raman spectroscopy. To remove surface impurities, the substrates underwent chemical cleaning using a 3:1 HCl:HNO<sub>3</sub> solution at 80°C for 50 minutes, followed by rinsing in water, acetone, and isopropanol. For each sample, the face having a single growth sector has been chosen using Diamond view setup as described in the chapter 2.

### 3.3.1.2 Growth conditions

For producing the stacking layers described in the Figure III.12, growth conditions given in Table III.6 have been used. Prior to the growth process, the surface underwent a preparation step involving etching with H<sub>2</sub>/O<sub>2</sub> (98:2) plasma for 30 minutes[26]. This etching procedure aimed to remove the top layer, which is typically damaged during the substrate polishing process, thereby ensuring an improved starting surface for the subsequent growth.

Layer	Intrinsic	Lightly boron doped	Heavily boron doped
(B/C) <sub>gas</sub> [ppm]	0	170	6000
Gas Flux [sccm]	200	200	200
CH <sub>4</sub> /Total gas	5%	6%	6%
O <sub>2</sub> /Total gas	0%	0.25%	0.25%
T [°C]	850	850	850
Microwave power [kW]	3	2.5	2.5
Pressure [mbar]	200	150	150

Table III.6 - Fixed conditions during the second experimental growth optimization

In order to limit the well-known memory effect when boron is introduced in a reactor, two different MPACVD machines were utilized for the growth of the different layers: one reactor dedicated to the growth of lightly and heavily boron-doped layers (SSDR machine), and another one to the growth of intrinsic layers.

For the heavily boron-doped layers, the growth was performed with the optimized conditions mentioned in the previous section. Lightly boron-doped layers were grown using the same conditions, but with a lower (B/C)<sub>gas</sub> ratio. The intrinsic diamond layers were grown using basic optimized growth condition for ultrapure diamond with a dedicated intrinsic diamond reactor[6].

### 3.3.1.3 Evaluation of Dislocation Density

To evaluate dislocation density, we followed the procedure developed in the lab and consisting in performing a plasma etching with  $H_2/O_2$  (98%/2%) in the same pressure and microwave power conditions than for the growth step, leading to etch pits formation [26]. As clearly demonstrated by LSPM [15], dislocation density can be estimated by statistically counting the number of etch pits.

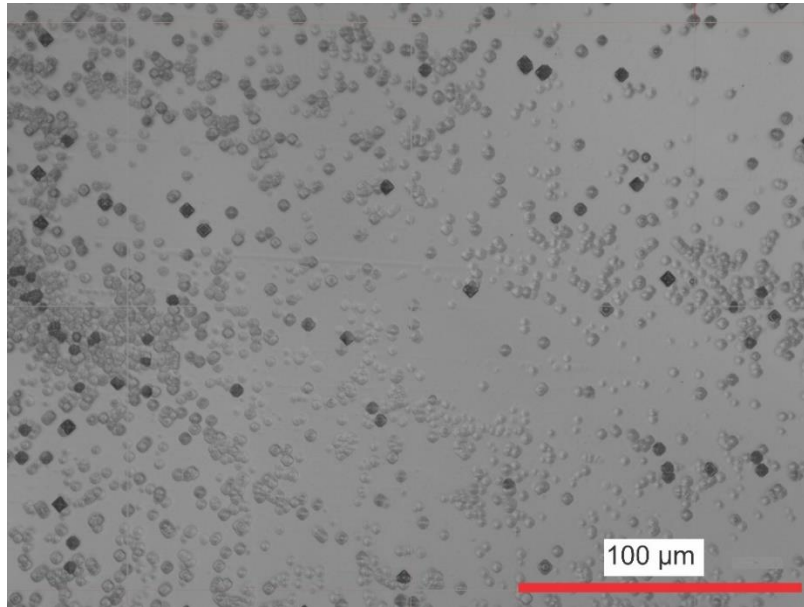


Figure III.13 - Typical CLSM picture of a magnified area obtained after plasma etching for etch-pits counting.

Thus, after the etching process, we utilized the Keyence VK 9700 CLSM to analyze the resulting surfaces. Using this device, the surface is divided into four  $100 \times 100 \mu m^2$  area enabling us, by using ImageJ software [27], to extract information from the images and count the number of etch-pits to determine dislocation density.

Nevertheless, we have to keep in mind that the procedure described is a semi-quantitative approach to estimate the dislocation density in a sample and should only be interpreted as a general trend, since the actual dislocation density can potentially slightly differ from the estimated value.

### 3.3.1.4 Description of the followed process

For each stacking layer configuration, the morphology before and after each growth step was analyzed using CLSM. Similarly, the crystalline quality of each layer was evaluated using Raman spectroscopy (Jobin-Yvon LabRam HR800) performed at room temperature with a 473 nm laser excitation before an etching step with  $H_2/O_2$  plasma for 10 minutes allowing to evaluate the dislocation density.

The Figure III.14 gives a summary of all the steps performed in this study.

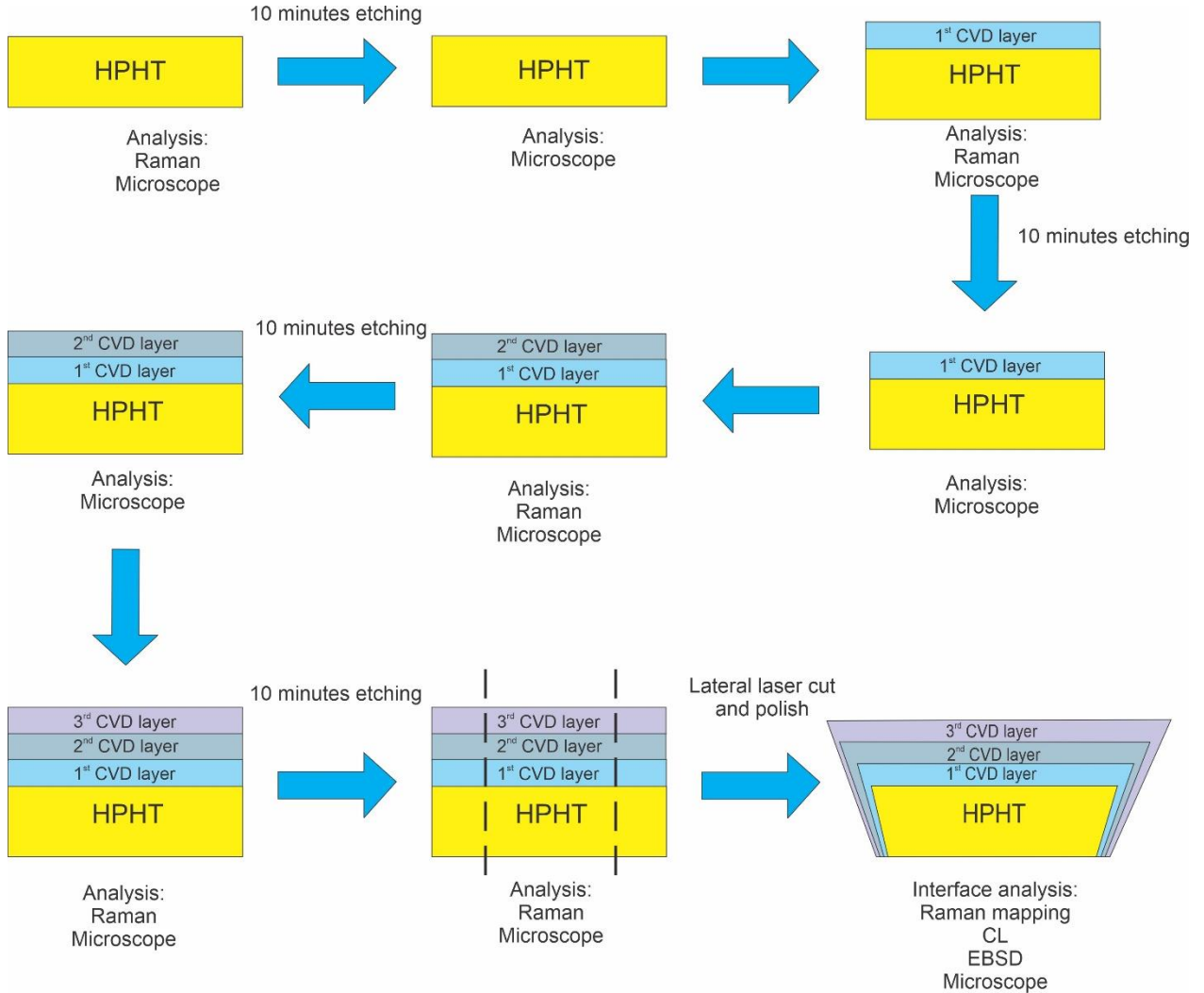


Figure III.14 – Summarized steps followed in this study

As previously described, the first step is the selection of four similar commercially available (100)-oriented HPHT substrates. The substrates underwent various analytical techniques such as CSLM and Raman spectroscopy. A 10-minute etching phase is then performed in order to estimate dislocation density which was around  $1 \times 10^5 \text{cm}^{-2}$  for the four substrates. The first chemical vapor deposition (CVD) growth was then performed, followed by new CSLM and Raman spectroscopy and another etching phase with dislocation counting.

This process is repeated until the desired number of CVD layers was achieved. Finally, the samples were sent to Almax company to undergo a lateral laser cutting and polishing and obtain a sample in

cross section, allowing observation and characterization of the different interface by Raman mapping, cathodoluminescence, and SEM imaging.

### 3.3.1.5 Results obtained from the stacking layer study

Figure III.15 shows the evolution of the Raman diamond peak of the different layers for two stacking layers configuration: the standard configuration with a buffer layer (Figure III.15 (a)) and the inverse configuration with a buffer layer (Figure III.15 (b)).

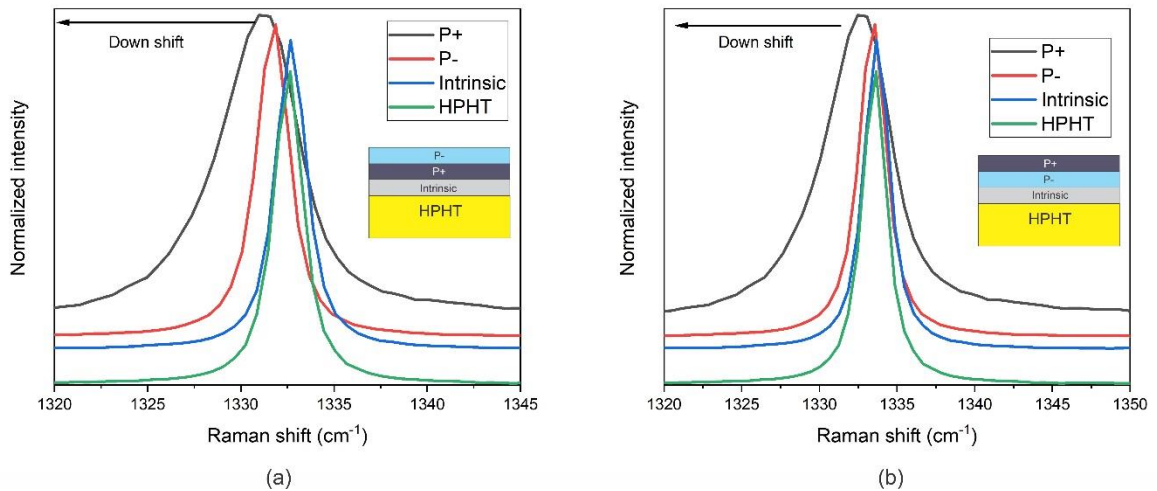


Figure III.15 - Raman diamond peak shift zoom of the different diamond layers; Boron doping leads to diamond peak enlargement and downshift

On these figures, we mainly focus on the FWHM of the intrinsic and  $p^-$  diamond peak since it gives an indication on the crystalline quality of diamond layers [28, 29]. Analyzing the  $p^-$  active layer for all the stacking configurations, we compiled the results in Table III.7 in which it can be observed that there is no major changes in the FWHM. It remains close to  $2\text{ cm}^{-1}$  regardless of the chosen configuration, indicating good crystalline quality.



For the heavily boron doped diamond, the FWHM enlarged from  $2 \text{ cm}^{-1}$  up to a range of  $4.1\text{-}6.5 \text{ cm}^{-1}$ , whereas its position downshifted by almost  $2 \text{ cm}^{-1}$ . Moreover, the asymmetry due the Fano effect is visible as well as the FWHM widening of the diamond peak and its downshift related to the compression stress of the layer [30]. These explanations are to be moderated by the fact that the Fano effect that we observe at higher boron concentration leads also to some shift of the Raman peak and increase of the FWHM.

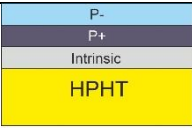
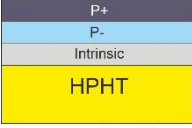
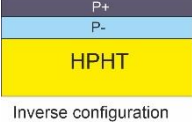
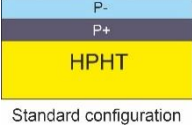
Configuration	HPHT FWHM	Intrinsic FWHM	P- FWHM	P+ FWHM
 <p>Standard configuration with buffer layer</p>	$2 \text{ cm}^{-1}$	$2.1 \text{ cm}^{-1}$	$2.1 \text{ cm}^{-1}$	$6.5 \text{ cm}^{-1}$
 <p>Inverse configuration with buffer layer</p>	$2 \text{ cm}^{-1}$	$2.1 \text{ cm}^{-1}$	$2.2 \text{ cm}^{-1}$	$5 \text{ cm}^{-1}$
 <p>Inverse configuration</p>	$2 \text{ cm}^{-1}$	NA	$2.2 \text{ cm}^{-1}$	$4.1 \text{ cm}^{-1}$
 <p>Standard configuration</p>	$2 \text{ cm}^{-1}$	NA	$2.1 \text{ cm}^{-1}$	$5.1 \text{ cm}^{-1}$

Table III.7 – Comparative table of the FWHM as an indicator of crystalline quality, making emphasis on the active layer (P-)

To further examine the influence of a high boron concentration on the FWHM, this value was plotted in the Figure III.16 as a function of boron concentration measured by SIMS for the samples E, F and G (heavily boron doped layers) and H and I (light boron doped layers).

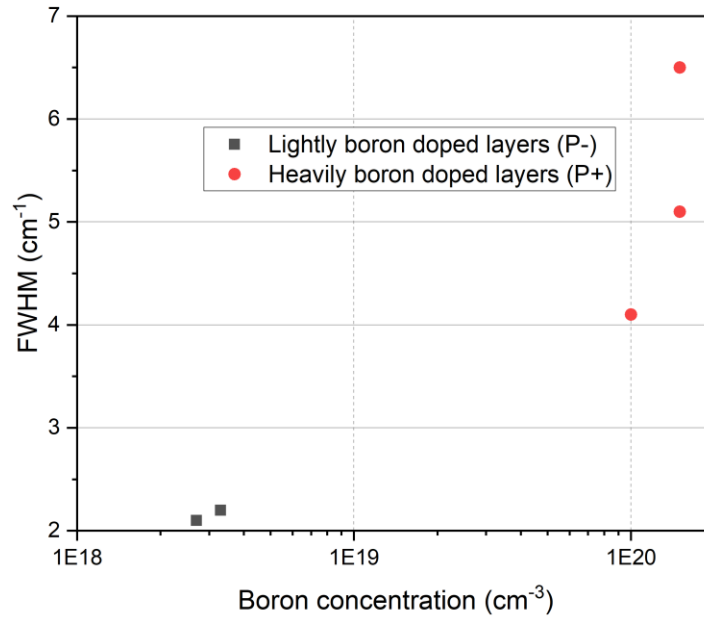


Figure III.16 – Evolution of the Raman diamond peak FWHM as function of boron doping level

The results showed that in the case of lightly boron-doped samples, the boron concentration was slightly higher than what is typically desired for the preparation of a vertical Schottky diode since the value is higher than  $1 \times 10^{18} \text{ cm}^{-3}$ . However, the film quality did not appear to be significantly affected. On the other hand, the FWHM for heavily boron-doped samples showed a strong increase which is not necessary due to deterioration in material quality.

Indeed, the lack of a clear discontinuity suggests that the broadening of the diamond Raman peak is primarily due to an increase in the doping level rather than a decrease in crystalline quality as already report by Boussadi et al [31]. This indicates that the film quality may remain relatively stable even with higher boron concentrations.

Beyond the crystalline quality of the P<sup>-</sup> layer, which seems not to be affected by the stacking layer configuration, we focused our attention on the threading dislocations. After the etching step of 10 minutes, etch pits counting were carried out for each grown layer, and the tendencies are depicted in Figure III.17.

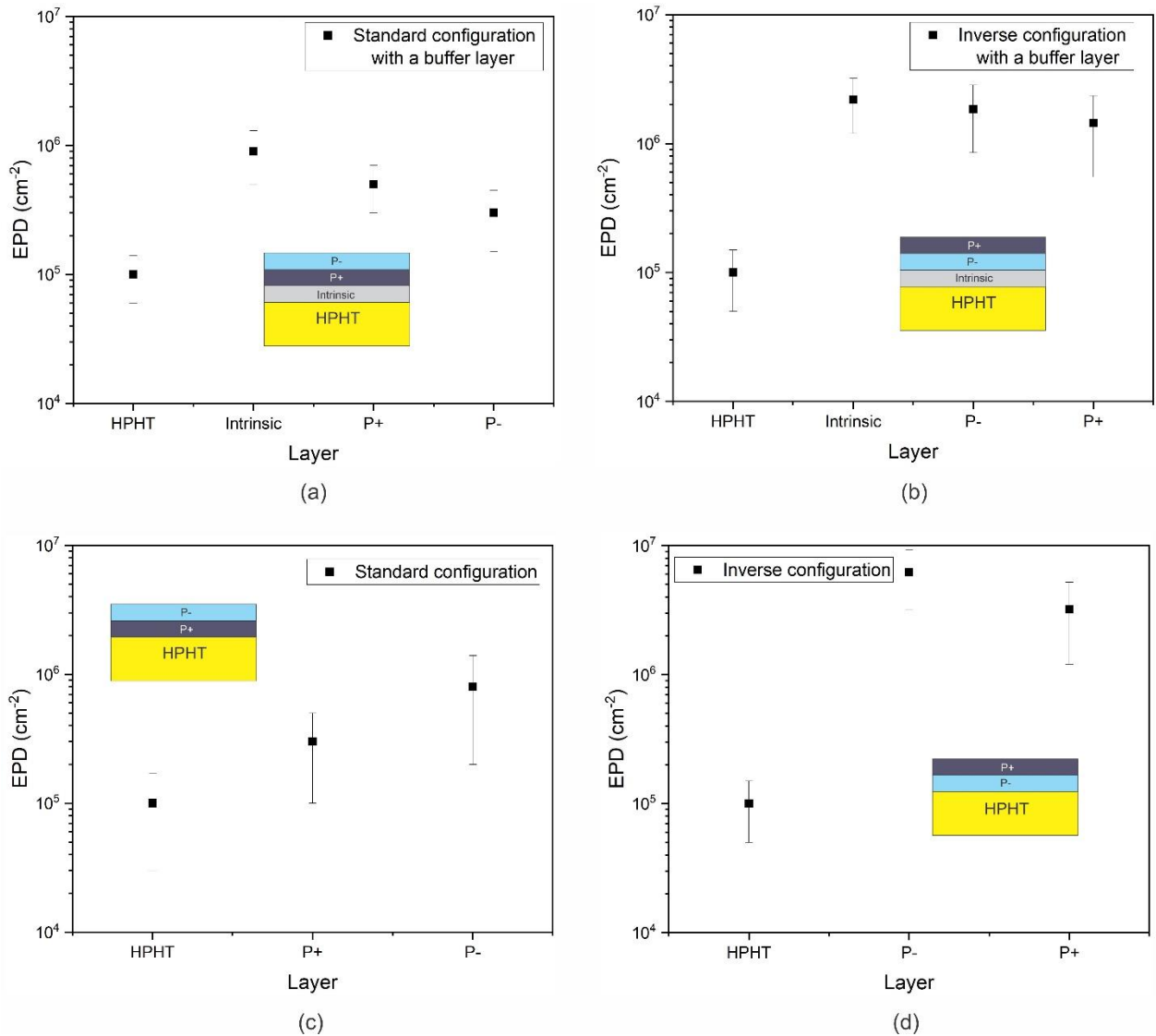


Figure III.17 - Evolution of the Etch-pits Density (EPD) on different stacking configuration layers. (a) Standard configuration, (b) Inversed configuration, (c) Standard configuration with buffer layer and (d) Inverse configuration with buffer layer.

The results of the dislocation density comparison between the different layers have shown some interesting tendencies. The first one is that an intrinsic buffer diamond layer just above the HPHT substrate does not seem to have a real advantage on the stacking configurations. In both cases the EPD increased by almost one order of magnitude.

One possible explanation could be attributed to the difference in terms of nitrogen concentration between the substrate and the intrinsic layer, which could induced some stress leading to dislocation formation.

On the other hand, the highly boron doped layers led to a different tendency since the EPD didn't increase so much and remained at the same order of magnitude or even decrease. This reduction in EPD in the boron doped layers could be attributed to the stress compensation induced by the high concentration of boron atoms in a similar manner than that related by S. Ohmagari et al.[32] in a study in which they introduced high levels of Tungsten.

In fact, authors explained that the propagation of dislocations in diamond films depends on the evolution of the strain in the grown film even if all the corresponding phenomenon are not completely understood and required more deep investigations.

As a partial conclusion, this study showed that EPD strongly increased when an intrinsic layer is deposited directly on HPHT substrate while the heavily boron doped layers showed a tendency to either keep constant or even decreased EPD. Thus, the standard configuration with  $p^-$  deposited on a  $p^+$  layer seems to be the most favourable configuration to contain dislocation density in the active layer.

In order to complete this study, the samples have been cut along the cross section to perform an interface analysis with the aim to have a better understating of the dislocation density improvement after the growth of highly boron doped layers.

### 3.3.2 Interface analysis

One of the most important aspects of the interface analysis is to follow the evolution of Raman and CL spectra along the growth direction in order to obtain a valuable insight into the growth process and the quality of the layers.

Figure III.18 (a) gives a visual representation of one of the fourth samples. It corresponds to the configuration (a) i.e. the deposition of a  $p^+$  layer on HPHT substrate followed by the deposition of the  $p^-$  layer. Figures III.18 (b) presents CSLM images of the complete cross-section area and Figure III.18 (c) shows a magnified view of the sample in which the distinction of the different layers based on the contrast is possible.

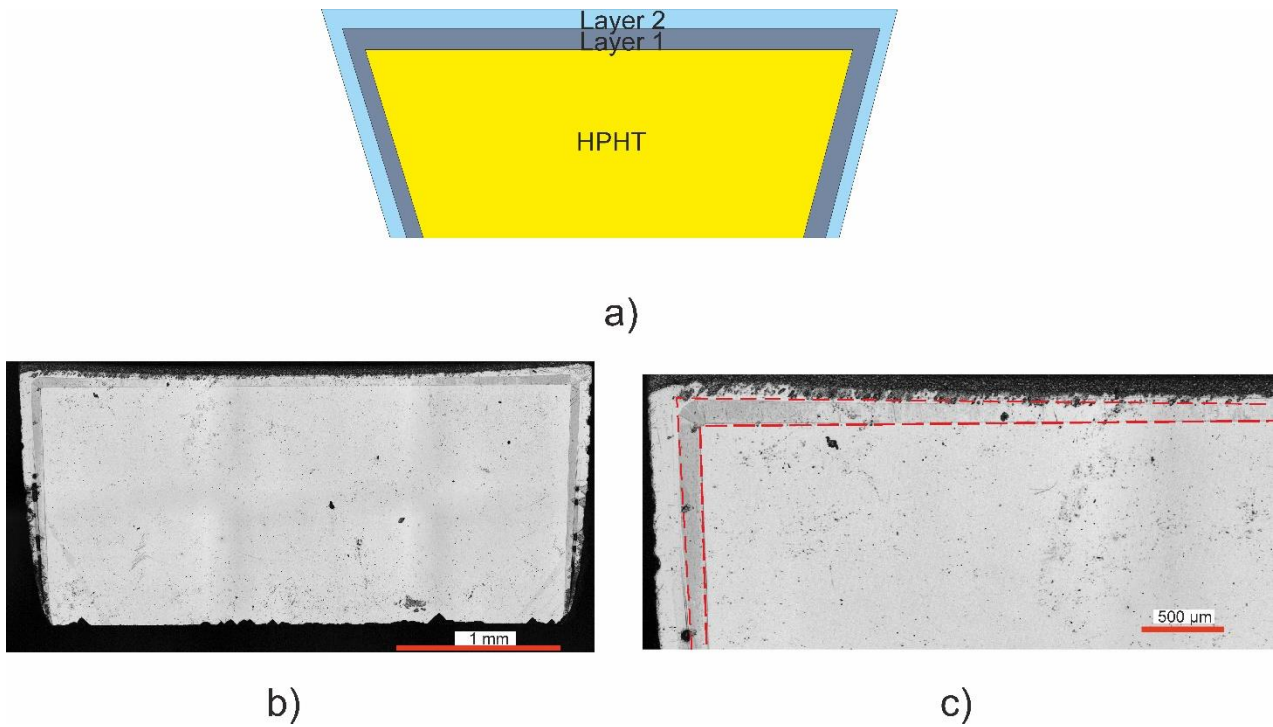


Figure III.18 - Cross-Section view of the Stacked Layers in configuration (a). (a) Schematic representation of the cross-section, (b) CSLM image of the complete cross-section. (c) Magnified view highlighting the distinct layers

### 3.3.2.1 Raman mapping

Raman mapping was carried out on the cross section in a  $250 \times 250 \mu\text{m}^2$  area covering the interface between the layers. The scanning step was  $10 \mu\text{m}$  along each axis.

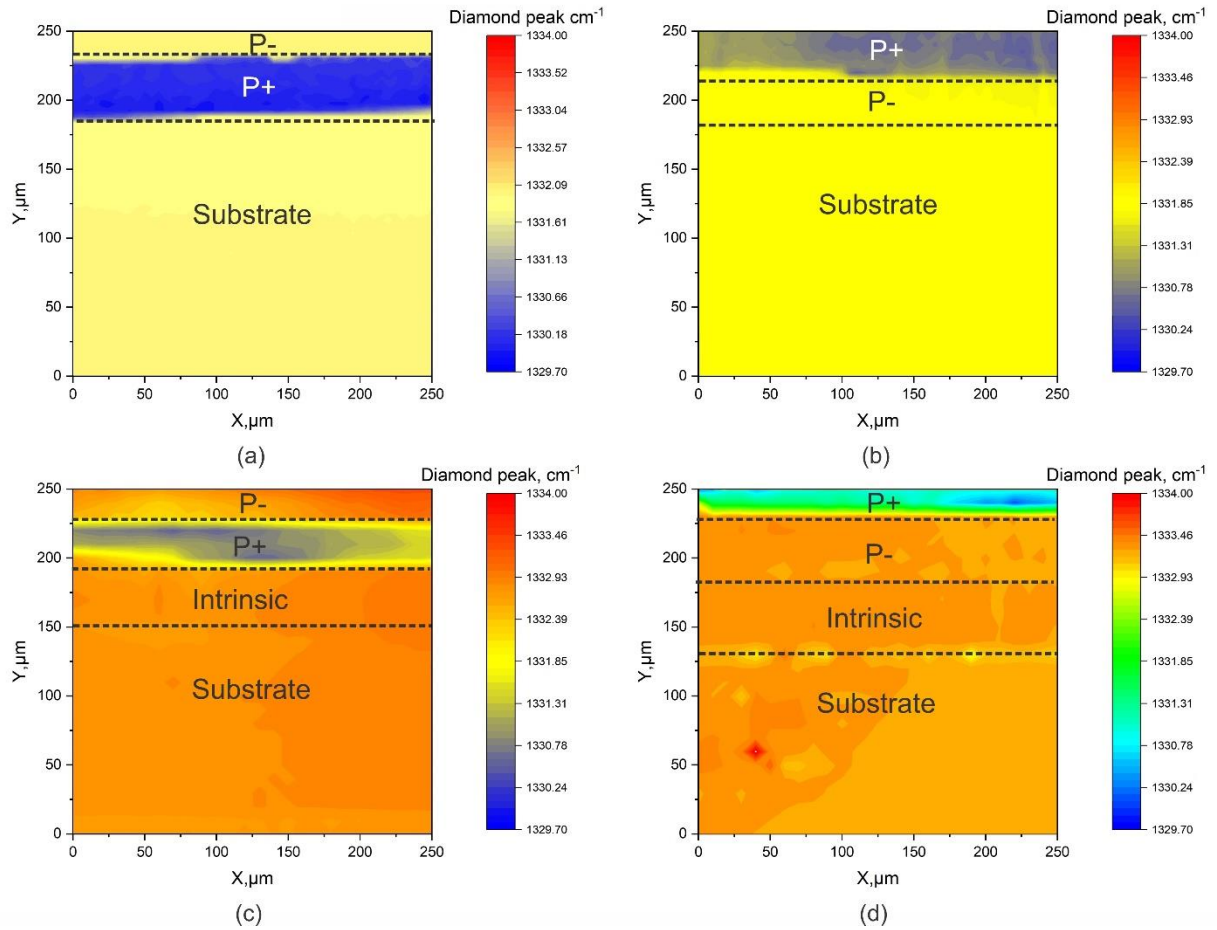


Figure III.19- Diamond peak Raman shift mapping of the four stacking cut samples. (a) Standard configuration, (b) Inversed configuration, (c) Standard configuration with buffer layer and (d) Inversed configuration with buffer layer.

The distribution of the Raman peak shift is presented for the fourth configurations in Figure III.19. The main information that must be kept in mind for the fourth characterized samples is that the growth of a  $p^+$  layer induced a strong downshift of almost  $2 \text{ cm}^{-1}$  compared to the unstressed diamond peak which is expected to be at  $1332.5 \text{ cm}^{-1}$ . This downshift is commonly attributed to the Fano effect. It is important to note, however, that alternative factors, such as tensile stress, could also contribute to the observed downshift as others works from LSPM [8].

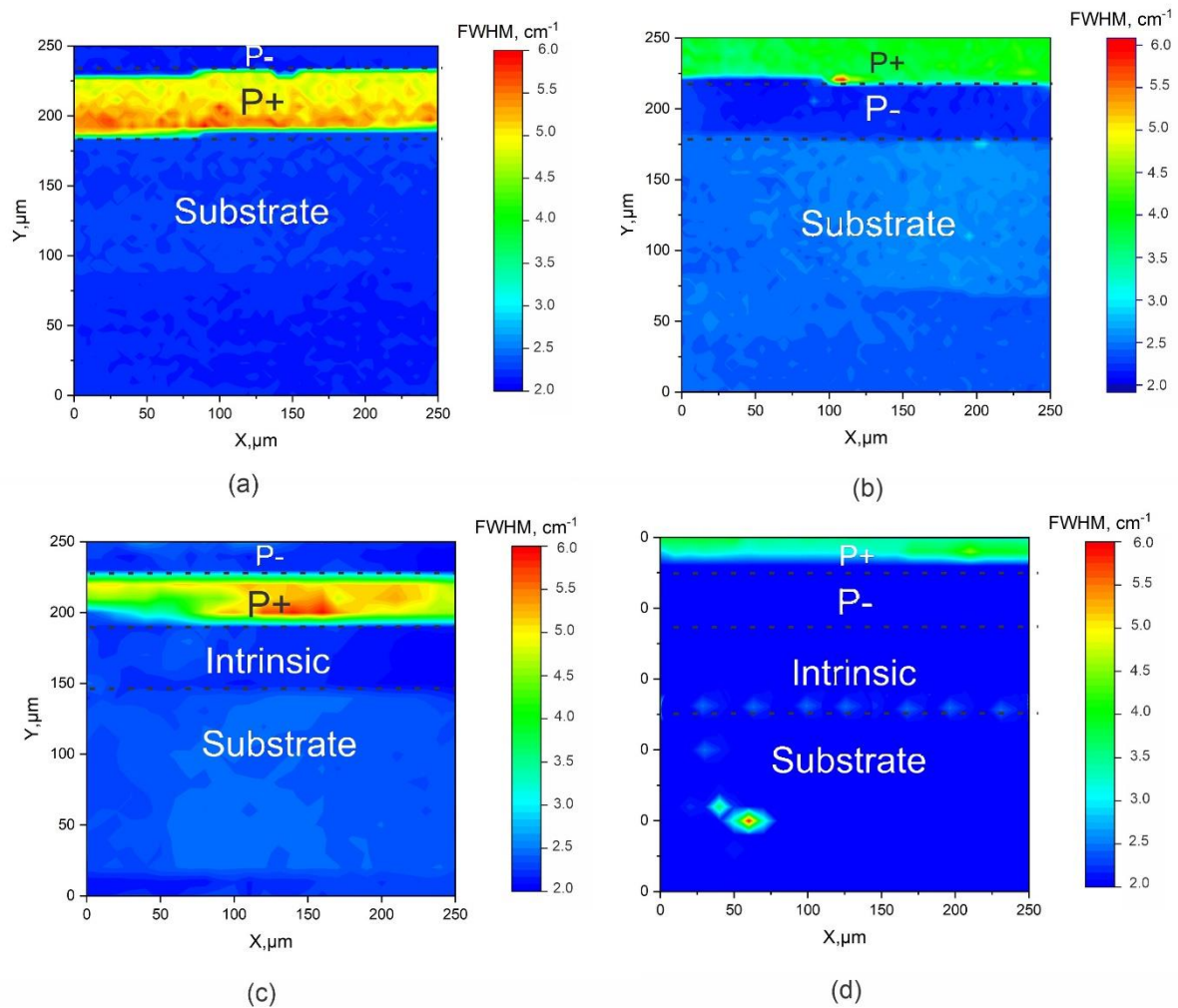


Figure III.20 - Raman mapping concerning the FWHM in different zones of the cut samples. (a) Sample A (standard configuration), (b) Sample B (Inversed configuration), (c) Sample C (standard configuration with buffer layer) and (d) Sample D (Inversed configuration with buffer layer)

The distribution of the FWHM of the diamond Raman peak has been also mapped in order to study the evolution of the crystalline quality of the samples along the growth. A FWHM close to  $2 \text{ cm}^{-1}$  was measured for all  $p^-$  layers even after a deposition over a  $p^+$  layer. This result demonstrates that the  $p^-$  quality is not affected by a growth on  $p^+$  rather than on an intrinsic CVD layer or directly on the HPHT substrate.

Based on the results obtained from the dislocation density study and the interface analysis, we showed that the growth of the p<sup>-</sup> active layer on heavily boron-doped layers rather than on an intrinsic layer or on HPHT substrate led to a significant improvement in the overall quality of the sample.

The results of the Raman mapping showed that a strong diamond peak downshift in the heavily boron-doped layers is obtained compared to the expected unstressed diamond peak, which could explain the decrease of dislocation density. Additionally, the results from the analysis of the FWHM indicated a good crystalline quality of the p<sup>-</sup> layer, even when deposited on a P+ layer.

In conclusion, the use of a heavily boron-doped layer instead of an intrinsic one to deposit the p<sup>-</sup> active layer leads to an increase of final sample quality. This information is important for the development of high-quality electronic devices that require the use of diamond layers in their fabrication processes.

Nevertheless, more studies must be performed to have a better understanding on the exact influence of the high doping level on the dislocation propagation.

#### 3.3.2.2 Cathodoluminescence analysis

To complete the previous study, CL analysis was conducted on the cross section of the samples heavily and lightly boron-doped layers in the standard configuration (a). The analysis was performed using a Jobin-Yvon HClue system attached to a Zeiss EVO-MA15 scanning electron microscope presented in Chapter 2. The CL spectra have been performed at 110 K using a liquid nitrogen-cooled stage in order to have a better defect signature. A 10 kV electron beam with a 20 nA current was applied.

This configuration provided the necessary energy and electron density for efficient electron excitation, enabling suitable CL emission.



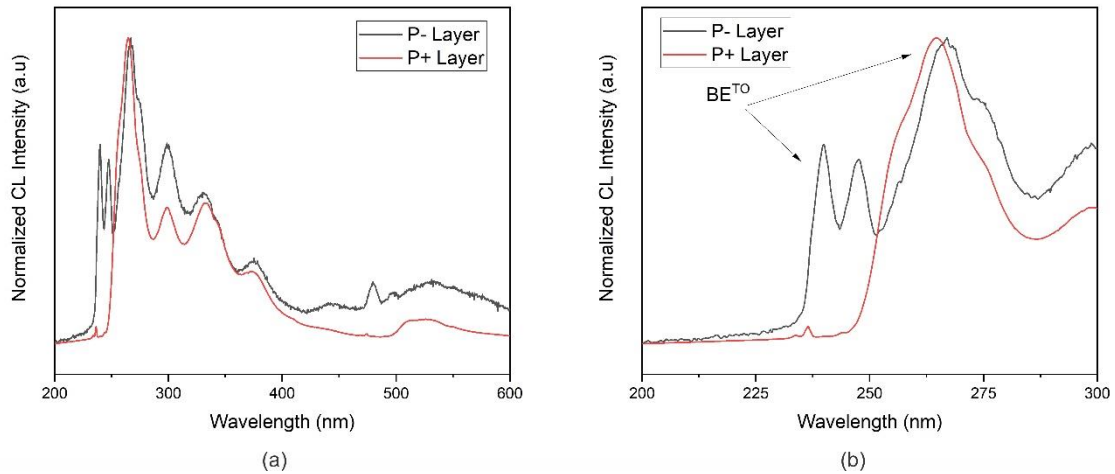


Figure III.21 - Cathodoluminescence spectra of  $p^+$  and  $p^-$  from the standard configuration: a) Full range and b) zoom in the excitonic region.

The obtained spectrum for the  $p^-$  layer, presented in Figure III.21 (a) and III.21 (b), is primarily dominated by the recombination emission of bound excitons to boron acceptors with the assistance of transverse optical phonons ( $BE^{TO}$ ). This emission exhibits a characteristic doublet structure [33] at approximately 230-250 nm clearly visible on Figure III.21 (b).

In addition, there are broader bands observed at 300, 330, and 370 nm, which may indicate the presence of defects. However, the intensity of this band is relatively moderate in comparison to the exciton emission. These observations confirm the high crystalline quality of the  $p^-$  grown layer even if it has been grown on  $p^+$  layer.

Cross-sectional CL images of the sample has been also performed at 300, 330 and 370nm and are presented on Figure III.22. These pictures reveal signs of dislocation propagation in the  $P^-$  layer since black lines showing non-luminescence are clearly observed. Unfortunately, due to technical limitations and time constraints, the detection and analysis of dislocation propagation using CL imaging as described in Chapter 2 were not fully explored in this study and are planned in the near future.

For the  $P^+$  layer, the  $BE^{TO}$  emission peak exhibits a significant shift towards lower energies (higher wavelength) with a moderate broadening, indicative of a decrease in the bandgap energy. This shift is consistent with the presence of very high boron doping levels [34].

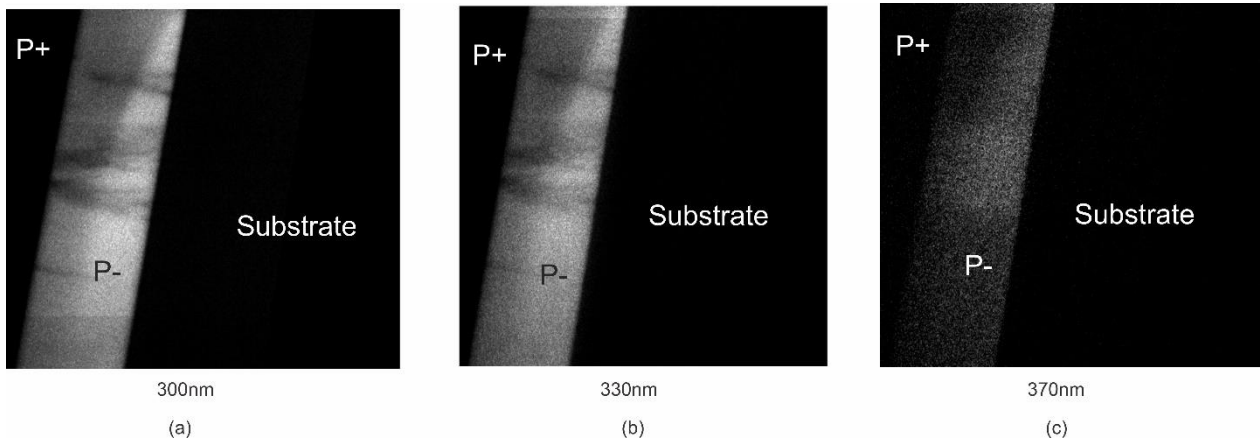


Figure III.22 - CL images taken in cross sections of the samples at different wavelengths

### 3.4 Conclusions

Based on the investigation realized in this chapter, the standard configuration consisting in growing a  $p^+$  layer directly on HPHT substrate before depositing the active  $p^-$  layer is recommended for improving diamond structure adapted for fabricating Schottky diodes.

This configuration allows limiting the increase of dislocation density and presents the benefit to be less time consuming in terms of microfabrication simplicity, for instance, removing a substrate on a thin  $p^-$  layer can be complicated rather than removing substrates from a thick  $p^+$  layer. The use of heavily boron-doped layers has been shown to improve the crystalline quality by inducing tensile stress levels, leading to a better overall sample quality even if the mechanisms involved are not completely clear and require further investigations.

The findings of this study can be utilized for the development of high-quality diamond-based electronic devices that require stable growth and improved crystalline quality.

Moreover, both Raman study and cathodoluminescence (CL) analysis confirmed the presence of high boron doping levels. The Raman study revealed a noticeable shift in the Raman peak, suggesting the possible presence of stress within the samples. While this shift could be associated with the high boron doping, it is important to consider other factors that may contribute to the observed stress. Additionally, the decrease in epitaxial layer propagation density (EPD) observed in highly boron-doped layers aligns with this presence of this stress. The combined findings from the Raman and CL studies provide further evidence of the impact of boron doping on the structural properties of the diamond layers.

### 3.5 References

1. Lin, C.R., et al., *The effect of the substrate position on microwave plasma chemical vapor deposition of diamond films*. Surface and Coatings Technology, 2006. **200**(10): p. 3156-3159.
2. Babchenko, O., et al., *Influence of surface wave plasma deposition conditions on diamond growth regime*. Surface and Coatings Technology, 2015. **271**: p. 74-79.
3. Fiori, A., *New generations of boron-doped diamond structures by delta-doping technique for power electronics: CVD growth and characterization*. 2012, Université de Grenoble.
4. Volpe, P.-N., *Fabrication of unipolar diamond devices for power electronics*  
*Réalisation de composants unipolaires en diamant pour l'électronique de puissance*. 2009, Université Joseph-Fourier - Grenoble I.
5. Tokuda, N., et al., *Surface roughening of diamond (001) films during homoepitaxial growth in heavy boron doping*. Diamond and Related Materials, 2007. **16**(4): p. 767-770.
6. Achard J., e.a., *High quality MPACVD diamond single crystal growth: high microwave power density regime*. Journal of Physics D: Applied Physics 40 (20), 2007: p. p. 6175-6188.
7. Issaoui, R., et al., *Thick and widened high quality heavily boron doped diamond single crystals synthesized with high oxygen flow under high microwave power regime*. Diamond and Related Materials, 2019. **94**: p. 88-91.
8. Issaoui, R., *Elaboration de films épais de diamant monocristallin dopé au bore par MPAVCD pour la réalisation de substrats de diamant P +*. 2011, Paris XIII.
9. Bernard, M., C. Baron, and A. Deneuveille, *About the origin of the low wave number structures of the Raman spectra of heavily boron doped diamond films*. Diamond and Related Materials, 2004. **13**(4-8): p. 896-899.
10. Mortet, V., et al., *Analysis of heavily boron-doped diamond Raman spectrum*. Diamond and Related Materials, 2018. **88**: p. 163-166.
11. Pruvost, F., E. Bustarret, and A. Deneuveille, *Characteristics of homoepitaxial heavily boron-doped diamond films from their Raman spectra*. Diamond and Related Materials, 2000. **9**: p. 295-299.
12. Pruvost, F. and A. Deneuveille, *Analysis of the Fano in diamond*. Diamond and Related Materials - DIAM RELAT MATER, 2001. **10**: p. 531-535.
13. Ing. M. Lamac, I.N.L., Msc. L. Iwanikov and Dr. V. Mortet. *Raman Tool*. Available from: <http://ofm.fzu.cz/raman-tool>.
14. Tallaire, A., et al., *Identification of Dislocations in Synthetic Chemically Vapor Deposited Diamond Single Crystals*. Crystal Growth & Design, 2016. **16**(5): p. 2741-2746.
15. Naamoun, M., et al., *Etch-pit formation mechanism induced on HPHT and CVD diamond single crystals by H<sub>2</sub>/O<sub>2</sub> plasma etching treatment*. physica status solidi (a), 2012. **209**(9): p. 1715-1720.
16. Fiori, A. and T. Teraji, *Plasma etching phenomena in heavily boron-doped diamond growth*. Diamond and Related Materials, 2017. **76**: p. 38-43.
17. Achard, J., et al., *The control of growth parameters in the synthesis of high-quality single crystalline diamond by CVD*. Journal of Crystal Growth, 2005. **284**(3): p. 396-405.
18. Gicquel A., e.a., *Validation of actinometry for estimating relative hydrogen atom densities and electron energy evolution in plasma assisted diamond deposition reactors*. Journal of Applied Physics 83 (12), 1998: p. p. 7504-7521.

19. Hassouni K., e.a., *Modeling of H<sub>2</sub> and H<sub>2</sub>/CH<sub>4</sub> Moderate-Pressure Microwave Plasma Used for Diamond Deposition*. Plasma Chemistry and Plasma Processing 18 (3), 1998: p. p. 325-362.
20. Achard, J., et al., *Freestanding CVD boron doped diamond single crystals: A substrate for vertical power electronic devices?* physica status solidi (a), 2012. **209**(9): p. 1651-1658.
21. Okushi, H., *High quality homoepitaxial CVD diamond for electronic devices*. Diamond and Related Materials, 2001. **10**(3): p. 281-288.
22. Baron, C. *Contribution à l'estimation de paramètres physiques à l'aide de modèles d'ordre réduit*. 2003.
23. Ogura, M., et al., *Misorientation-angle dependence of boron incorporation into (0 0 1)-oriented chemical-vapor-deposited (CVD) diamond*. Journal of Crystal Growth - J CRYST GROWTH, 2011. **317**: p. 60-63.
24. Umezawa, H., Y. Kato, and S.-i. Shikata, *1 Ω On-Resistance Diamond Vertical-Schottky Barrier Diode Operated at 250 °C*. Applied Physics Express, 2013. **6**(1): p. 011302.
25. Tarelkin, S., et al., *Power diamond vertical Schottky barrier diode with 10 A forward current*. physica status solidi (a), 2015. **212**(11): p. 2621-2627.
26. Tallaire, A., et al., *Oxygen plasma pre-treatments for high quality homoepitaxial CVD diamond deposition*. physica status solidi (a), 2004. **201**(11): p. 2419-2424.
27. *ImageJ software*. Available from: <https://imagej.nih.gov/>.
28. Widmann, C.J., et al., *Homoepitaxial growth of single crystalline CVD-diamond*. Diamond and Related Materials, 2016. **64**: p. 1-7.
29. da Silva Neto, J., et al., *Growth and Characterization of Polycrystalline CVD Diamond Films Obtained by MWPACVD at High Power 2,45GHz Microwave Discharge*. Materials Research, 2022. **25**.
30. Di Liscia, E., *Stress Analysis on Single-Crystal Diamonds by Raman Spectroscopy 3D Mapping*. Materials Sciences and Applications, 2013. **04**: p. 191-197.
31. Boussadi, A., et al., *Thick heavily boron doped CVD diamond films homoepitaxially grown on (111)-oriented substrates*. Diamond and Related Materials, 2017. **79**: p. 108-111.
32. Ohmagari, S., et al., *Large reduction of threading dislocations in diamond by hot-filament chemical vapor deposition accompanying W incorporations*. Applied Physics Letters, 2018. **113**(3): p. 032108.
33. Dean, P.J., *Bound Excitons and Donor-Acceptor Pairs in Natural and Synthetic Diamond*. Physical Review, 1965. **139**(2A): p. A588-A602.
34. Baron, C., et al., *Cathodoluminescence of highly and heavily boron doped (100) homoepitaxial diamond films*. Diamond and Related Materials, 2006. **15**(4-8): p. 597-601.

# **Chapter IV: Growth of large and thick boron doped single crystal diamond**

## Summary

4	Chapter IV: Growth of large and thick boron doped single crystal diamond .....	122
4.1	Introduction .....	124
4.2	Lateral growth technique .....	125
4.2.1	Advantages and limitations of lateral growth .....	125
4.3	Conditions promoting lateral growth .....	125
4.3.1	First approach for lateral growth .....	127
4.3.2	Higher methane and oxygen levels during boron doped diamond deposition .....	130
4.3.3	Second approach using 1% oxygen in the gas phase .....	131
4.3.4	Third approach using 2% oxygen in the gas phase .....	134
4.4	Methods to obtain large and thick boron doped substrates .....	140
4.4.1	Widening of a 3x3mm <sup>2</sup> substrate .....	140
4.4.2	Widening of a 5x5mm <sup>2</sup> substrate .....	143
4.4.3	Overgrowth on macroscopic hole .....	145
4.4.4	Overgrowth on hole array on heteroepitaxial substrate .....	151
4.5	Conclusions .....	157
4.6	Perspectives .....	158
4.7	References .....	159

## 4.1 Introduction

The production of large and thick diamond substrates is a crucial step in the development of industrial applications based on diamond materials. Various methods, such as chemical vapor deposition (CVD) and high-pressure high-temperature (HPHT) techniques have been employed to achieve this goal [1-5].

However, the growth of high-quality diamond material over large areas remains a significant challenge. Moreover, the incorporation of boron atoms into diamond lattices during growth can be challenging due to its low solubility and the tendency to form amorphous boron carbide phases.

In recent years, there have been attempts to grow large and thick boron-doped single crystal diamond substrates using CVD methods [6, 7]. One promising approach involves the use of large single crystal diamond substrates as a template for the growth of heavily boron-doped diamond layers.

However, this approach is challenging due to the difficulty in obtaining large, high-quality single crystal diamond substrates with low dislocation density [8, 9].

Lateral growth techniques have been shown as promising in reducing dislocation density and improving electronic properties compared to conventional growth methods [3, 7]. Therefore, in this chapter we will investigate the potential of using lateral growth techniques to produce large and thick boron-doped single crystal diamond substrates.

We will provide an overview of the conditions that promote lateral growth, the methods used to obtain large and thick boron-doped substrates, and the potential obstacles and risks associated with these techniques.

We will also investigate the potential of the growth of large and thick boron-doped single crystal diamond substrates in order to reduce dislocation density, these films being expected for a subsequent use as freestanding CVD substrates by their potential to be the base for manufacturing vertical power devices.

## 4.2 Lateral growth technique

Lateral growth technique has emerged as a promising solution for producing high-quality diamond films. This technique involves preferential growth of diamond crystals in the lateral direction, limiting the formation of dislocations and defects due to their deviations. As the underlying mechanisms of the lateral growth technique are not yet fully understood, further investigations are necessary to optimize this growth strategy.

The technique of lateral growth has its origins in semiconductor material synthesis, where it has successfully yielded to high-quality thin films of materials like silicon, gallium arsenide or gallium nitride [10-13]. In the context of diamond synthesis, the lateral growth method has been already developed for intrinsic material and allowed producing diamond films with better properties in terms of dislocation density [3].

### 4.2.1 Advantages and limitations of lateral growth

Previous studies have demonstrated the potential to develop large-area heteroepitaxial (H-CVD) diamonds surfaces [14]. However, the quality of such material falls far below the requirements for electronic devices, particularly in terms of dislocation density, which can reach up to  $10^9 \text{ cm}^{-2}$ .

By thickening diamond close to 1 mm, this dislocation density can be reduced around  $10^7 \text{ cm}^{-2}$  but remains too high for developing efficient electronic devices [15]. More recently, researchers developed lateral growth technique on heteroepitaxial substrates and succeeded in reducing dislocation density by two orders of magnitude in the lateral growth regions [16]. Nevertheless, despite its advantages, the lateral growth technique on H-CVD has some limitations.

One limitation is the challenge of achieving high ratio between lateral and vertical growth rate, which requires careful optimization of growth conditions, making it challenging to implement in large-scale production. Furthermore, it should be noted that this technique has never been tested for boron-doped diamond.

## 4.3 Conditions promoting lateral growth

In order to identify the optimal growth conditions that promote lateral growth in boron-doped diamond films, a systematic approach was developed, involving the variation of different growth parameters and monitoring their effects on the growth rate and crystal quality. One of the main parameter was the evaluation of the ratio between the lateral growth rate (LGR) and the normal growth rate (NGR), which is the main criterion to assess lateral expansion.



A high LGR/NGR ratio ( $>1$ ) is indicative of successful lateral growth, resulting in the desired widening of the diamond film's surface. Threading dislocations in diamond are known to follow the growth direction and targeting the widening of the material during growth. This enhances the development of the dislocations from the center to the edges which may limit their impact on the performance of the obtained material.

These conditions are crucial and will allow developing growth strategies having an impact on extended defect density by bending threading dislocations using specific substrate geometries as already shown at LSPM [3, 17, 18]. Some examples are given in Figure IV.1.

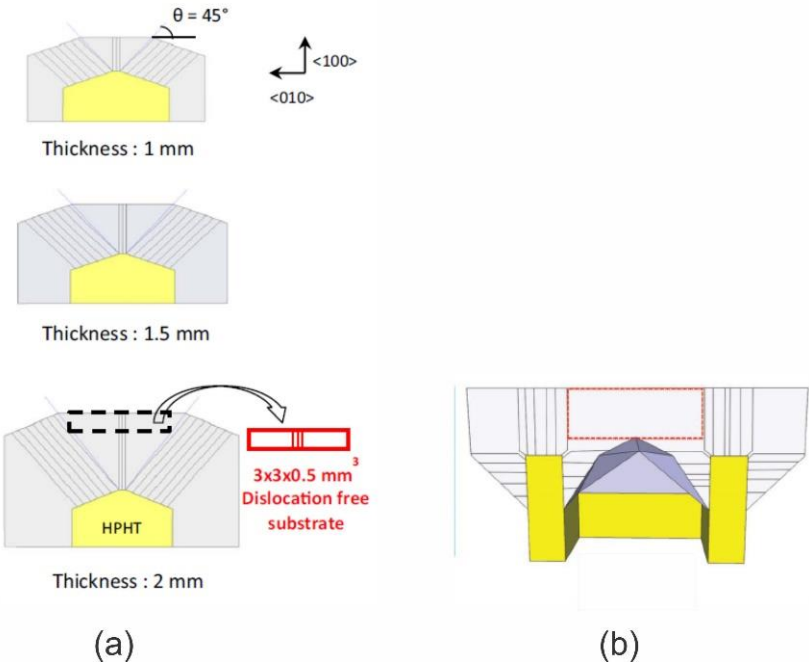


Figure IV.1 - Schematics of dislocation propagation. (a) Growth on pyramidal shape substrate leading to an improvement of dislocation density by controlling the widening of the upper face [3, 17, 18]. (b) Growth on a pierced substrate allowing strongly limiting dislocation density when  $LGR > NGR$  [3, 17, 18][3, 17, 18]

In this PhD thesis, the primary objective of our approach was to understand the influence of key parameters on lateral growth during boron doped diamond growth and effectively reduce the occurrence of threading dislocations, thereby enhancing the overall material quality.

#### 4.3.1 First approach for lateral growth

Thanks to the favorable results obtained in the previous chapter, which included high-quality surfaces and smooth textures, our initial step was to test the developed recipe by extending the deposition time as long as possible for strongly thickening boron doped material. The objective was to investigate whether lateral growth could be observed on the sample by keeping similar quality obtained for shorter deposition times.

The experimental conditions used are detailed in Table IV.1, and a commercially available (100)-oriented 1b HPHT substrate was utilized. Prior to the growth process, the surface underwent a preparation step involving etching with H<sub>2</sub>/O<sub>2</sub> (98:2) plasma for 30 minutes [19].

This etching procedure aimed to remove the top layer, which is typically damaged during the substrate polishing process, and prepare the edges of the sample, thereby ensuring an improved starting substrate for the growth.

1 <sup>st</sup> set of growth parameters	
Substrate	HPHT – 1b <100>
Pressure	150 mbar
MW Power	2.5 kW
Total gas flux	200 sccm
CH <sub>4</sub>	6%
O <sub>2</sub>	0.25%
Temperature of the sample	850 °C ± 30 °C
B/C ratio	6,000 ppm
Precursor gas	Diborane
Thickness deposited	500 μm
Time	120 h

Table IV.1 – Growth conditions during the first approach for lateral growth optimization

Figure IV.2 presents the Raman spectrum of the sample which shows the Fano effect signature and a broadened peak around 600 cm<sup>-1</sup>, a FWHM of 5 cm<sup>-1</sup> and the characteristic diamond peak shifted to the left at 1328 cm<sup>-1</sup> compared to the characteristic diamond peak usually localized at 1332.5 cm<sup>-1</sup>.

All these characteristics suggest that the sample was heavily boron doped as expected in the growth condition used and already discussed in the previous chapter. The Raman web tool gives us a doping value of approximately  $2 \times 10^{20}$  at  $\text{cm}^{-3}$  for measurements performed at several locations of the sample without showing strong dispersion in doping level.

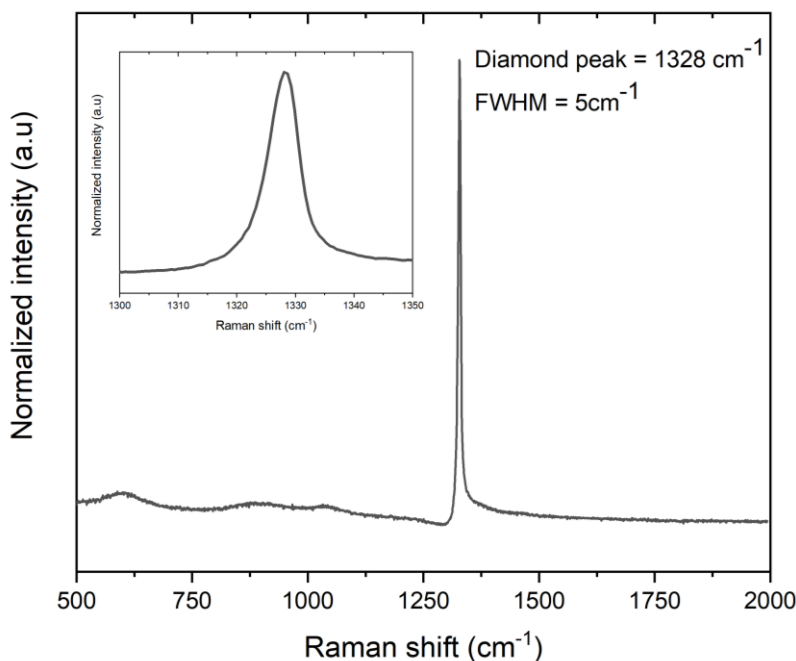


Figure IV.2 – Raman spectrum of the sample grown using the extended time recipe detailed in Chapter III.

Figure IV.3 (a) displays the complete surface image of the sample obtained after 120 hours of deposition leading to a  $500 \mu\text{m}$  thick layer.

The surface morphology appears to have some etch pits, those are visible. Figure IV.3 (b) shows a magnified area where some etch pits are visible, but they do not appear to be extensive and could be due to oxygen in the gas phase or a possible increase in temperature in the final deposition hours that also could enhance this phenomenon.

It is also noticeable that the corners broke during the growth due the possible apparition of (111) faces which are known to be very defective. The lateral dimensions of the sample were increased but only by  $175 \mu\text{m}$  per side which is much lower than the CVD thickness. To claim similar lateral and vertical growth rates, the sample should have increased by at least  $500 \mu\text{m}$  per side.

The primary objective of achieving a significantly enlarged area fell short of our expectations, as we only obtained an increase from a HPHT of  $3.1 \times 3.1 \text{ mm}^2$  to approximately  $3.45 \times 3.45 \text{ mm}^2$  resulting in a LGR/NGR ratio of approximately of 0.36, which is a low value to expect a favorable effect on the development of growth strategy for reducing dislocation density.

Thus, the previous optimized growth conditions doesn't allow reaching a LGR/NGR ratio  $> 1$  and the task of obtaining conditions that specifically promote lateral growth in boron-doped diamond could be more challenging than expected because the growth process involves not only methane and hydrogen as for intrinsic material but also diborane and oxygen, which should also play important roles in terms of growth rate.

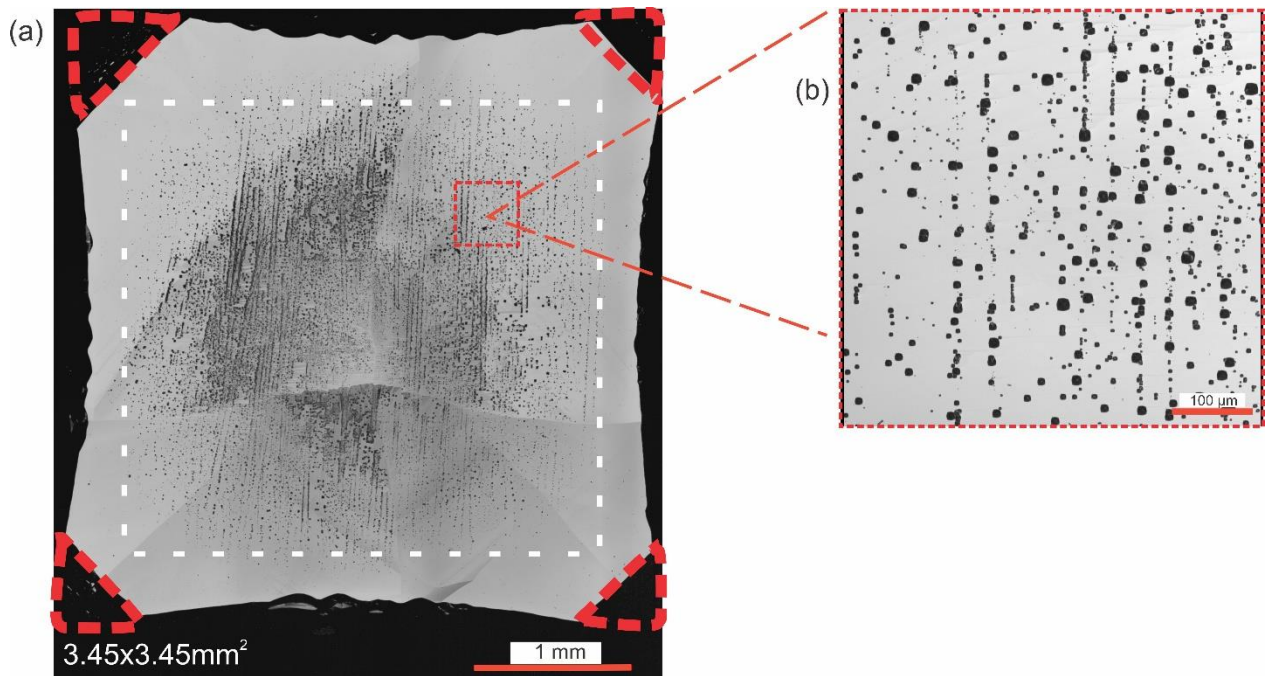


Figure IV.3 – CLSM images of the first recipe tested. The footprint of the original substrate is marked with white dotted square and the (111) faces, marked in red, indicate broken corners. (a) CLSM image showing the complete surface of the sample. (b) A magnified area of the sample, with etch-pits marks prominently highlighted.

We also performed electrical resistivity measurements on this sample and a value of 0.87  $\Omega\cdot\text{cm}$  was obtained. This value is relatively close to the reported value by Issaoui et al. in 2012 (0.26  $\Omega\cdot\text{cm}$ ) for their samples with the highest boron doping level [20]. It is important to note that our measurements were conducted prior to the deposition of electrical contacts, thus our samples may differ from those in previous reports, potentially contributing to the observed differences in resistivity. To establish a better correlation between resistivity and boron concentration, additional measurements using thinner probes and under controlled conditions are necessary, as well as SIMS.

#### 4.3.2 Higher methane and oxygen levels during boron doped diamond deposition

In order to modify and try to promote lateral overgrowth in boron-doped diamond deposition, we extended further initial works developed by Issaoui et al [7] consisting in increasing the levels of oxygen and methane in the gas mixture. In this paper, it was described that the presence of oxygen could decrease vertical growth and promote lateral growth, leading to the formation of high-quality diamond films with large surface areas.

Although the underlying mechanism is not yet fully understood, it is thought to be related to oxygen's role in surface reconstruction and etching. Studies suggest that oxygen can react with carbon species on the diamond surface, leading to surface etching and restructuring, which could, in turn, promote the formation of preferential growth sites for lateral overgrowth.

Some other studies [7, 21-23] have also investigated the effect of oxygen levels on the morphology and quality of boron-doped diamond films grown by microwave plasma-enhanced chemical vapor deposition. They showed similar results indicating that higher oxygen levels led to a significant increase in lateral overgrowth and the formation of high quality, single crystal diamond films.

However, as an increase of the oxygen level during the growth process can lead to enhanced surface etching [7, 21], an increase in methane concentration is necessary to compensate the etching effect and maintain a relatively high growth rate. It is crucial though, to optimize the methane concentration along with other growth parameters, such as substrate temperature and gas flow rate, because using higher methane levels can result in plasma instability, soot formation, and an increase in defects like non-epitaxial crystallites.

Thus, finding a compromise that allows for the widening of heavily boron-doped diamond films keeping an acceptable growth rate while minimizing soot formation is essential and very challenging.

Other factors, such as the diborane concentration in the gas can also play important roles in determining the morphology and quality of the resulting diamond films. Finally, in this work we have been referred to previous work of LSPM [7, 18] that has investigated a range of growth conditions to promote lateral overgrowth in boron doped diamond films.

#### 4.3.3 Second approach using 1% oxygen in the gas phase

Taking into account the outcomes achieved from this previous work and involving an increase of methane and oxygen concentrations, we proceeded to a second attempt to establish reliable parameters for lateral growth. In this experiment, we utilized a growth recipe with 10% of methane and 1% of oxygen, aiming to enhance the lateral growth rate. The detailed parameters employed for this growth are described in Table IV.2.

To promote a higher growth rate, we also slightly increased the couple microwave power-pressure settings. The diborane concentration was maintained at 6,000 ppm, consistent with the previous recipe found in chapter III in order to achieve the desired level of boron doping. Prior to the growth process, the surface underwent a preparation step involving etching with H<sub>2</sub>/O<sub>2</sub> (98:2) plasma for 30 minutes.

2 <sup>nd</sup> set of growth parameters	
Substrate	HPHT – Ib <100>
Pressure	170 mbar
MW Power	2.7 kW
Total gas flux	200 sccm
CH <sub>4</sub>	10%
O <sub>2</sub>	1%
Temperature of the sample	880 °C ± 30 °C
B/C ratio	6,000 ppm
Precursor gas	Diborane
Thickness deposited	580 μm
Time	120h

Table IV.2 - Growth conditions used during the second approach for lateral growth optimization

Figure IV.4 presents the Raman spectrum of the sample which shows a pronounced Fano effect suggesting that sample grown in these conditions was heavily doped. The diamond peak is found at  $1327\text{cm}^{-1}$ , showing the same tendency than before.

The FWHM of the sample found in this sample is  $14\text{ cm}^{-1}$  related to the doping-induced disorder in heavily boron-doped diamond. To have an estimation of boron doping, we used the Raman web tool that gave a value of approximately  $6 \times 10^{20}$  at  $\text{cm}^{-3}$ . Different measurements were performed among the sample in different areas without a notable difference.

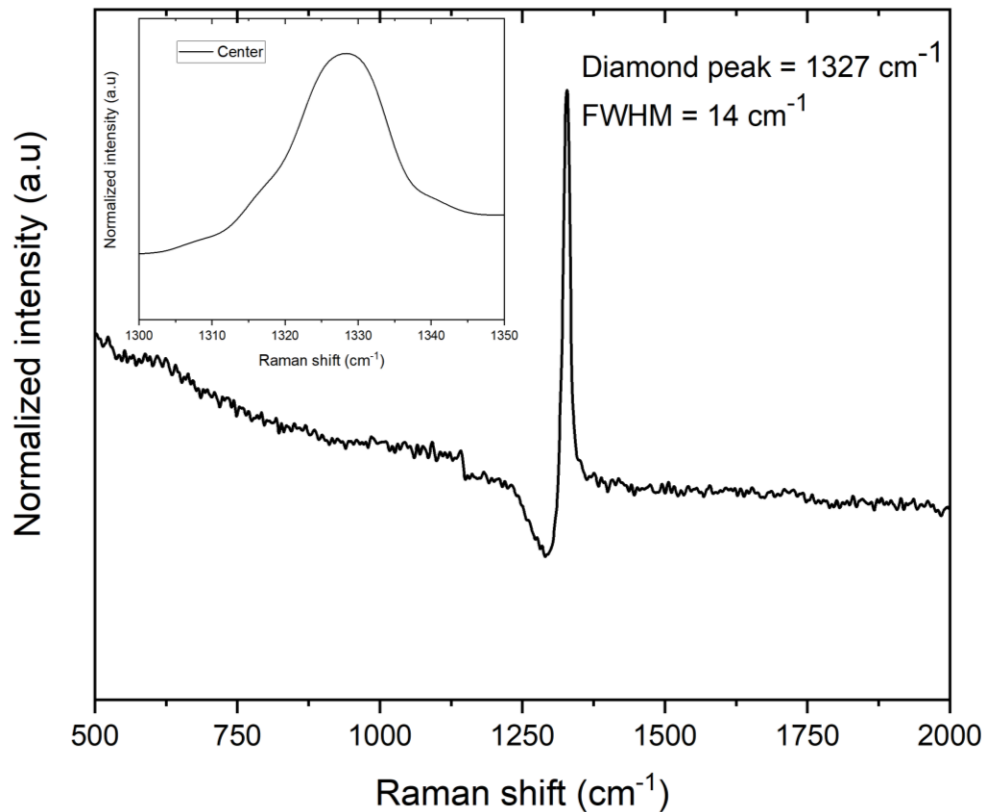


Figure IV.4 - Raman spectrum of the of the sample grown in the second approach with 1% oxygen in the gas phase

After 120 hours of deposition, the total surface area achieved was  $4.3 \times 4.3\text{ mm}^2$  (Figure IV.5 (a)) with  $580\text{ }\mu\text{m}$  of diamond growth. While the overall surface appears smooth, the corners show signs of stress since two of them broke, probably due to the appearance of large (111) faces highlighted in red. Nevertheless, in these growth conditions, each side was widened by  $600\text{ }\mu\text{m}$ . The lateral growth rate appears to be higher than before and closer to the normal growth rate, resulting in a LGR/NGR ratio of approximately 1.

These results suggest an enhancement in lateral growth, suggesting that higher concentrations of oxygen and methane contribute to promoting lateral expansion without too much reducing normal growth rate.

However, it is important to note that the use of these growth conditions during long period of time may lead to uncomfortable situation, particularly in terms of reactor performance. The subsequent sections will delve into a detailed analysis of these issues.

Figure IV.5 (b) shows a magnified area where some etch pits are visible, but they do not appear to be extensive and could be due to higher oxygen levels that promotes etching.

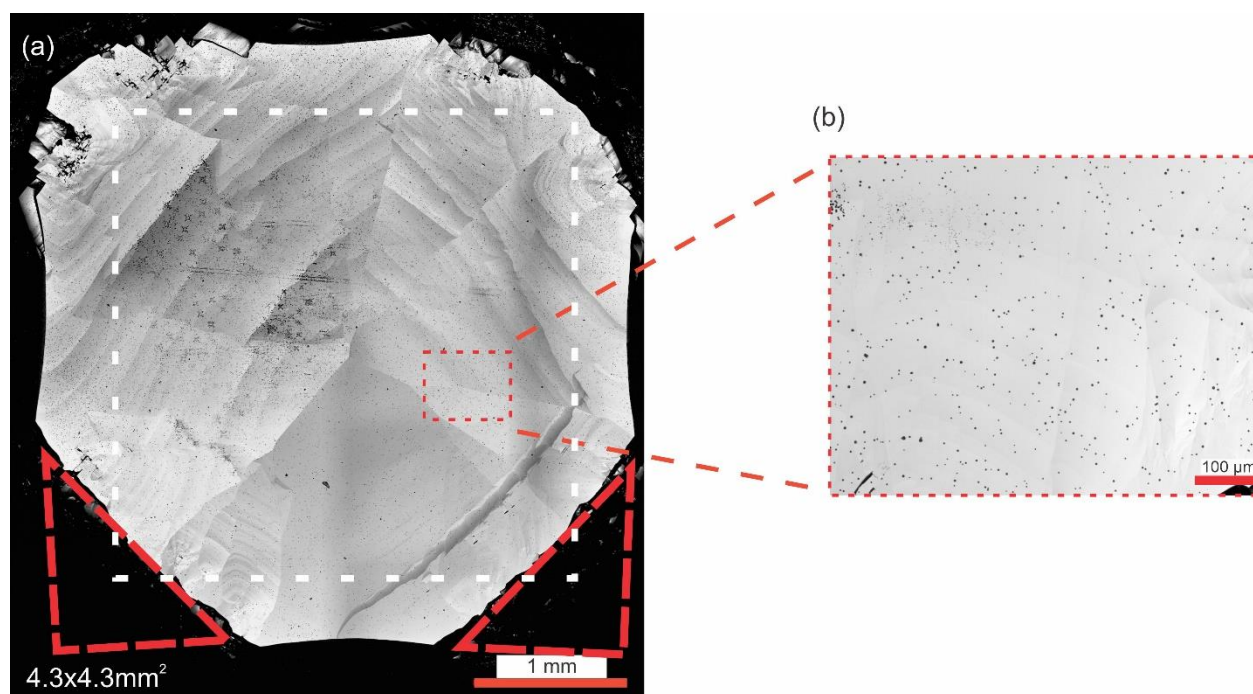


Figure IV.5 – CLSM images of the second test sample. The footprint of the original substrate is marked with white dotted square. The (111) faces are marked in red indicating broken corners; (a) complete 4.3x4.3mm<sup>2</sup> surface area and (b) A magnified area of the sample, with etch-pits marks

Finally, for this case, the electrical resistivity measurements on these samples was found to be 0.7  $\Omega$ -cm which is very close to the values determined for the previous sample. As a partial conclusion, such conditions seem to promote lateral growth but the morphology of the sample clearly shows the appearance of large (111) faces at the corners which are not favorable for obtaining large crystals.



#### 4.3.4 Third approach using 2% oxygen in the gas phase

In order to go further and try to limit the appearance of (111) faces during the growth, we increased the oxygen level in the gas phase up to 2% but keeping the methane concentration at 10% and the diborane level at 6,000 ppm, as in the previous approach. The growth parameters used during the growth are presented in table IV.3.

In this study, we propose the fabrication of two different samples: sample A, consisting in a heavily boron-doped layer, and sample B, consisting in a lightly boron-doped layer achieved through non-intentional doping (NID) taking advantage of the reactor memory effect with diborane. By investigating the differences in lateral growth improvement between these two doping levels, we aim to gain valuable insights into the impact of doping on lateral expansion.

3 <sup>rd</sup> set of growth parameters	
Substrate	HPHT – 1b <100>
Pressure	170 mbar
MW Power	2.7 kW
Total gas flow	200 sccm
CH <sub>4</sub>	10%
O <sub>2</sub>	2%
Temperature of the sample	850 °C ± 30 °C
B/C ratio	6,000 ppm for sample A and 0 ppm for sample B
Precursor gas	Diborane
Thickness deposited	950µm for sample A and 400µm for sample B
Time	170h for sample A and 121h for sample B

Table IV.3 - Growth conditions used during the third approach for lateral growth optimization

The Raman spectra of the samples A and B are shown in Figure IV.6. For sample A (Figure IV.6 (a)), a broadened peak at around 600 cm<sup>-1</sup> and a high-pronounced Fano effect are observed suggesting a heavy boron doping level confirmed by the Raman web tool with a value of approximately 3x10<sup>20</sup> cm<sup>-3</sup>. The diamond peak is localized at 1326 cm<sup>-1</sup> with a full width at half maximum of 10 cm<sup>-1</sup>, showing the same tendency than before.

In the case of sample B, we note the presence of a diamond peak at  $1329\text{ cm}^{-1}$ , characterized by a full width at half maximum (FWHM) of  $2.2\text{ cm}^{-1}$ . This implies a high crystalline quality for the non-intentionally doped (NID) diamond with a lower shift to lower wavenumbers of the diamond peak than for the high boron doped sample.

The FWHM in this case is relatively similar to those of intrinsic samples, further attesting the good crystalline quality. The estimated boron doping levels from the Raman web tool is approximately  $3 \times 10^{19}\text{ cm}^{-3}$ , which remains very high for non-intentionally doped material. This point highlights the significant contamination in the dedicated reactor used for boron doping which will require, to achieve lower doping levels essential for a Schottky diode the use of a different reactor dedicated to very low doping level.

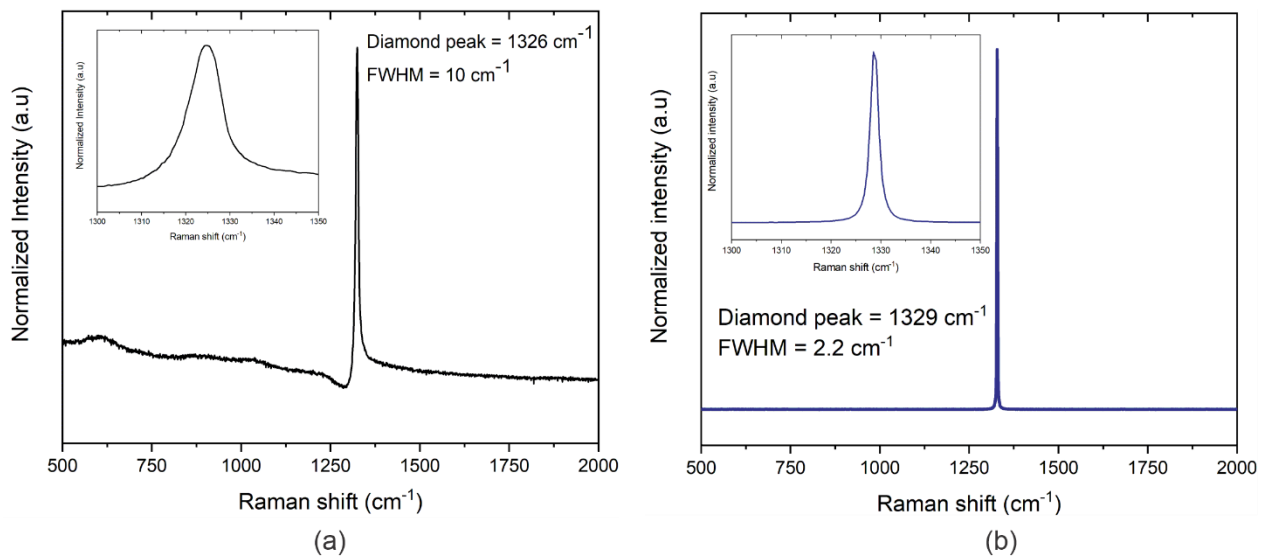


Figure IV.6 – Raman spectra performed on the 2 grown samples; (a) Sample A; heavily boron doped and (b) Sample B; non-intentionally doped (NID)

Figure IV.7 displays the surfaces of samples A and B. In sample A (Figure IV.7 (a)), the deposition during 170 hours resulted in a surface area increase from  $3.1 \times 3.1\text{ mm}^2$  to  $5 \times 5\text{ mm}^2$ , with  $950\text{ }\mu\text{m}$  deposited.

This means a widening of  $950\text{ }\mu\text{m}$  per side, turning into approximately the same LGR and NGR leading to a LGR/NGR equal to 1, value similar to the previous conditions using 1% of  $\text{O}_2$ . Nevertheless, in these specific conditions, it is possible to enhance both the lateral growth rate (LGR) and normal growth rate (NGR) without negatively affecting the resulting sample morphology.

Moreover, beyond the improvement of the growth rate, these conditions also lead to more favorable morphologies for enlarged substrates since the size of (111) faces is reduced.

In the case of the lightly boron-doped sample which is depicted in Figure IV.6 (b), it exhibited an enlargement from  $3.1 \times 3.1 \text{ mm}^2$  to  $4 \times 4 \text{ mm}^2$ .

This means that around  $450 \mu\text{m}$  were added per side after a deposition time of 121 hours with a deposited thickness of  $400\mu\text{m}$ . The LGR/NGR ratio for this sample was also close to 1 showing that diborane concentration didn't affect this ratio but in this case, the NGR being lower, a longer deposition duration will be required for similar enlargement.

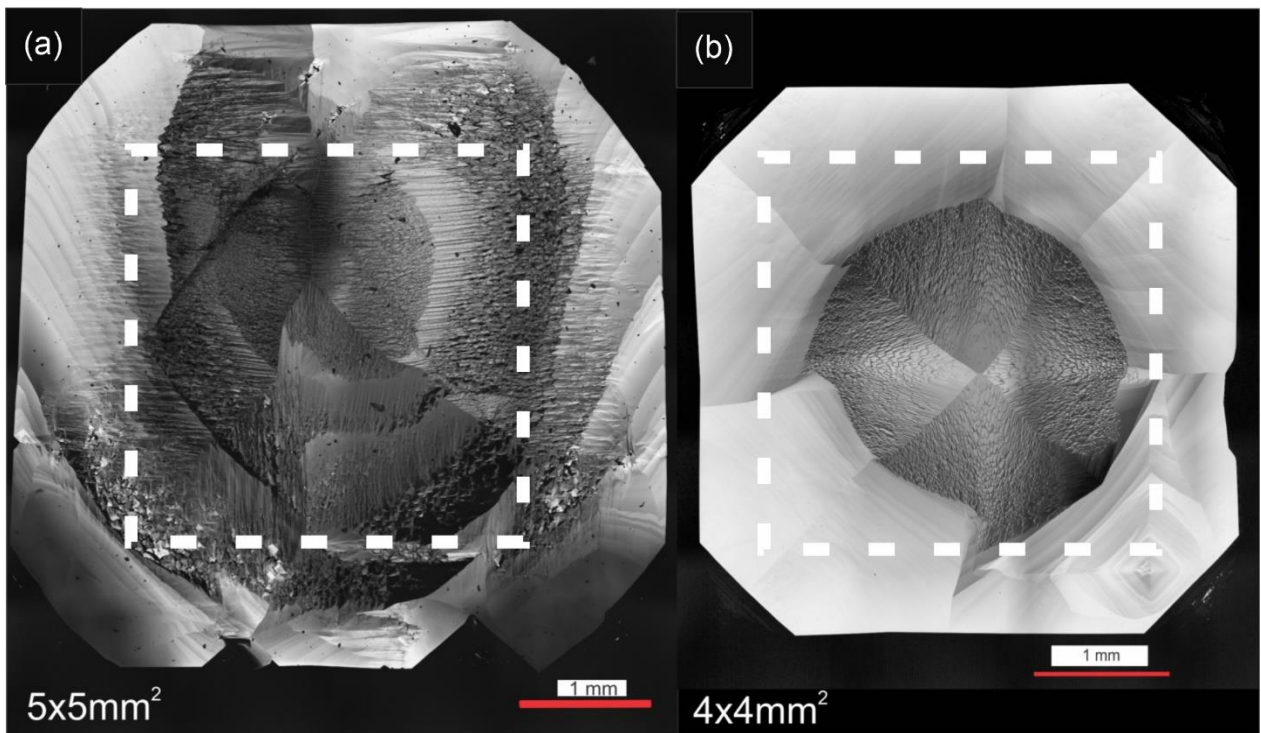


Figure IV.7 – CLSM images of the third approach performed with their respective footprint mark with a white dotted square. (a) Heavily boron doped  $5 \times 5 \text{ mm}^2$  sample, (b) lightly boron doped sample of  $4 \times 4 \text{ mm}^2$

Lastly, the electrical resistivity measurement performed on the heavily-doped sample was found to be equal to  $0.62 \Omega\text{-cm}$  and similar to the previous ones showing that the modification of  $\text{O}_2$  concentration didn't affect doping efficiency.

In addition to these promising results, it is worth emphasizing the adverse effects of using high amounts of methane and oxygen in the gas phase. Indeed, promoting lateral growth in boron-doped diamond under these conditions can have negative effects on machinery, efficiency, and deposition

quality. These risks also pose a threat to equipment safety. In this section, we will discuss some of the common issues we faced during all this thesis work, associated to heavily boron doped diamond growth, especially when performing lateral growth.

The continuous gas injection during long period of time deposition can lead to soot formation, negatively impacting temperature control and potentially causing overheating of the reactor chamber walls. This soot can cause blockages, reducing the cooling system's effectiveness, leading to temperature control issues, and potentially causing thermal stress and structural damage to the equipment.

This problem is enhanced specially by the use of higher oxygen levels to enhance lateral growth during boron-doped diamond long time deposition, which can increase soot formation.

This soot, depicted in Figure IV.8 (a), forms inside the antenna and emerges from the gas-dosing shower during growth. This requires, after each growth process, to clean the shower (shown in Figure IV.8 (b)), in the reactor which is time-consuming.

If this cleaning is not performed, over time, the deposited soot can harden and completely obstructs the gas injection as shown in Figure IV.8(c), posing significant risks to both the reactor and the quality of the diamond deposition.

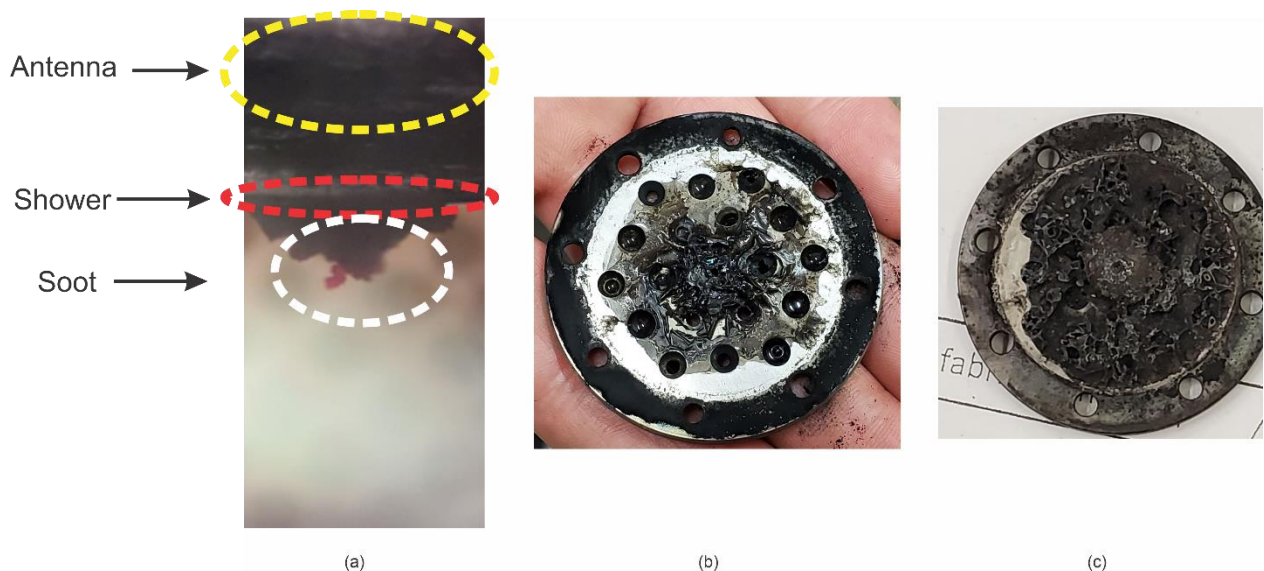


Figure IV.8 - Soot Formation Problem: (a) Soot formed during the growth at the top of the chamber over the shower; (b) the shower removed for cleaning after deposition; and (c) the soot formation mixture hardened after some time, forming a blockage.

Soot formation remains then a significant challenge and further research is needed to develop more effective strategies for minimizing its impact on boron-doped diamond film growth efficiency and quality.

Finally and despite the problems of soot formation, we further investigate the effect of growth parameters on widening of boron doped diamond and more particularly the amount of methane in the gas phase.

#### 4.3.4.1 Methane influence on lateral growth

In this study, a last sample was grown by increasing the methane concentration to 11%, keeping all the other parameters constant. The growth conditions are given in the table IV.4.

4 <sup>th</sup> set of growth parameters	
Substrate	HPHT – Ib <100> with (100) lateral faces
Pressure	170 mbar
MW Power	2.7 kW
Total gas flux	200 sccm
CH <sub>4</sub>	11%
O <sub>2</sub>	2%
Temperature of the sample	850 °C ± 30 °C
B/C ratio	6,000 ppm
Precursor gas	Diborane
Thickness deposited	850 μm
Time	150h

Table IV.4 - Growth conditions used during the fourth approach for lateral growth optimization

Figure IV.9 shows the surface of the sample after 150 hours of growth under the specified conditions. While there is an evidence of lateral growth, the surface morphology of the sample is a disaster since numerous non-epitaxial particles are clearly visible.

This damage could be attributed to the increased incorporation of boron when higher methane concentrations is used in the deposition process as already observed by Okushi et al. [24] and Baron et al.[25]. It could be at the origin of the presence of sp<sup>2</sup> phase during the growth leading to non-epitaxial crystallites.

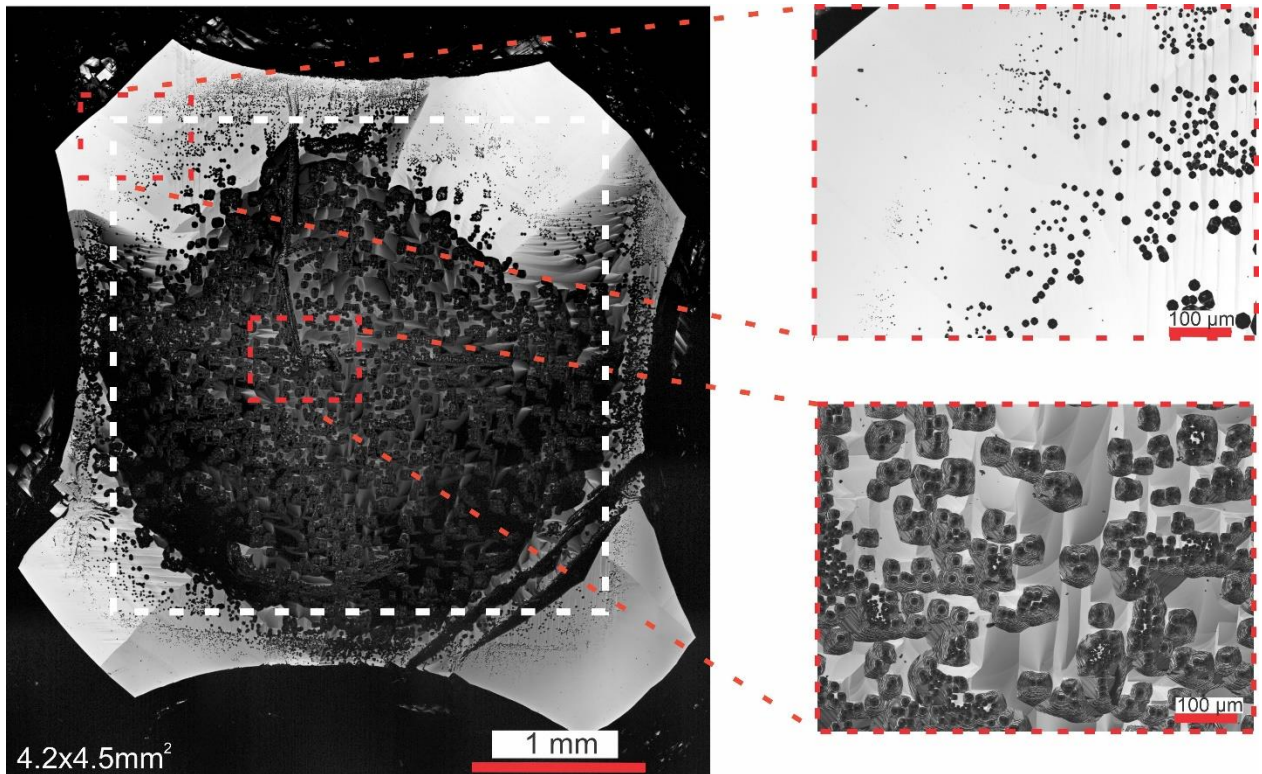


Figure IV.9 - CLSM images of the complete surface with increased methane. The footprint of the original substrate is marked with white dotted square. The zoomed-in areas depict a rough region in the center of the sample.

Based on the results obtained and the observed limitations associated with higher methane concentrations, it is indeed reasonable to conclude that increasing the methane concentration beyond 10% may not yield to a better surface quality in the context of this study.

With the identified optimal conditions of 10% methane and 2% oxygen concentrations, the focus can now shift towards exploring methods to enlarge diamond substrates while addressing the challenge of dislocation reduction.

In the upcoming sections, we will delve into the various methods investigated in this thesis work that utilize these optimal growth conditions to promote lateral growth and produce high-quality diamond films in terms of dislocation density with effective doping.

#### 4.4 Methods to obtain large and thick boron doped substrates

Throughout this thesis work, various methods were explored to achieve the goal of enlarging diamonds while also addressing the challenge of reducing dislocations. Different types of substrates were employed, ranging from simple commercial HPHT substrates to higher-quality CVD substrates. Additionally, modified HPHT and heteroepitaxial substrates were utilized in an attempt to decrease dislocations density.

The subsequent sections will provide an overview of the different methods explored and the corresponding results obtained. The findings obtained from these investigations will contribute to the broader understanding of diamond growth and provide valuable insights for future research in the field.

##### 4.4.1 Widening of a 3x3mm<sup>2</sup> substrate

The first method to obtain large and thick boron doped diamond substrates is through the widening of a small initial substrate, which has been already discussed in the previous paragraph. It has been possible to increase the substrate size from 3.1 x 3.1 mm<sup>2</sup> to 5 x 5mm<sup>2</sup> using 2% of oxygen and 10% of methane. This promoted lateral growth and resulted in a diamond substrate with a larger surface area and thickness than the original substrate.

In this section, we will focus on the possibility to remove the initial substrate in order to obtain freestanding heavily boron doped substrate with a larger surface. The ability to produce such substrates offers significant benefits, particularly when considering the fabrication of a Schottky diode and more generally, power electronic components.

A larger substrate will give the possibility to obtain larger active area for the device, which can enhance its performances particularly for improving current handling capabilities. This increased active area provides more space for the Schottky contact, enabling efficient charge transfer and reducing the on state resistance.

Raman spectroscopy analysis after removing the initial substrate and polishing the CVD layer is presented in Figure IV.10 (a) confirming that the diamond possessed high quality with the absence of any graphitic phase and a high doping level as depicted previously.

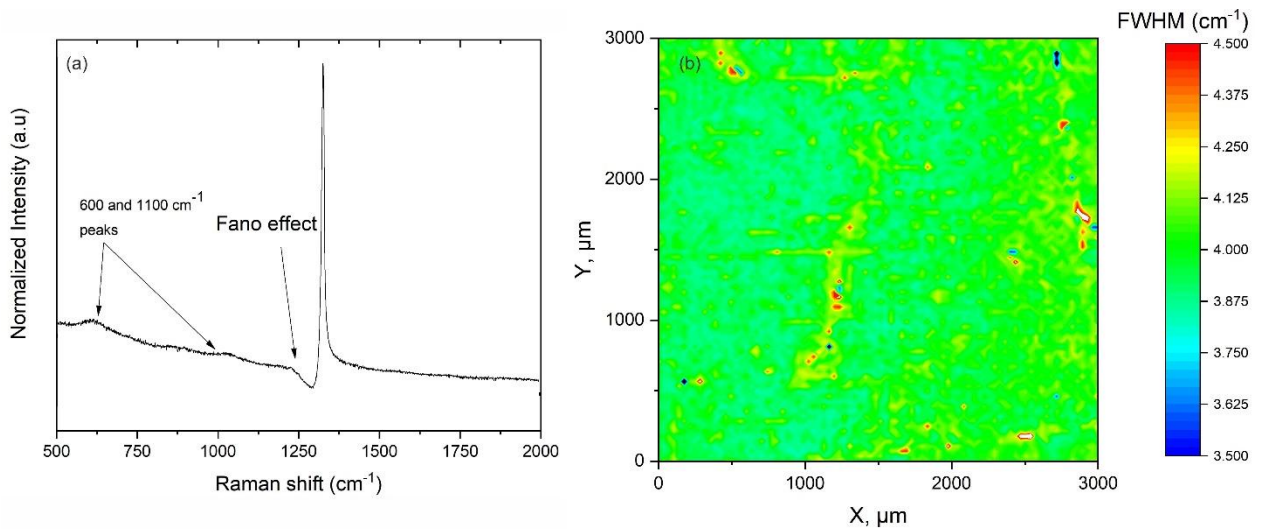


Figure IV.10 – Raman analysis of the 5x5 mm<sup>2</sup> sample: (a) Raman spectrum of the resulting CVD sample obtained and (b) 3x3 mm<sup>2</sup> Raman mapping

A mapping of the FWHM of the diamond peak has been performed and is presented in the Figure IV.10 (b). A value around 4 cm<sup>-1</sup> was found in the majority of the sample, showing a high uniformity among all the cut and polished CVD layer.

These results confirms the potential of using a high oxygen flow to widen small initial substrates and produce large, highly boron-doped diamond substrates with excellent quality and uniformity.

Figure IV.11 shows the surface morphology of the sample before and after cutting and polishing process performed by Almax Company. One corner of the sample appears to be broken after the polishing process and moreover, some cracks are visible on the samples, these cracks being localized close to the initial substrates.

They highlight the presence of some stress in the material revealed by the laser cutting step and that this is a very critical step that should be improved to limit as much as possible the appearance of crack related to the stress. In particular, the use of a water guided laser beam as developed by Synova Company could be an alternative since it allows to strongly reduce the local temperature of the sample during the process of cutting. Such a cutting system has been recently acquired at LSPM and will be tested in further work.

Nevertheless, we demonstrated the possibility of widening a small initial substrate by adjusting the growth conditions to obtain a large and thick boron doped diamond substrates.



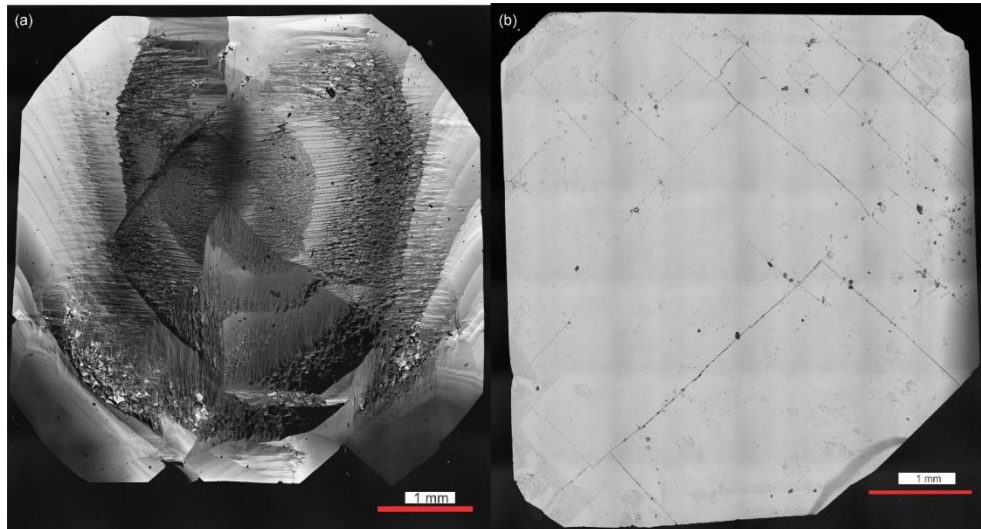


Figure IV.11 – CLSM images of 170h deposition sample as grown (a) and after laser cut and polishing (b)

Finally, SIMS measurements performed at GEMaC indicate an inhomogeneity of the doping level at the surface but the characterization has been performed on the side that was near the substrate. An explanation to such a behavior could be that the substrate was not totally removed after the cutting and polishing step. Nevertheless, after 1  $\mu\text{m}$  of etching during SIMS operation, the boron doping concentration is homogeneous and around  $4 \times 10^{20} \text{ at/cm}^3$ , which is relatively similar to the doping level found using the Raman web tool ( $5 \times 10^{20} \text{ at/cm}^3$ ). These results are very encouraging for the development of high boron-doped CVD substrates for high-power applications.

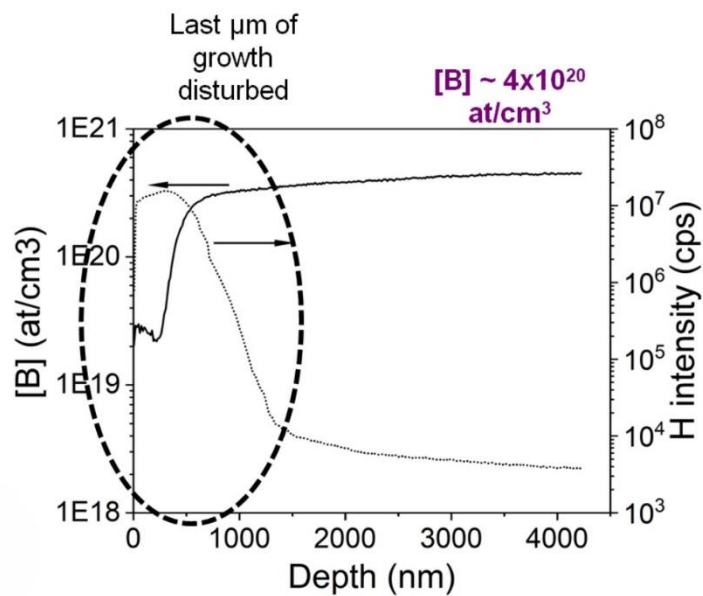


Figure IV.12 – SIMS measurements of the heavily boron doped 5x5mm<sup>2</sup> sample

#### 4.4.2 Widening of a 5x5mm<sup>2</sup> substrate

The objective of using a 5 x 5 mm<sup>2</sup> single crystal diamond is to further increase the size of heavily boron-doped CVD diamond substrates which still strongly hampers industrial development of diamond material.

Unfortunately, it remains very difficult to find 5 x 5 mm<sup>2</sup> HPHT substrates and this study has been made using a CVD single crystal diamond substrate. Moreover, it was impossible to find a high quality 5 x 5 mm<sup>2</sup> substrate with all faces oriented along (100) direction and the substrate we used had (110) oriented lateral faces.

The growth conditions used was the previously ones and reported in table IV.5.

Fixed growth conditions	
Substrate	CVD 5x5 mm <sup>2</sup> substrate <100> with (110) lateral faces
Pressure	170 mbar
MW Power	2.7 kW
Total gas flux	200 sccm
CH <sub>4</sub>	10%
O <sub>2</sub>	2%
Temperature of the sample	850 °C ± 30 °C
B/C ratio	6,000 ppm
Precursor gas	Diborane
Thickness deposited	1.2 mm
Time	260h

Table IV.5 - Growth conditions used during the approach widening a 5x5mm<sup>2</sup> substrate

The Raman spectroscopy analysis showed that the grown diamond did not exhibited graphitic phase. The diamond peak was observed at 1320 cm<sup>-1</sup>, suggesting a higher compressive stress in comparison to previous samples synthesized, including those described in the previous chapter.

Additionally, the Fano effect was more pronounced in this sample, with huge peaks at 600 and 1100  $\text{cm}^{-1}$ , suggesting a very high level of boron doping. The FWHM was broadened up to 12  $\text{cm}^{-1}$ , which may be attributed to higher doping-induced disorder resulting from increased levels of boron doping while the boron doping concentration estimated by the Raman web tool was approximately of  $6.4 \times 10^{20}$  at  $\text{cm}^{-3}$ .

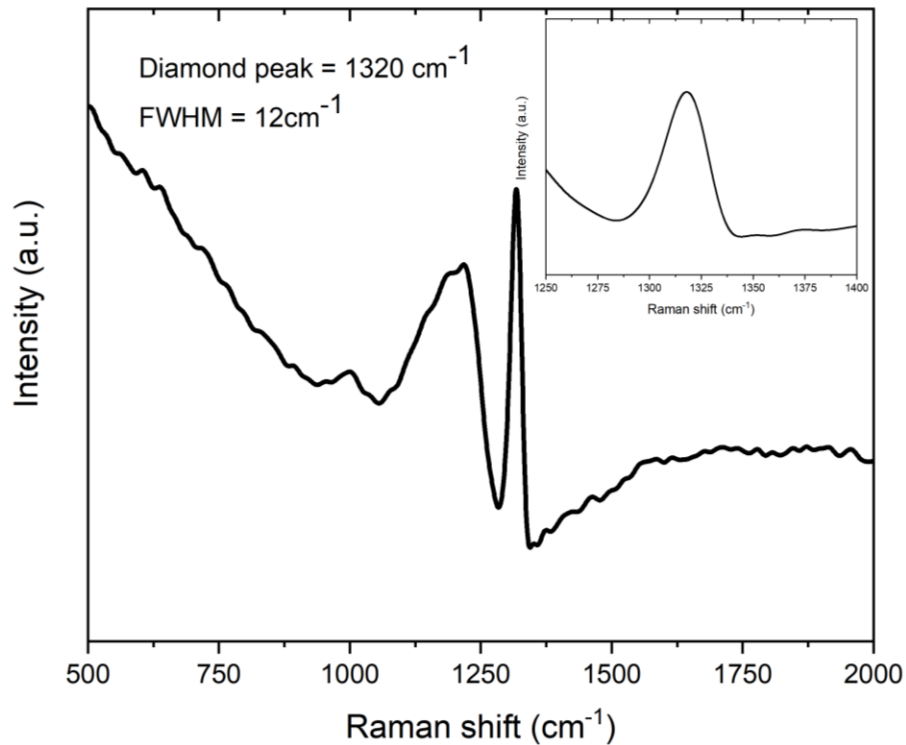


Figure IV.13 - Raman spectra of the resulting 6.5x6.5cm<sup>2</sup> sample

Figure IV.14 displays the morphology of the sample as grown and most of the surface is free non-epitaxial crystallites. We only see the occurrence of twinning and non-epitaxial crystallites at the edges and at the corners of the sample.

However, after a deposition duration of 260 hours resulting in a thickness of 1.2 mm, the sample was widened by only 1.5mm, which correspond to 750  $\mu\text{m}$  per side. Consequently, the lateral growth rate is less than the normal growth rate, leading to a LGR/NGR ratio around to 0.6. This is a lower value compared to previous results, indicating a less favorable lateral growth with substrates having (110) faces at the edge.

It indicates that if the aim is to enlarge as much as possible a substrate during the growth, a prerequisite is the use of an initial substrate with 6 (100)-oriented faces.

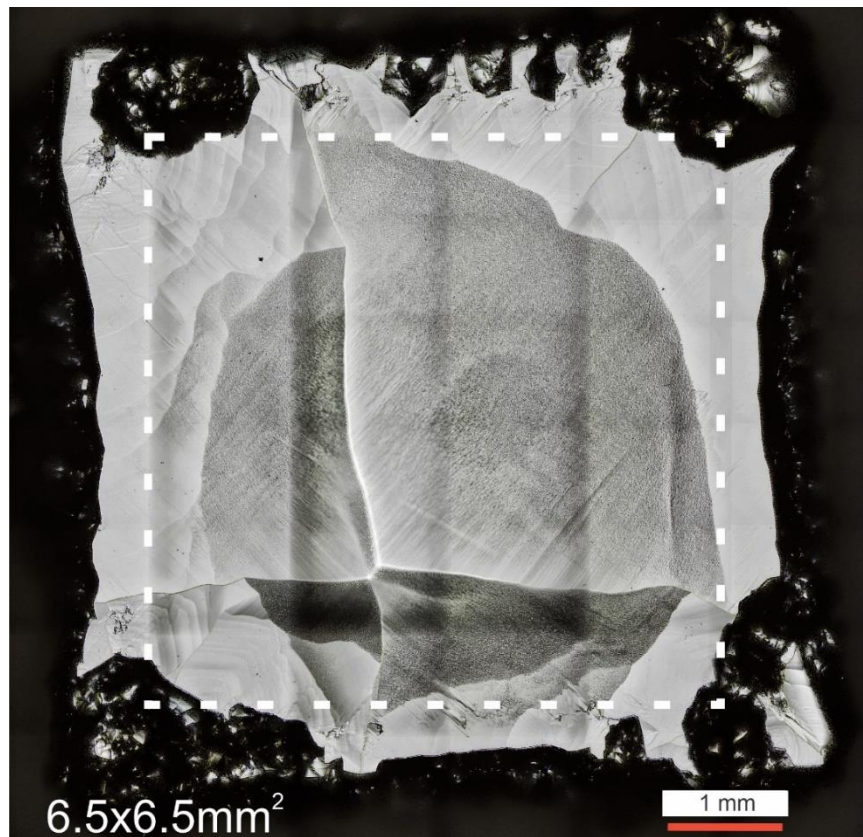


Figure IV.14 – CLSM image of the whole surface of the grown sample on a 5x5 mm<sup>2</sup> CVD substrate. The footprint of the original CVD substrate is marked with white dotted square

#### 4.4.3 Overgrowth on macroscopic hole

##### 4.4.3.1 Use of pierced substrates as a way to reduce dislocations

The use of a pierced substrate with a macroscopic hole for diamond growth has been shown to be a promising method for reducing threading dislocations [3]. This approach, proposed by Alexandre Tallaire and his collaborators, involves the use of a substrate with a pre-existing hole which is overgrown during the growth process. The only condition for succeeding in reducing dislocations is to promote growth condition leading to a LGR/NGR > 1.

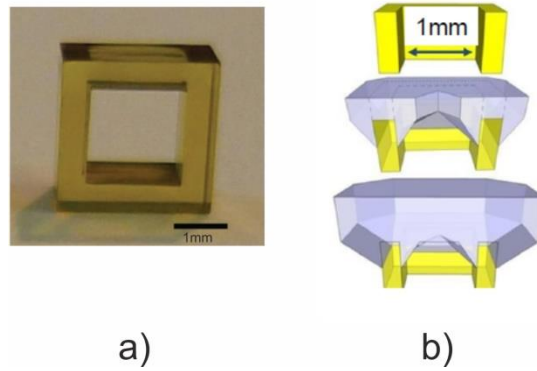


Figure IV.15 – (a) Picture of a pierced diamond substrate as example and (b) cross-section schematics illustrating the growth of the CVD layer (blue) on the HPHT substrate (yellow)[3]

Figure IV.15 shows a typical image of the pierced substrate used for the further experiments in this work. All the HPHT substrates were Ib type with 6 (100)-oriented faces and with dimensions of 3 x 3 x 1.5 mm<sup>3</sup>. The substrates were prepared by Almax company by laser cutting of the central part.

#### 4.4.3.2 Substrate with 1 x 1 mm<sup>2</sup> pierced hole

For the first try, we chose to prepare a substrate with a relatively small square hole of 1 x 1 mm<sup>2</sup> in order to limit the thickness required to fully overgrown it. The growth conditions for this sample are listed in Table IV.6 and correspond to the conditions leading to the larger widening of the substrate.

Fixed growth conditions	
Substrate	HPHT 1x1 mm <sup>2</sup> pierced substrate – Ib <100>
Pressure	170 mbar
MW Power	2.7 kW
Total gas flux	200 sccm
CH <sub>4</sub>	10%
O <sub>2</sub>	2%
Temperature of the sample	850 °C ± 30 °C
B/C ratio	6,000 ppm
Precursor gas	Diborane
Thickness deposited	1 mm
Time	230h

Table IV.6 - Growth conditions used for the first approach to fulfill the first pierced substrate

Despite the smooth lateral surface as shown in Figure IV.16, we can see that one of the corners broke due the possible appearance of (111) faces. However, even after a deposition time of 230 hours resulting in a thickness of 1 mm, it was not possible to achieve full diamond coverage over the hole.

A smaller square-shaped area measuring approximately  $500 \times 500 \mu\text{m}^2$  remained unfilled. More surprising, we can observe that the sample was widened by 2 mm, which means that each side was increased by 1 mm, which is coherent with the deposited thickness and the LGR/NGR ratio previously determined with these growth conditions.

It seems that the external lateral growth rate and the internal lateral growth rate are not similar since the LGR/NGR is only 0.5 in the latter case.

Some points could explain this behavior but further analysis should have to be performed. Actually, it is possible that the temperature close to the hole region which is at the center of the sample is lower than the temperature at the edge of the substrate.

This difference could strongly impact the LGR/NGR ratio. It could be also associated to the misorientation of the lateral faces of the holes and of the samples, which could be slightly different and induced different LGR inside the hole and at the external part of the sample.

Raman spectroscopy analysis revealed high-quality diamond with no evidence of graphitic phases and the classical signature of highly boron doped diamond with two peaks at  $600$  and  $1100 \text{ cm}^{-1}$  and the Fano effect. The estimated boron doping concentration determined by the Raman web tool, was approximately  $3 \times 10^{20} \text{ at cm}^{-3}$ .

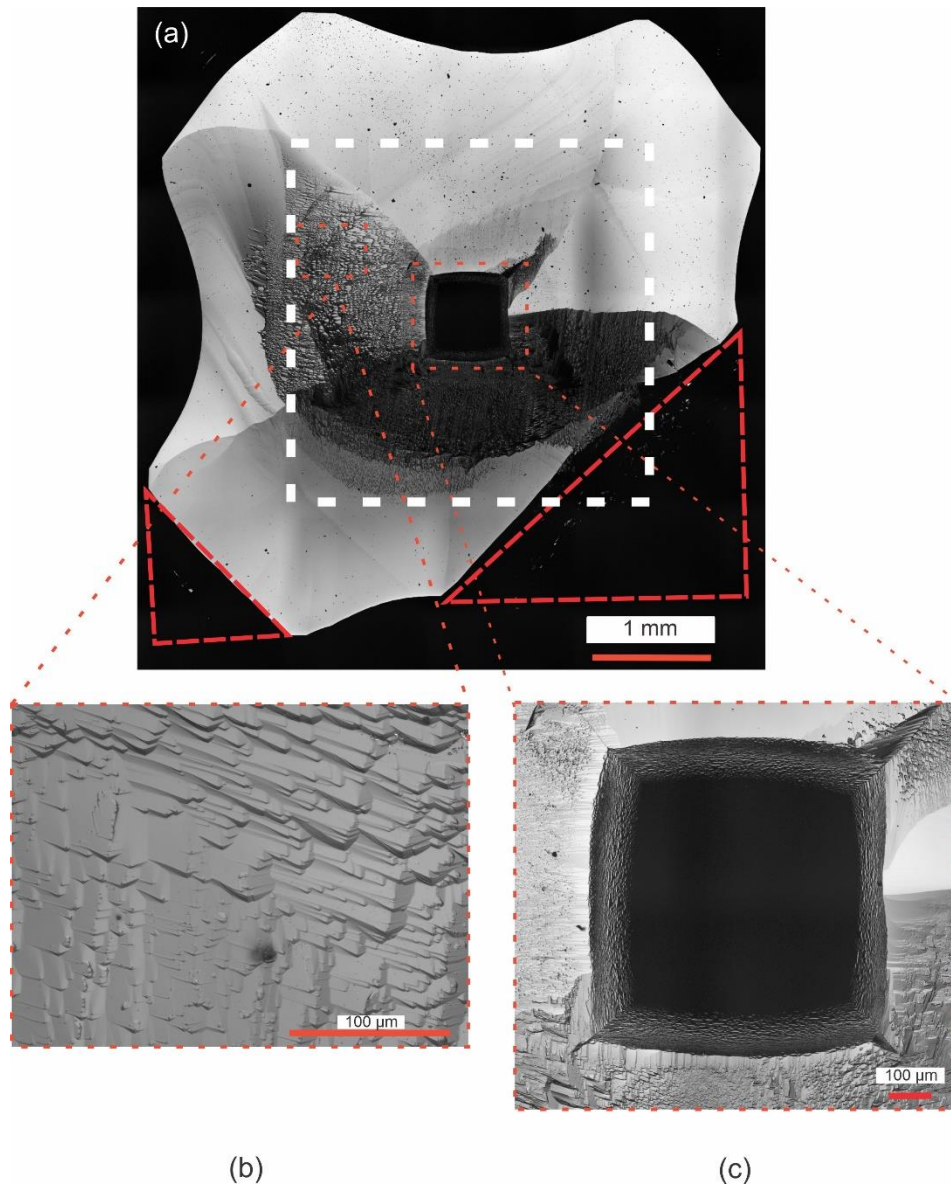


Figure IV.16 - CLSM image of the complete surface as well as magnification of different areas. The footprint of the original substrate is marked with white dotted square. The  $(111)$  faces, marked in red, indicate broken corners; (a) CLSM image showing the complete surface of the sample. (b) A magnified area of the sample nearby the center and (c) A magnified area of the unfilled hole.

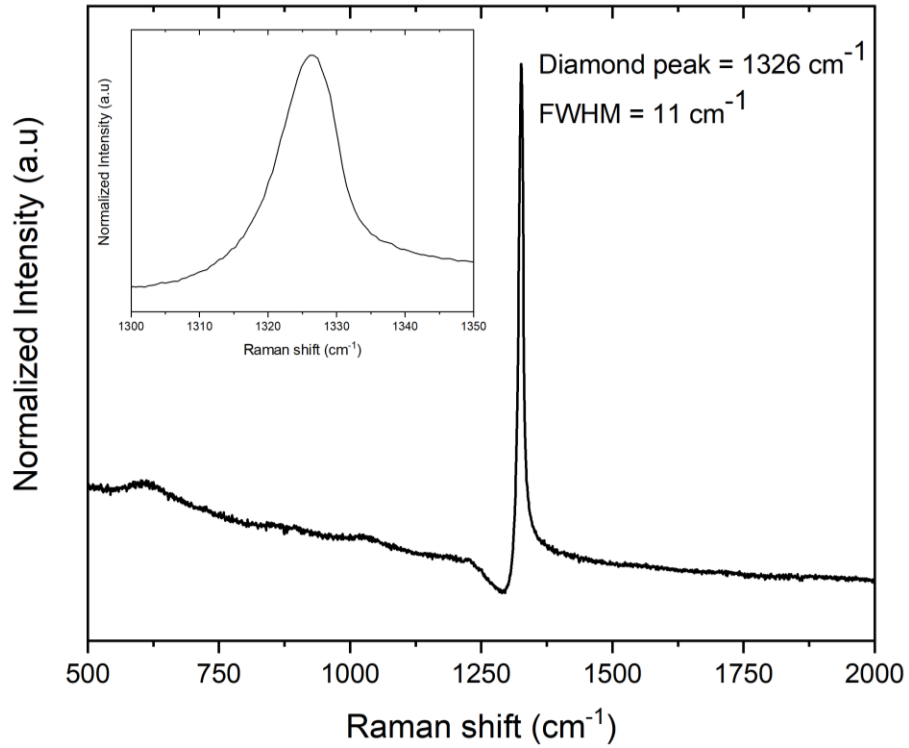


Figure IV.17 - Raman spectra of the resulting  $1 \times 1 \text{ mm}^2$  pierced sample

As a conclusion, despite our best efforts, we were unable to completely fill the hole in the sample even after 230 hours of deposition. It seems that the internal growth rate to fill the hole is lower than the external growth rate and then we try, in a new attempt to reduce the size of the square pierced hole.



#### 4.4.3.3 Substrate with 800 x 800 $\mu\text{m}^2$ pierced hole

For the second HPHT pierced sample, we chose a squared area of 800 x 800  $\mu\text{m}^2$ . The growth conditions for this sample are listed in Table IV.7.

Fixed growth conditions	
Substrate	HPHT 800x800 $\mu\text{m}^2$ pierced substrate – Ib <100>
Pressure	170 mbar
MW Power	2.7 kW
Total gas flux	200 sccm
CH <sub>4</sub>	10%
O <sub>2</sub>	2%
Temperature of the sample	850 °C $\pm$ 30 °C
B/C ratio	6,000 ppm
Precursor gas	Diborane
Thickness deposited	1.3 mm
Time	180h

Table IV.7 - Growth conditions used for the first approach to fulfill the second pierced substrate

Unfortunately, as for the previous sample, it was impossible to achieve a complete filling of the hole even after 180 hours of deposition. Figure IV.18 illustrates the growth progression from the initial stage, after 58 hours of deposition, and finally after 180 hours, resulting in a 1.3 mm thick layer with an approximate surface area of 5 x 5 mm<sup>2</sup>.

This means that 1mm was added per side. This 2<sup>nd</sup> try confirmed that the external lateral growth exceeded the internal lateral growth, preventing complete coverage of the internal hole.

Specifically, the external growth rate remains similar to the normal growth rate, giving a LGR/NGR of approximately 1. On the other hand, the internal growth rate is relatively slower leading to a LGR/NGR of approximately 0.3.

This implies that the presence of the hole have an impact on the current growth conditions, hindering the complete filling of the pierced area during the growth process. As explained before, it could be due to a variation of the local temperature close to the hole. Indeed, we observed that the control of temperature became very challenging towards the end of the deposition due to soot formation.

Consequently, it might lead to an increase of it, difficult to observe during the final hours. But this tendency could be confirmed by the etching effect observed in Figure IV.18 (c), already described in Chapter III, and reinforced when the temperature is higher.

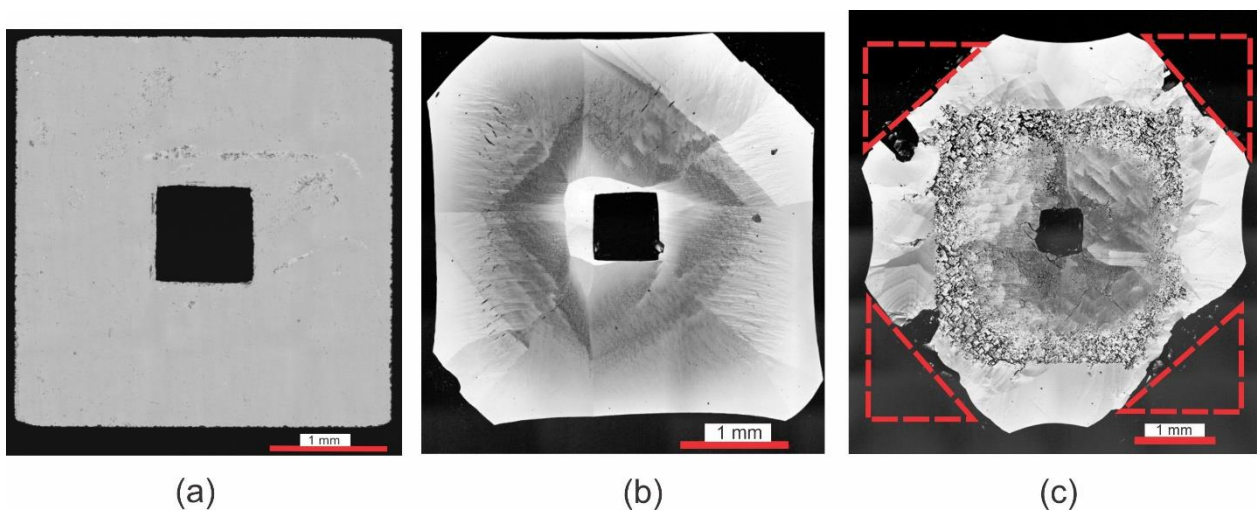


Figure IV.18 - Confocal laser scanning microscope images of the deposition evolution of the sample a) HPHT pierced substrate; b) deposition after 58h and c) final deposition after 180h

This increase of temperature could lead to a larger gradient of temperature especially because thermal conductivity is usually reduced when boron doping is present [25, 26]. This gradient could induce local modifications of growth rate explaining why the hole is not fully covered even after a long period of growth.

#### 4.4.4 Overgrowth on hole array on heteroepitaxial substrate

Heteroepitaxial diamond growth involves the deposition of diamond films on substrates made of a different material, such as Ir/MgO or Ir/YSZ/Si. The main interest of this material is to offer the possibility of growing large substrates even if dislocation density remains as high as  $10^7 \text{ cm}^{-3}$ . Various techniques have been developed to try to reduce this density and improve the quality of heteroepitaxial diamond films, including overgrowth on hole arrays [18] and other patterned structures[26].

The diamond substrates used in this study were supplied by Augsburg Diamond Technology GmbH and measured  $10 \times 10 \times 0.7 \text{ mm}^3$ . The substrates were grown on an Ir/YSZ template with lateral and top faces oriented along the  $\langle 100 \rangle$  direction before being lifted off and polished to optical quality on both sides. The advantage of starting from a large substrate is the possibility to create hole arrays on the substrates having different sizes. Two different hole sizes with lateral faces oriented along the  $\langle 100 \rangle$  direction were produced, with dimensions of  $800 \times 800 \mu\text{m}^2$  and  $500 \times 500 \mu\text{m}^2$ . A confocal laser scanning microscope image of the prepared substrate is shown in Figure IV.19.

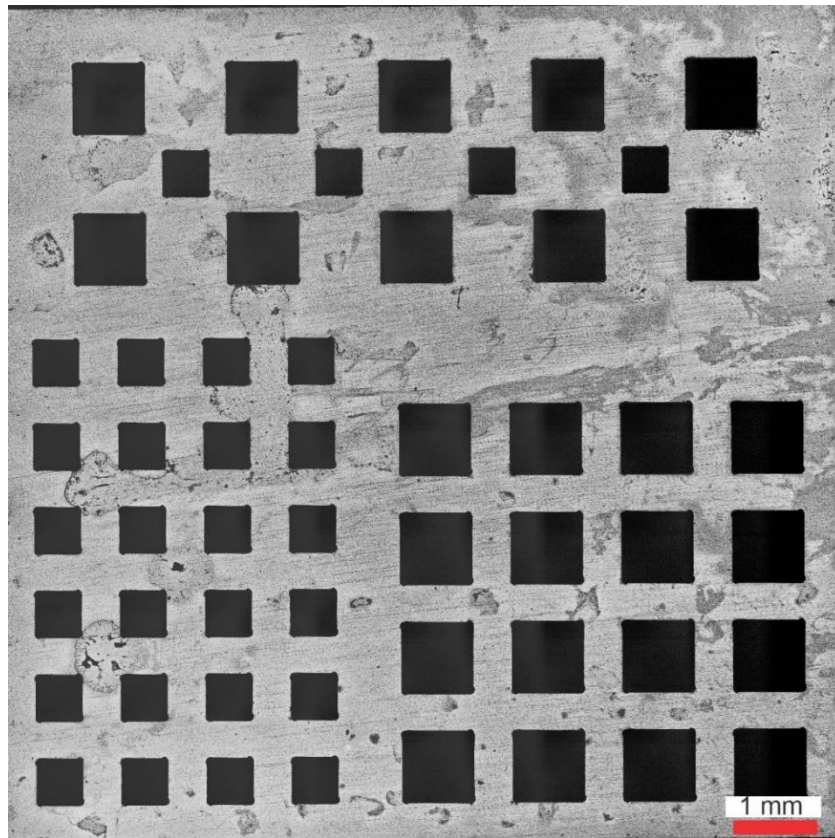


Figure IV.19 - Confocal laser scanning microscope image of the HCVD substrate sample used

The experimental conditions used for this process are presented in Table IV.8.

Fixed growth conditions	
Substrate	Heteroepitaxial substrate <100>
Pressure	170 mbar
MW Power	2.7 kW
Total gas flux	200 sccm
CH <sub>4</sub>	10%
O <sub>2</sub>	2%
Temperature of the sample	850 °C ± 30 °C
B/C ratio	6,000 ppm
Precursor gas	Diborane
Thickness deposited	1 mm
Time	260h

Table IV.8 - Growth conditions for the attempt to fulfill the Heteroepitaxial substrate

According to Raman analysis, the sample showed high boron doping levels, which were indicated by the appearance of an intense peak at 1200 cm<sup>-1</sup>. The characteristic diamond peak was also observed with a highly pronounced Fano effect. Its position is around 1322 cm<sup>-1</sup> showing the same tendency with a shift to lower wavenumber values, which is, as we have already mentioned, related to both high boron doping level and stress.

Nevertheless, the shift is very strong which could be indicative of a much higher stress in the deposited layer which is well accepted in the case of heteroepitaxial diamond. The FWHM was broadened up to 20 cm<sup>-1</sup>, which may be attributed to higher doping-induced disorder resulting from increased levels of boron doping. Nevertheless, it is not the case since the boron doping concentration has been estimated by the Raman web tool to approximately 3x10<sup>20</sup> at cm<sup>-3</sup>.

This broadening corresponds more likely to a reduction of diamond quality when the growth is performed on heteroepitaxial substrate.

Finally, a Raman mapping was also conducted in the close vicinity of a unfilled hole showing that the sample is relatively homogeneous. The white area corresponds to the unfilled hole.

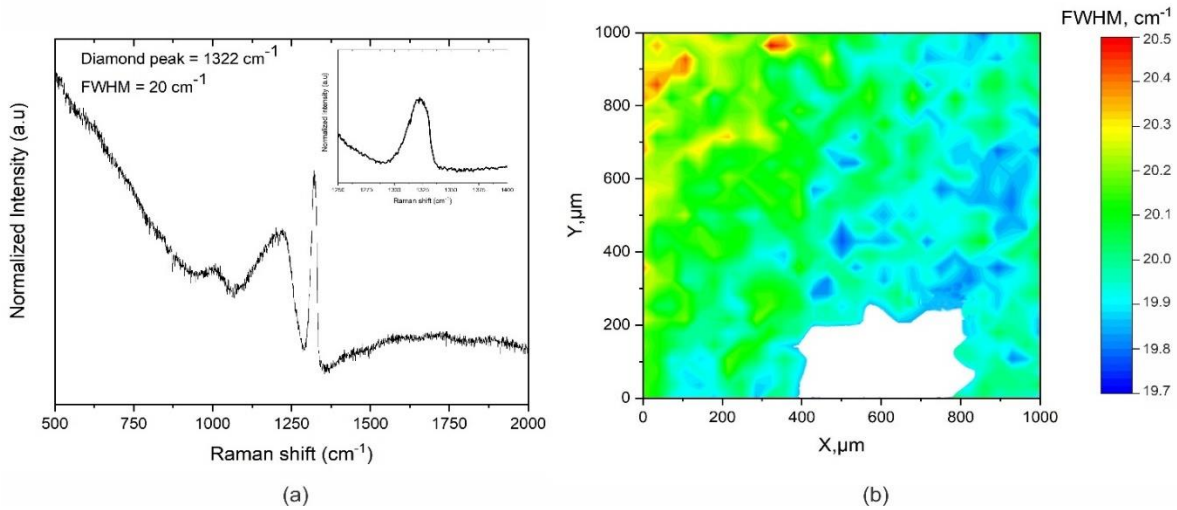


Figure IV.20 – Raman analysis of the HCVD sample. (a) Raman spectrum of the sample. (b) Raman mapping depicting the FWHM across a 1 x 1 mm<sup>2</sup> area. The white area represents the region that could not be filled during the growth process

The observation of the surface showed that the sample had experienced a fracture during the growth process likely due to stress. Despite this problem, we were able to successfully deposit a heavily boron-doped layer with a thickness of 1mm after a 260-hour deposition period.

However, it should be noted that due to the sample's fracture, a colder zone was present (refer to Figure IV.21) leading to a very limited and defective diamond deposition in this area which will not be discussed in this part and will be excluded from further analysis.

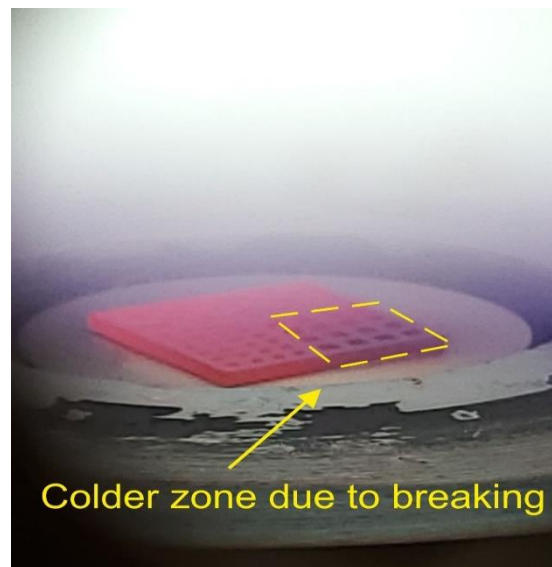


Figure IV.21 – Photography of heteroepitaxial sample during growth. Dashed yellow zoned highlights a cooler zone due to breaking.

In the part of the sample grown at a stable temperature, after a 260 hour deposition, the sides increased by 250  $\mu\text{m}$  each, resulting in a LGR/NGR ratio of approximately 0.5. This ratio is significantly lower than the ratio found on HPHT substrates under the same conditions, showing that heteroepitaxial material has a different behavior in terms of growth mode. It will imply further efforts to adapt the growth conditions for this specific substrate type but the time required for these adaptations exceeds didn't allow me to carry out these developments.

If now we focus on the internal lateral growth, we can see that the side of a 800 x 800  $\mu\text{m}^2$  holes decreases by about 200  $\mu\text{m}$ . Similarly, the 500 x 500  $\mu\text{m}^2$  holes also showed a 200  $\mu\text{m}$  decrease per side. This results in a LGR/NGR ratio of approximately 0.4 whatever the initial size of the hole. As for HPHT substrate, this ratio is lower than the ratio obtained for the lateral sides which is very specific to the growth of boron doped material since was not the case when similar works were performed by Mehmel et al with intrinsic diamond growth on pierced heteroepitaxial substrates[18].

Thus, even if this technique showed promising results, its use in the case of boron-doped layer remains very challenging and requires further investigations.

Figure IV.22 shows a portion of the HCVD sample surface, specifically highlighting some of the unfilled holes. It's crucial to note that the image presented here focus on the more successful area of the sample post-growth.

The less successful or problematic areas have been omitted for clarity and focus in this particular discussion. Further exploration and analysis would be required to fully understand the challenges encountered in those areas.

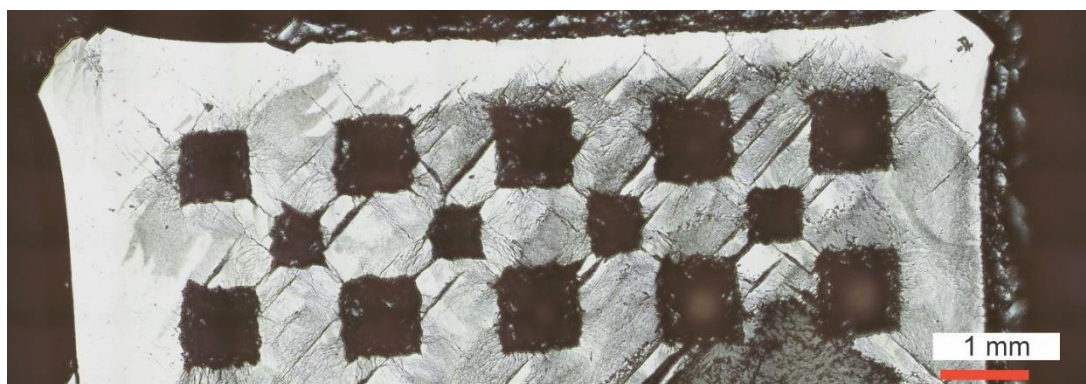


Figure IV.22 - CLSM image of the HCVD sample area with hole array of 500 $\mu\text{m}$  and 800 $\mu\text{m}$

As a partial conclusion, we can say that the use of a HCVD substrate with a hole array showed promising results for the deposition of thick and large intrinsic material but for boron-doped layers, the process was impeded by substrate breakage due to the high level of stress generated during the deposition process.

Despite this problem, a 500  $\mu\text{m}$  thick boron-doped diamond layer was successfully deposited, although the holes in the substrate were not fully overgrown. Further work is needed to address the issue of substrate breakage and to optimize the deposition conditions to achieve full holes closure. Overall, this study provides valuable insights into the challenges and opportunities of using HCVD substrates for diamond deposition and highlights the need for pursuing research in this area.

## 4.5 Conclusions

In conclusion, we have made significant strides in optimizing strategies for expanding heavily boron-doped diamond films using lateral growth techniques. By investigating and optimizing possible process parameters, we achieved lateral growth rates that, in some instances, were larger than the normal growth rate, even with high levels of boron.

Our findings also suggest that combining pierced and laser pierced substrates with lateral growth could be an effective strategy to mitigate dislocation formation. However, the precise conditions that allow a higher internal growth rate must be identified. The fact that pierced holes in the substrate cannot be filled as soon as diborane is added to the gas mixture remains unclear, necessitating further investigation.

Another key conclusion is the potential benefit of starting with intrinsic substrates to reduce dislocation density. By first mitigating dislocations on these substrates and then proceeding with a heavily boron-doped layer, in that case we hope to create a better starting point from a dislocation perspective. While this approach may not prevent the addition of many dislocations at the growth resumption, it provides a promising avenue for further exploration.

Our work demonstrates the potential of lateral growth techniques for producing high-quality, heavily boron-doped diamond films for a wide range of applications. While challenges remain, our results suggest that continued research in this area could lead to significant improvements in the efficiency and performance of diamond-based devices. Detailed perspectives for future work are provided in the following section.



## 4.6 Perspectives

In addition to the conclusions drawn from our study, there are several promising perspectives that can be pursued in further research on the growth of heavily boron-doped diamond films using lateral growth techniques:

- Optimization of lateral growth parameters: our study has provided valuable insights into the impact of process parameters on lateral growth rates and boron doping levels such as the modification of the oxygen and methane concentration in the gas mixture but further optimization of these parameters is needed. Indeed, the set of parameters used in our last results still leads to the appearance of (111) faces which are well known to be very defective. Condition allowing an increase of growth rate in (111) direction could allow reducing their size and improve the global quality of the grown substrates.
- Developing dedicated characterization methods that could give a hint on dislocation propagation like a transversal cut over the pierced unfilled hole substrates: indeed, the high doping level of these samples makes CL imaging very challenging due to the darkness of the grown layer, for instance.
- Characterization of electronic properties: while our focus has been on the growth aspects and achieving high levels of boron doping for near-zero resistance, future research could delve into a comprehensive characterization of the electronic properties of the p- layer deposited on these heavily boron-doped diamond substrates. This includes studying carrier mobility, conductivity, and the impact of doping on the band structure. Understanding these properties is crucial for the development of diamond-based electronic devices, and while we acknowledge that mobility may be poor in these highly doped substrates, it is the specific properties of the p- layer that will be of particular interest.
- Integration to device fabrication: the successful growth of heavily boron-doped diamond films using lateral growth techniques presents a significant opportunity for their integration into practical device structures. As demonstrated in Chapter III in which we focused on fabricating a Schottky diode through a stacking layer, further research can now concentrate on the fabrication of specific devices, including high-power electronic devices, sensors, and quantum computing elements, utilizing these films. This integration necessitates advancements in multiple areas, such as device design, processing techniques, and characterization methods.

## 4.7 References

1. Gsell, S., et al., *A route to diamond wafers by epitaxial deposition on silicon via iridium/yttria-stabilized zirconia buffer layers*. Applied Physics Letters, 2004. **84**(22): p. 4541-4543.
2. Gicquel A., e.a., *CVD diamond films: from growth to applications*. Current Applied Physics 1 (6) 2001, 2001: p. p. 479-496.
3. Tallaire, A., et al., *Reduction of Dislocations in Single Crystal Diamond by Lateral Growth over a Macroscopic Hole*. Advanced Materials, 2017. **29**(16): p. 1604823.
4. Yamada, H., et al., *A 2-in. mosaic wafer made of a single-crystal diamond*. Applied Physics Letters, 2014. **104**(10): p. 102110.
5. Yamada, H., et al., *Fabrication of 1 Inch Mosaic Crystal Diamond Wafers*. Applied Physics Express, 2010. **3**(5): p. 051301.
6. Kwak, T., et al., *Boron-Doped Single-Crystal Diamond Growth on Heteroepitaxial Diamond Substrate Using Microwave Plasma Chemical Vapor Deposition*. physica status solidi (a), 2020. **217**(12): p. 1900973.
7. Issaoui, R., et al., *Thick and widened high quality heavily boron doped diamond single crystals synthesized with high oxygen flow under high microwave power regime*. Diamond and Related Materials, 2019. **94**: p. 88-91.
8. Lloret, F., et al., *Boron-Doping Proximity Effects on Dislocation Generation during Non-Planar MPCVD Homoepitaxial Diamond Growth*. Nanomaterials (Basel), 2018. **8**(7).
9. Barbay, C., et al., *Dislocations imaging in low boron doped diamond epilayers using Field Emission Scanning Electron Microscopy (FE-SEM)*. Applied Surface Science, 2019. **495**: p. 143564.
10. Zavabeti, A., et al., *Two-Dimensional Materials in Large-Areas: Synthesis, Properties and Applications*. Nano-Micro Letters, 2020. **12**(1): p. 66.
11. Rantamäki, R., et al., *Epitaxial Lateral Overgrowth of Gallium Arsenide Studied by Synchrotron Topography*. MRS Online Proceedings Library (OPL), 1999. **570**: p. 181.
12. Zheleva, T.S., et al., *Pendeo-epitaxy: A new approach for lateral growth of gallium nitride films*. Journal of Electronic Materials, 1999. **28**(4): p. L5-L8.
13. Li, J., et al., *Study on Nucleation and Growth Mode of GaN on Patterned Graphene by Epitaxial Lateral Overgrowth*. Crystal Growth & Design, 2023.
14. Mayr, M., et al., *Correlation between surface morphology and defect structure of heteroepitaxial diamond grown on off-axis substrates*. physica status solidi (a), 2014. **211**(10): p. 2257-2263.
15. Stehl, C., et al., *Efficiency of dislocation density reduction during heteroepitaxial growth of diamond for detector applications*. Applied Physics Letters, 2013. **103**: p. 151905-151905.
16. Mehmel, L., *Deposition of doped and intrinsic heteroepitaxial diamond films on Ir/SrTiO<sub>3</sub>/Si (100) multilayer stacks*  
*Épaissement et dopage de films de diamant hétéroépitaxiés sur substrats multicouches Ir/SrTiO<sub>3</sub>/Si (100)*. 2019, Université Paris-Nord - Paris XIII.
17. Boussadi, A., et al., *Reduction of dislocation densities in single crystal CVD diamond by confinement in the lateral sector*. Diamond and Related Materials, 2018. **83**: p. 162-169.
18. Mehmel, L., et al., *Dislocation density reduction using overgrowth on hole arrays made in heteroepitaxial diamond substrates*. Applied Physics Letters, 2021. **118**(6): p. 061901.
19. Tallaire, A., et al., *Oxygen plasma pre-treatments for high quality homoepitaxial CVD diamond deposition*. physica status solidi (a), 2004. **201**(11): p. 2419-2424.

20. Issaoui, R., et al., *Evaluation of freestanding boron-doped diamond grown by chemical vapour deposition as substrates for vertical power electronic devices*. Applied Physics Letters, 2012. **100**(12): p. 122109.
21. Butler, J.E., et al., *Thin film diamond growth mechanisms*. Philosophical Transactions of the Royal Society of London. Series A: Physical and Engineering Sciences, 1993. **342**(1664): p. 209-224.
22. Liu, D.-Y., et al., *Effect of oxygen on regulation of properties of moderately boron-doped diamond films*. Chinese Physics B, 2022. **31**(12): p. 128104.
23. Wang, R., et al., *Morphology, defects and electrical properties of boron-doped single crystal diamond under various oxygen concentration*. Materials Letters, 2022. **322**: p. 132345.
24. Okushi, H., *High quality homoepitaxial CVD diamond for electronic devices*. Diamond and Related Materials, 2001. **10**(3-7): p. 281-288.
25. Baron, C. *Contribution à l'estimation de paramètres physiques à l'aide de modèles d'ordre réduit*. 2003.
26. Ichikawa, K., et al., *High crystalline quality heteroepitaxial diamond using grid-patterned nucleation and growth on Ir*. Diamond and Related Materials, 2019. **94**: p. 92-100.

## **General conclusions and outlook**

My doctoral research journey was primarily focused on mastering the growth of high-quality, thick, and large boron-doped monocrystalline diamond films. The aim was to mitigate the propagation of threading dislocation, thereby enhancing the potential of boron-doped diamond for various applications, especially in power electronics. This research was divided into four main chapters, each dedicated to a specific aspect of the study. This general conclusion aims to summarize the key findings and contributions from each chapter, providing a holistic perspective on the conducted research.

The first chapter highlighted the unique properties of diamond and the challenges in utilizing them. The synthesis of high-quality diamond material, controlling dopant concentration, and reducing dislocations were identified as key to unlocking diamond's potential. The second chapter detailed the experimental techniques and characterization methods used, providing a comprehensive understanding of the diamond samples. The third chapter presented the results of boron-doped diamond film growth, emphasizing the importance of controlling the thickness, doping level, and defect density of the p- layer in the development of vertical Schottky diodes.

The findings suggested that growing a p+ layer directly on an HPHT substrate before depositing the active p- layer was recommended for improving diamond structure adapted for fabricating Schottky diodes. The use of heavily boron-doped layers was shown to enhance the crystalline quality by inducing stress levels that somehow limit the dislocation propagation, leading to an overall improvement of the sample quality. These findings can be utilized for the development of high-quality diamond-based electronic devices that require stable growth and improved crystalline quality.

The results presented in the final chapter of this thesis made significant progress in optimizing strategies for extending heavily boron-doped diamond films using lateral growth techniques. By investigating and optimizing different parameters, we achieved lateral growth rates that, in some instances, were larger than the normal growth rate, even with high boron doping levels. We also experimented the limitation of threading dislocations using substrate with holes array and conditions leading to lateral growth. Even if this strategy was very effective with intrinsic materials, we showed that the overgrowth of the holes is impossible with boron doping growth.

Nevertheless, the thickness achieved and the lateral growth rates are notable accomplishments. Moreover, the utilization of different substrates such as HCVD, CVD and HPHT is also noteworthy, as they can serve as a foundation for extending boron-doped diamond substrates. Additionally, it has been shown that oxygen content in the gas phase plays a pivotal role in achieving the optimal parameters for lateral growth. However, further research is essential to refine these parameters and minimize reactor malfunctions because, for instance, those oxygen levels with extended depositions can be harmful to the reactor.

The work conducted during this thesis represents a significant advancement in the boron-doped diamond field, with unique studies on crystals with thicknesses surpassing 1 mm and high boron concentrations. The application of these substrates in the electronics sector is already underway, and future research areas include plasma modeling, understanding soot formation, and improving dislocation propagation in heavily boron-doped films.

The application of single-crystal diamond in industrial power electronics is tied to the ability to synthesize large functional surface areas. Despite progress, further research should explore various paths, such as deposition on heteroepitaxial substrates, the use of larger CVD substrates, and the simultaneous growth of multiple diamond layers. The presence of extended defects in diamond single crystals remains a challenge, and further studies are needed to understand and mitigate threading dislocations.

In conclusion, the research has paved the way for the use of boron-doped monocrystalline diamond films in power electronics, with projects like MOVEToDiam building upon this work. However, several growth-related questions remain, presenting exciting opportunities for future research. The impact of oxygen, different substrate sizes, and other factors will likely be areas of continued exploration. With continued support and active pursuit of these research directions, diamond-based electronic components may become an integral part of future everyday life.